FPDC

fracture proof design corporation

8305030412 830428
PDR ADOCK 05000286
P PDR

PASNY Contract 80-121, Change Order 5

Final Report, March 25, 1983
Revision 2, April 11, 1983

Report Number 83-154

FRACTURE MECHANICS ANALYSIS OF THE INDIAN POINT UNIT 3 NUCLEAR GENERATING STATION STEAM GENERATOR GIRTH WELD CRACKS

Prepared by

FRACTURE PROOF DESIGN CORPORATION
77 Maryland Plaza
St. Louis, MO 63108

Principal Investigators

Keyren H. Cotter
Paul C. Paris

Prepared for

The Power Authority of the State of New York
10 Columbus Circle
New York, NY 10019

PASNY Project Manager

James V. Brunetti
Civil-Structural Department, Design and Analysis

REPORT APPROVAL COVER SHEET

Client: Power Authority of the State of New York

Contract/PO Number: 80-121 Job Number: 150

Project Plant: Indian Point Unit 3

Report Title: Fracture Mechanics Analysis of the Indian Point Unit 3 Nuclear Generating Station Steam Generator Girth Weld Cracks

Report Number: 83-154 Rev: 2

The work described in this Report was performed in accordance with the FPDC Quality Assurance Program. The signatures below verify the accuracy of this Report and its compliance with applicable Quality Assurance requirements.

Prepared By: R H Potts Date: April 11, 1983

Reviewed By: Paul C. Paris, Sr. Date: April 11, 1983

Approved By: Hans Kattenbelt Date: April 11, 1983

REVISION RECORD

Rev. No.	Prepared	Reviewed	Approved	Approval Date	Revision

INDEX

1-0 INTRODUCTION 1-1
1-1 BACKGROUND 1-1
1-2 STATEMENT OF THE PROBLEM 1-2
1-3 OBJECTIVE 1-2

2-0 CRACK STABILITY CRITERIA 2-1
2-1 CRACK DRIVING FORCE 2-1
2-2 FRACTURE TOUGHNESS CONSIDERATIONS 2-2
2-3 TEARING STABILITY CONSIDERATIONS 2-2
2-3.1 Theory 2-2
2-3.2 The J-T Diagram 2-5
2-3.3 Extrapolation of Jmat-Tmat Curve 2-6

3-0 SSY BASED ANALYSIS 3-1
3-1 J-INTEGRAL ESTIMATION 3-1
3-1.1 Circumferential Cracks 3-1
3-1.2 Longitudinal Cracks 3-2
3-1.3 Tearing Stability for SSY Conditions 3-3
3-1.4 Plastic Zone Instability Failure 3-3

4-0 STRESS ANALYSIS 4-1
4-1 PRESSURE STRESS ANALYSIS 4-1
4-1.1 Axisymmetric Idealization 4-1
4-1.2 P-Convergent 3-D Idealization 4-2
4-2 THERMAL STRESS ANALYSIS 4-3
4-3 WELD RESIDUAL STRESSES 4-4
4-4 CRACK SURFACE PRESSURE 4-4
4-5 COMBINATION OF STRESSES 4-5
4-6 PWHT STRESS ANALYSIS 4-6

5-0 RESULTS 5-1
5-1 FATIGUE CRACK GROWTH 5-1
5-2 LEAK-BEFORE-BREAK 5-2
5-2.1 Material Properties. 5-2
5-2.2 Leak Rate Analysis 5-3
5-2.3 Crack Stability for LBB. 5-4
5-3 PRESSURIZED THERMAL SHOCK 5-4
5-4 DISCUSSION 5-5

6-0 CONCLUSIONS 6-1

7-0 REFERENCES 7-1

APPENDIX A, MATERIAL PROPERTIES A-1
A-1 SOURCE OF DATA A-1
A-2 DATA REDUCTION A-1
A-3 PROCEDURE FOR CALCULATING Tmat A-5
A-4 PROCEDURE FOR CALCULATING Jmod A-5
A-5 RESULTS A-6
A-6 REFERENCES A-7

APPENDIX B, FPDSSM B-1
B-1 THE SLICE SYNTHESIS METHOD B-1
B-2 THEORY B-1
B-3 APPLICATIONS B-3
B-4 VERIFICATION OF SLICE SYNTHESIS SOLUTIONS B-4
B-5 REFERENCES B-4

APPENDIX C, HEAT TRANSFER CALCULATIONS C-1

EXECUTIVE SUMMARY

An analysis of postulated "crack-like" defects that might remain in the Indian Point 3 steam generators after completion of the girth weld repair program was undertaken. The specific objective was to satisfy safety and economic considerations underlying the existence of such crack-like defects. 2

Part-through surface cracks were postulated to exist in the worst location of the girth weld and fatigue crack growth computations were performed. It was determined that cracks having a surface length of six times the depth and a depth of .25 inches would take more than six times the remaining operating life to propagate through-the-wall of the vessel. In a similar analysis, with cracks having a depth of one-quarter of the wall thickness, it required over three times the remaining operating life to propagate through the vessel wall. This task also involved performing a detailed stress analysis of the girth weld region under various thermal and pressure transients. The results of the stress analysis were found to differ from the original Westinghouse stress analysis report. 2

Consideration was also given to generalized leak-before-break criteria. This involved determining the longitudinal and circumferential crack lengths that result in readily detectable leak rates of nominally ten gallons per minute. Then, demonstrating that both longitudinal and circumferential cracks, that cause such leak rates, have excellent margins of stability. This was achieved. It was demonstrated that cracks having lengths in excess of 20 inches were stable and exhibited considerable margins of safety.

A postulated accident condition of pressurized thermal shock involving introduction of 70F feedwater into a "hot" steam generator under design pressure was also evaluated. It was shown that, even if large cracks are present, the cracks behave in a stable manner and the generator does not rupture. 2

Section 1

INTRODUCTION

1-1 BACKGROUND

The Power Authority of the State of New York (Authority) is currently in the process of repairing extensive cracking in girth welds in the Indian Point 3 steam generators. The cracks are located in the upper shell to lower shell transition cone girth weld. The repair procedure consists of grinding out cracks detected by liquid penetrant and other NDE techniques, and, if required, replacing the metal so removed with weld filler metal. After completion of the weld repair procedure, the regions subjected to weld repair are stress-relieved at a temperature of 1150F for 4 hours. 2

Based on the known extensive cracking in the original weld, it is both prudent and conservative to postulate, for safety analysis purposes as well as economic factors, that cracks may still be present in the region after completion of the repair. If such cracks are postulated to be present, then several factors must be considered. These include: the stability of the largest crack in the worst location under the most severe stresses that can be expected to occur in the steam generator vessel; the growth of cracks due to repeated fatigue loads or by some environmentally enhanced stress-corrosion cracking mechanism; the leak-before-break condition that resulted in the leaking of the steam generator during operation must be generalized to show that a general leak-before-break premise is valid for all postulated defect locations; and, lastly, Section XI criteria must be considered regarding permissible defect sizes and inspection limits. 1

In addition to the foregoing questions, it is also relevant to consider the effect of the localized thinning associated with the repair procedure. Specifically, it is necessary to define any effect that would result from the wall not having its original full thickness due to the weld repair procedure.

1-2 STATEMENT OF THE PROBLEM

Before placing the steam generator back into service, it is necessary to resolve the questions posed in Section 1-1. These questions have both operational safety and economic impact. The safety aspects must be addressed in order to demonstrate to the USNRC and the Authorized Inspector (AI) that placing the Unit back into operation is justified based on conservative assumptions as to the repair and the presence of any detected or undetected crack-like defect(s). The economic considerations arise because of the need to be assured that any such crack-like defect(s) will not result in a near term unscheduled outage. 2

1-3 OBJECTIVE

The objective of the study will be to quantify the behavior of crack-like defects such as those shown in Figure 1-1. This requires determination of stresses, crack growth rates, crack stability and fatigue loads. 2

Figure 1-1 Postulated Initial Crack Size

ASME SECTION XI REF. FLAW

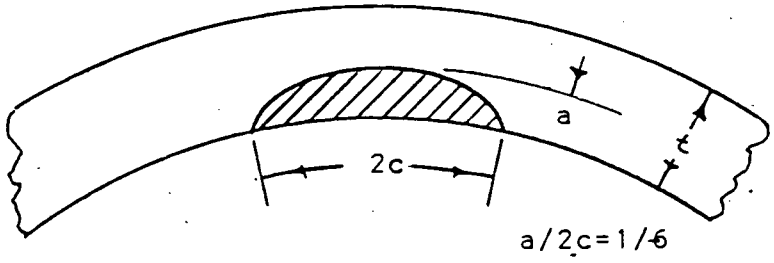

Section 2

CRACK STABILITY CRITERIA

In order to analyze the stability of cracks in nuclear vessels using fracture mechanics methodology, it is necessary that the material properties, distribution of crack sizes and shapes, applied loads (or stresses) and the crack stability criteria be specified. As all but the crack stability criteria are readily quantifiable, only this aspect will be discussed.

2-1 CRACK DRIVING FORCE

Crack stability is usually evaluated by comparing the value of a crack driving force parameter with the resistance of the material to crack extension. The crack driving force parameters can be grouped into those applicable to cases involving limited (small) amounts of crack-tip plasticity and those with large amounts of crack-tip plasticity, including net-section yielding. The former is often referred to as small-scale yielding (ssy) and the latter as large-scale yielding (lsy). For ssy cases, the crack driving force is usually described in terms of the associated values of the crack-tip stress-intensity factor, K. For lsy cases, K is not applicable and the parameter is described in terms of the value of the J-integral, J_{app}. J_{app} is also valid for the ssy regime.

The analysis of crack problems is the ssy regime involves the use of the methods of linear-elastic fractiure mechanics (LEFM). For the analysis of lsy problems, elastic-plastic fracture mechanics will be relied upon.

2-2 FRACTURE TOUGHNESS CONSIDERATIONS

For ssy problems, the crack driving force based on LEFM is defined in terms of the stress-intensity factor, K. And, for stability, the K computed for the applied stress and crack size of interest must be less than the fracture toughness, K_{Ic}, of the vessel material. Stability can also be defined in terms of the J-integral, which, for LEFM, can be computed from $J=(K^2/E')$ as further discussed in Section 3-1. The parameter J_{Ic} can be considered a toughness that is equivalent to the K_{Ic} fracture toughness or crack growth initiation toughness, and thus for $J_{app}<J_{Ic}$, stability is insured. Because J is used throughout this report, consideration of LEFM methods is presented in terms of J. A J_{Ic} approach to stability (i.e., not including stable growth above J_{Ic}) is not acceptable for lsy problems because it is far too conservative.

Exact J solutions are typically not available for lsy for the postulated crack geometries and loading. Thus, ssy estimates of J are developed for the crack geometries of interest using the accepted practice of basing J estimates on plastic zone corrected stress-intensity factor solutions (i.e., $K(a+r_y)$). (Note that estimates of J based upon K solutions, that is, LEFM, result in unconservative estimates of J as the plastic limit conditions of the cracked section are approached.)

2-3 TEARING STABILITY CONSIDERATIONS

2-3.1 Theory

Before utilizing tearing stability methods for typical problems, it is worthwhile to review a bit of theory. In the application of LEFM to brittle

materials, crack instability is assumed to be incipient when $K>K_{Ic}$. Physically, this is interpreted as an instability that accompanies the onset of crack extension. But, for tough materials, it is known that crack instability does not generally accompany the onset of crack extension. Rather, the K (or J) at instability can be well above the K_{Ic} (or J_{Ic}) point. It is important, from design and safety considerations, to be able to take advantage of the higher J values (or loads) that co-exist with the stable crack extension but, until the recent development of the tearing modulus concept, it was not possible. Analysts had been faced with the problem of using a J_{Ic} value for instability predictions unless representative R-curves could be developed which were typical of the significant material dimensions actually used in the structures of interest.

Solutions to problems that rely on the tearing stability approach involve expressing the intensity of the crack-tip deformation field by an appropriate elastic-plastic crack driving force parameter. Based on the fracture parameter, the behavior or growth of cracks can be expressed functionally. It follows that the use of a parameter like J infers that crack growth is controlled or determined by the value of the parameter. This logic leads to the term "J-controlled growth." Typically, the quantifying of the fracture parameter is accomplished by computing the value of the path independent J-integral, developed by Rice[8], either by use of direct integration around the crack-tip or by use of any one of a number of acceptable estimation schemes. Relative to any J computation, it is interesting to note that the phrase elastic-plastic fracture mechanics infers that problems involving plasticity can be analyzed for any type of loading. But Rice[8] proved the path independence of J only for the idealized case of no crack growth and a material which exhibits "non-linear elastic" behavior. Unfortunately, real materials do not behave exactly as non-linear elastic

materials and the problems of interest involve crack growth. However, the violation of this idealized behavior is not sufficient to invalidate the path independence of the J-integral if certain restrictions are met. Based on a need for these restictions, Hutchinson and Paris[9] set-forth strict theoretically based guidelines for J-controlled crack growth. Extensions beyond those limits are possible under the conditions discussed in Reference [4].

Although the value of J is indicative of the intensity of the crack-tip deformation field, it is not alone sufficient for resolution of the question of stability. To resolve this, Paris, et al.[1] defined a non-dimensional parameter, called the tearing modulus, which assumed the validity of J-controlled growth. It is applicable to material property data and applied loads alike, and is expressed as

$$T = \frac{E}{\sigma_o^2} \frac{dJ}{da} \tag{2-1}$$

where E is the elastic modulus, a is the crack length, σ_o is a flow stress, and J is the J-integral. J controlled growth requires that the crack extension, da, occurs under the equilibrium condition

$$J_{app} = J_{mat}, \tag{2-2}$$

which applies whether or not stability of the crack extension is present. In this expression, J_{mat} is the value of J on the material J-resistance curve, and the J_{app} is the computed value of the J-integral for a given load and crack length. For a crack under the preceeding equilibrium conditions stability is determined

from

$$T_{app} < T_{mat} \qquad \text{(stable)} \tag{2-3}$$

$$T_{app} > T_{mat} \qquad \text{(unstable)} \tag{2-4}$$

where T_{mat} is determined from the material J-R curve and T_{app} is dependent upon the crack geometry and loading existing in the actual structure.

The very power of this approach stems, in part, from the fact that the use of tearing stability methods is applicable to both the ssy and lsy regime.

This stability criteria has been experimentally verified for several specimen types. Paris, et al.[1], were the first to demonstrate applicability through experiments using A471 steel 3-point bend bars in a test system of variable compliance. The variable compliance feature was used as a means of controlling the T_{app}. Similarly, Zahoor and Kanninen[10] tested circumferentially cracked 4-inch diameter TP304 stainless steel pipes in 4-point bending, and Gudas and Joyce[11] evaluated several materials of varying degrees of toughness in 4-point bending.

2-3.2 The J-T Diagram

For safety assessments of nuclear piping systems that are based on the tearing modulus stability concept, it is convenient to present the results using a J-T diagram. The J-T diagram compares the applied (or calculated) values of J and T with the material (invariant characteristic of a material) values. That is, the J_{app} vs. T_{app} response is compared with the J_{mat} vs. T_{mat} curve to determine

whether the T_{app} value is less (or greater) than the T_{mat} value for the J_{app} value specified. If the $T_{app} < T_{mat}$, then stability is assured; and, conversely for instability. A sample J-T diagram is shown in Figure 2.1.

The material curve shown on Figure 2.1, was derived from a J-resistance curve for the material of interest. The details of this can be found in Appendix A. Note in Figure 2.1, that the T_{app} values are dependent upon the J_{app}. For cases where the T_{app} is less than the T_{mat} values, stable crack behavior is assured. On the other hand, a lower T_{mat} value corresponding to higher J_{app} values can cause unstable behavior.

2-3.3 Extrapolation of the J_{mat}-T_{mat} Curve

For applications that require J_{mat} values greater than those available from the J-resistance curve, the assessment of whether a system is stable or unstable based on a J-T diagram may require extrapolation of the material curve. One way of extrapolating the resistance curve is to assume that the material continues to tear with the same slope. Recent experiments on stainless steel plate [22] indicate that this assumption may be valid. This would mean that, in the extrapolated regime, the T_{mat} remains constant. The extrapolation of the material curve on the J-T diagram would then be the vertical line extending from the maximum J_{mat} value point on the material curve. This is shown as 1-C in Figure 2.1.

An alternative to this extrapolation is to assume that there is no further increase in the J-resistance with crack growth. Such a behavior would imply that the T_{mat} reduces to zero in the extrapolated regime. That is, on a J-T diagram, the extrapolated material curve would take the form of the horizontal line noted

as 1-0 in Figure 2.1.

These two extrapolations represent the upper and lower bounds of resistance curve behavior for continued growth. In reality, the T_{mat} value is expected to decrease gradually with increase in the J_{mat} value[23], and experiments indicate that it does, leading to the possibility of a zero value of the T_{mat} at some higher J_{mat} value. One accepted approach is to follow Paris[4] and construct a tangent to the material curve. This approach is noted as line 1-T in Figure 2.1 and is accepted as valid throughout this report. 1,2

The validity of J-controlled growth is dependent upon the satisfaction of several requirements. One of these is that ω be "large". For typical A302B ferritic steel, valid J-resistance curves may have over 1 inch of crack growth and ω values that range from 5 to 10. Considering T_{mat} to decrease abruptly to zero, simply implies that the ω value, which is proportional to T, also decreases to zero. Note, that for small size specimens, the limit of Δa is on the order of 0.05 inches at ω=3 and having a method of extrapolation is necessary to avoid unreasonable conservatism. This would invalidate the assumptions of J-controlled growth, and any assessment of the stability of the vessel would be subject to serious error. J-resistance curves need to be developed to include extended amounts of crack growth while satisfying the J-controlled growth requirement. Because of these limitations, the assumption of the tangent extrapolation of the T_{mat} curve is felt to be the most acceptable method. 1,2

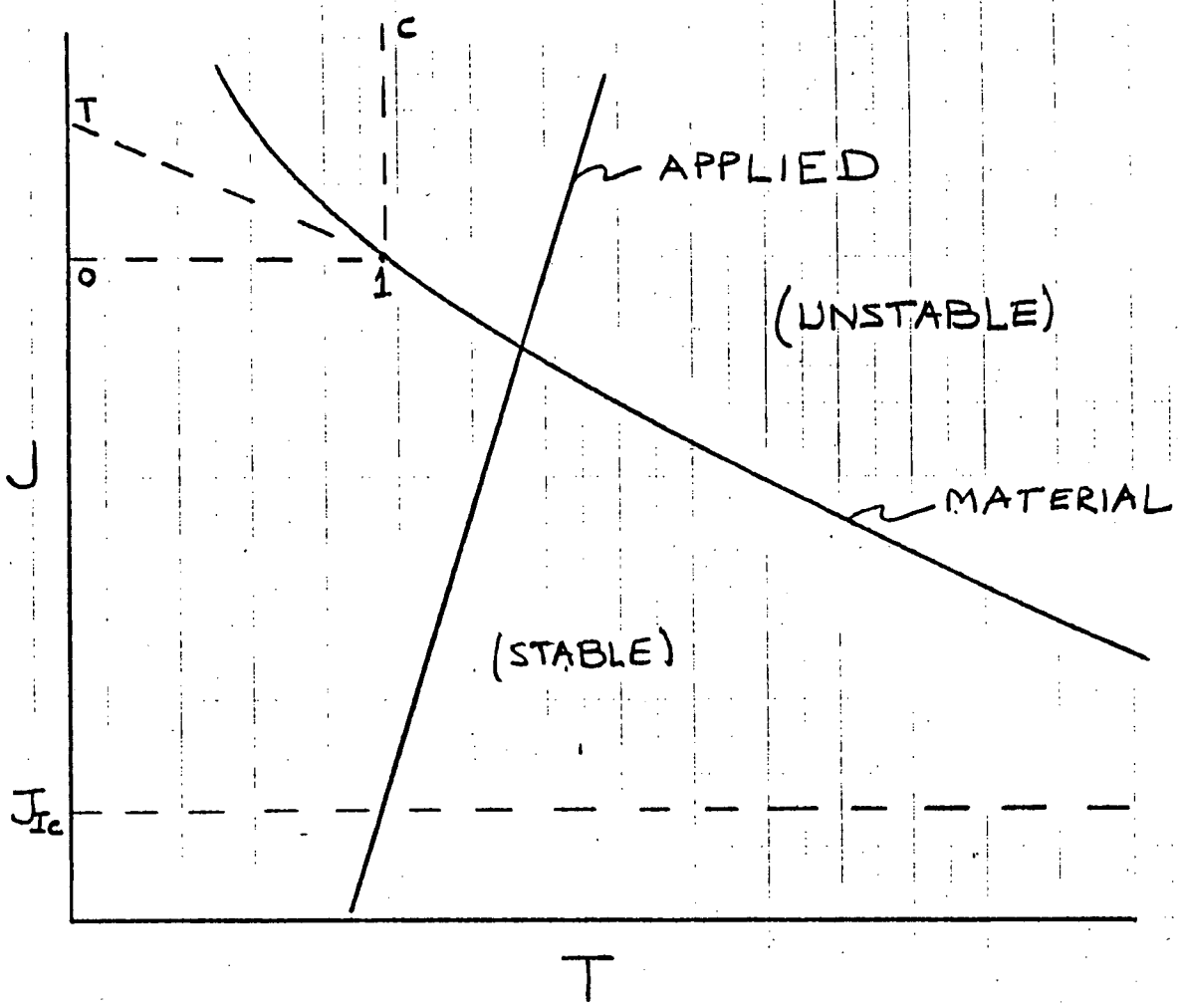

Figure 2-1 Schematic of J-T Stability Diagram

Section 3

SSY BASED ANALYSIS

3-1 J-INTEGRAL ESTIMATION

For the ssy regime, the J-integral, J_{app}, can be estimated using the relation

$$J_{app} = K_I^2/E' \tag{3-1}$$

where $E'=E$ for plane stress, $E'=E/(1-v^2)$ for plane strain, K_I is the opening mode plastic zone corrected stress-intensity factor, E is the elastic modulus and v is Poisson's ratio.

3-1.1 Circumferential Cracks

For circumferential cracks, the K_I consists of contributions from three types of loads: axial load, bending moment and membrane stress due to pressure. The K_I due to pressure loading, K_m, was obtained by utilizing the solutions from Reference [15], giving

$$K_m = \sigma_m/\overline{\pi R\theta}\ F_m \tag{3-2}$$

where σ_m is the membrane stress (axial) and F_m is a shell correction factor that depends upon the length of the crack and the geometrical dimensions of the shell.

The K_I due to the applied axial tension load is

$$K_t = \sigma_t/\overline{\pi R\theta}\ F_t \tag{3-3}$$

where F_t depends upon the same parameters as F_m. The function F_t can be derived

from the recent work of Erdogan and Delale[16]. FPDC has developed its own approximate, but conservative, expression for F_t which was used in this study. σ_t is the stress (tension) due to the axial load F

$$\sigma_t = F/(2\pi Rt) \tag{3-4}$$

Similar to the tension loading case, FPDC had previously developed an estimate of K for the externally applied bending load; and the K due to this loading is

$$K_b = \sigma_b/\overline{\pi R\tau}\ F_b \tag{3-5}$$

where F_b is a correction factor for a circumferential crack in a shell subjected to a bending load. σ_b is the maximum bending stress due to the external moment, M,

$$\sigma_b = M/Z \tag{3-6}$$

where Z is the elastic section modulus. The total K_I due to these three types of loading is

$$K_I = K_m + K_t + K_b \tag{3-7}$$

Equations (3-7) and (3-1), when combined together, give the functional form for J_{app}.

3-1.2 Longitudinal Cracks

The computation of crack stability for longitudinal flaws is based on plastic zone corrected stress-intensity factor solutions. For a longitudinal through crack in a pipe or vessel

$$K = S_h/\sqrt{\pi c}\ F(\lambda) \tag{3-8}$$

where S_h is the hoop stress, c is half the crack length, $\lambda=c//\sqrt{Rt}$ and the shell correction term $F(\lambda)=(1.+\ 1.25\lambda^2)^{.5}$. J_{app} can be found as before from Equation (3-1).

3-1.3 Tearing Stability for SSY Conditions

The form for T_{app} can be found by differentiating the equation for J_{app}, following Equation (3-1) and (3-7) or (3-8), with respect to crack length, giving

$$T_{app} = \frac{dJ_{app}}{da}\frac{E}{\sigma_o^2} \tag{3-9}$$

Then, using Equations (2-2) through (2-4), the stability of the crack can be determined.

3-1.4 Plastic Zone Instability Failure

Vasquez and Paris [20] have shown that situations exist in which the gradient with respect to the crack size of the elastic stress field at the tip of the crack becomes sufficiently large that the plastic zone cannot maintain stable static equilibrium and plastic zone instability occurs, followed by the propagation (or unstable extension) of the crack. This mode of unstable extension is called a "plastic zone instability failure" (or PZIF). The functional form of the PZIF criterion is given by

$$K^2_{pzif} = 2\pi\sigma_o^2 c_{eff}/P_z \tag{3-10}$$

where $P_z=1+2\lambda F'/F$, and c_{eff}, λ and $F(\lambda)$ are the plastic zone corrected terms described in Equation (3-8).

Section 4

STRESS ANALYSIS

Performance of fatigue crack growth analysis requires the determination of the stresses associated with the various transients shown in Table 4-1. As these transients have both thermal and pressure components, both thermal stress analyses and detailed pressure stresses must be determined.

4-1 PRESSURE STRESS ANALYSIS

In order to develop detailed stresses through-the-wall of the steam generator at the girth weld, it was necessary to perform a finite element stress analysis. The PAFEC 75 computer program was used for these purposes.

4-1.1 Axisymmetric Idealization 2

The mesh used for the analysis is shown in Figure 4-1. Appropriate boundary conditions were used to accomodate the axisymmetric idealization using 8 noded isoparametric quadrilateral elements and the h-convergent [24] formulation. 1
Details of the girth weld region are shown in Figure 4-2, and the results for a unit pressure load of 1000 psi are shown in Figure 4-3. It is interesting to note that the axial stresses, σ_{zz}, are larger than the hoop components, $\sigma_{\theta\theta}$. To determine the increase in stress that would result from localized thinning due to grinding out circumferentially oriented cracks and not replacing the metal with weld filler metal, as shown schematically in Figure 4-4, the idealization shown in 1
Figure 4-5 was utilized. The details of the thinned girth weld region is shown in Figure 4-6. The thinning takes the form of a 4:1 blend ratio and with a minimum

through-wall thickness of 3 inches. This is contrasted with the thickness in Figure 4-2 which is 3.5 inches at the girth weld. The results for the stress analysis, with a unit pressure load of 1000 psi and local thinning, are shown in Figure 4-7. Again, the axial component is noted to be larger than the hoop component. 1

4-1.2 P-Convergent 3-d Idealization

For the case of local longitudinal thinning, as shown schematicaly in Figure 4-8, a 3-d analytical approach is required. 2

The finite element model shown in Figure 4-9 consisted of 200 p-convergent type elements, using 3 elements through the thickness. In the area of interest, that is, the notch due to local thinning, p=3 and p=2 elsewhere. The portion modelled consisted of an 8 degree sector, extending 15 inches above the girth weld to 14 inches below. The boundary conditions along the edges assumed radial symmetry. The notch was conservatively modelled as 8 x 1 inches with a taper along long edges only. A single cubic (p=3) wedge was used for the taper. A prior analysis of vessel had been performed using axisymmetric shell elements. The stresses from this shell analysis were used to give surface traction loading at top and bottom of 3-d model. A single restraint was applied in axial direction. The applied load and the internal pressure of 1000 psi were self-equilibrating. The results of the 3-d stress analysis, for cases with and without local longitudinal thinning under unit pressure loading of 1000 psi, are shown in Figure 4-10. 2 2

4-2 THERMAL STRESS ANALYSIS

Table 4-1 is taken from the original Westinghouse design stress analysis [14]. It is noted in Table 4-1 that the hot-standby transient (HSB) has initial and final temperatures of 547 and 70F. This represents the temperature range at the thermal sleeve in the feedwater nozzle. Because of the large thermal stresses that would result from this large temperature variation if it were applicable to the girth weld, it was necessary to examine the thermal response in more detail. A heat transfer analysis was performed assuming that 70F feedwater was introduced into saturated steam-water at 547F. A plan view of the feedwater ring is shown in Figure 4-11. The small circles around the feedwater ring indicate J-tubes from which the feedwater enters the generator. It is the flow of this 70F water through the J-tubes into the generator and subsequent mixing with the 547F water (or steam) that will determine the magnitude of the thermal stresses. Details of this analysis are included in Appendix C. It was determined that the actual thermal response within the generator causes a temperature change from 547F at the beginning of feedwater flow to a minimum temperature of 517F prior to reaching equilibrium. Thus, the thermal response shown in Table 4-1 is correct for the feedwater nozzle but is unduly conservative for the girth weld. Accordingly, it was modified to reflect the actual response developed in Appendix C.

There are many load cases shown in Table 4-1. Rather than perform heat transfer calculations and associated thermal stress analysis for all conditions, it was determined that it would be simpler to conservatively bound the thermal responses. Accordingly, bounding is accomplished by selecting three cases. The cases selected were the heat-up cool-down transient (HU/CD), the loss of secondary pressure with return to power (LSPr), and the hot-standby (HSB). The idealization

of these transients that was used for computational purposes is listed in Table 4-3. This methodology is considered conservative in all cases.

The thermal stresses were computed using the properties shown in Table 4-2. The PAFEC 75 program was used to determine the thermal response and stresses. The axisymmetric idealization of Figure 4-1 was used for the computation. Eight-node isoparametric elements were used throughout as with Section 4-1.1. The outside of the generator was assumed insulated and the inside heated or cooled by convection according to the rates Table 4-3. 2

4-3 WELD RESIDUAL STRESSES

In order to be conservative in the analysis, weld residual stresses were assumed to be present after PWHT (Section 4-6) and were included in the analysis. 2 The estimate relies on the methodology of Ferril, Juhl and Miller [13]. The computation of the weld residual stress follows from the equation

$$\sigma(x) = \sigma_y(.12 - .72x + .72x^2)$$

where $x = a/t$ is the normalized wall position and σ_y = yield stress of the 2 material at the temperature at 400F. The idealization shown in the above equation is valid for a double-vee type of weld. Although the weld procedure for original manufacture of the vessel is for a single-vee, the presence of the repair weld[19] suggests the double-vee is a more reasonable approximation.

4-4 CRACK SURFACE PRESSURE

The proper computation of stress intensity factors, which is the purpose for performing these stress analyses, requires including the contribution due to crack

surface pressure (CSP). Crack surface pressure contributions to total stress are included only for cracks on the ID of the SG which are exposed to water or steam. It is not included for imbedded cracks or cracks in the OD.

4-5 COMBINATION OF STRESSES

The stresses determined in the preceding sections must be combined in order to get total stresses through-the-wall of the vessel. A typical case is shown in Figure 4-12. It is noted that the pressure stress, thermal stress, weld residual stress, and crack surface pressure are included in the summation to obtain a total stress that varies through-the-wall of the vessel. 2

Upon review of stresses, pressures and temperatures in the complete analytical load spectrum of Table 4-1, it was noted that the pressure variations of many of the transients can be bounded as was shown for thermal transients in Section 4-2. Thus, the analysis is simplified to that shown in Table 4-3. Most of the transients from Table 4-1 can be bounded by either the Group 1A or Group 1B analysis transient. The remaining transients, which are considered separately, are the HSB, LSP, HU/CD, and hydrotest. Table 4-1 indicates a hydrotest pressure equal to design pressure, p_{des}. Conservatively, the crack growth predictions are performed using a hydrotest pressure equal to 1.25 p_{des}. 2

Figures 4-13 through 4-17 show the maximum and minimum axial stress excursions associated with the foregoing six transients for the case of no thinning due to grinding. From these maximums and minimums, the stress ranges to be used for computing the stress intensity factor range in the subsequent fatigue crack growth analysis are computed. Three other sets of stress ranges are compiled similar to Figure 4-13 through 4-17. They are: axial stress with local 2

thinning, hoop stress with no local thinning and hoop stress with local thinning. The axial stresses are then used for the analysis of circumferentially oriented cracks and the hoop stresses for longitudinally oriented cracks.

4-6 PWHT STRESS ANALYSIS

The localized heating associated with the post-weld heat transient (PWHT) or stress-relief procedure is such that the rather sizeable thermal gradients might cause thermal stresses. These thermal stresses could, in turn, result in local yielding due either to their magnitude or to the reduction in yield stress at elevated temperature.

Accordingly, a finite element analysis was performed to determine the thermal stresses associated with the PWHT procedure. This also involved determining the thermal response or heat-transfer characteristics of the generator during the PWHT. 2

Based on preliminary calculations, it was determined that the heat-up and cool-down rates were slow enough that they could be approximated by the steady-state temperatures of the wall. The idealization shown in Figure 4-10 was used to determine the steady-state temperature distribution. Then, the methods used in Section 4-2 were followed to compute thermal stress. Based on assumed average material properties at 600F, the PWHT stresses were determined.

Table 4-1 Design Transients, IP 3 Steam Generators

TRANS	N_i	T_1	T_2	ΔT	T_{ave}	P_1	P_2	ΔP
HU/CD	200	100	547	±447	324	0	1005	1005
LOAD/UNLOAD	29200	547	513.8	±33.2	530.4	1005	769.8	±235.2
R. TRIP	400	513.5	545	+31.5	529	1003	769	234
LOSS OF LOAD	80	513.8	545	+31.2	529	1003	769	234
POWER BLACKOUT	10	547	70	-477	309	1005	0	1005
LOSS OF FLOW	80	547	513.8	32.2	530	1003	792	211
LSPr/with RTP*	6	513	205	308	359	764	12	-752
LSPr/no RTP*	6	513	240	273	376.5	764	25	-739
+10% STEP	2000	501.5	517.5	+16	509.5	690	795	+105
-10% STEP	2000	528.8	513.5	-15.3	521.2	876	768	-108
+20% STEP	2000	510	520	+10	515	744	812	+68
-20% STEP	2000	527	517	-10	522	870	792	-78
100% → 60% STEP	200	530	513	-17	521.5	885	764	-121
50% → 0% STEP	200	528	545	+17	536.5	1003	870	-133
100% → 0% STEP	80	527	545	+18	536	1003	873	-130
+5% STEP	2000	517.5	507.5	-10	512.5	728	795	+67
-5% STEP	2000	515	526	+11	520.5	855	778	-77
HSB	25000	547	70	-477	309	1005	0	-1005
HYDROTEST	50	70	70	0	70	0	1085	+1085

* LSPr = Loss of Secondary Pressure, RTP = Return to Power

Table 4-2 Material Properties, Thermal Stress Analysis

Temps (F)	k (Btu/hr-ft²-F)	a (ft²/hr)	ρ (lb/ft³)	$\alpha x10^{-6}$ (/F)	$Ex10^{6}$ (psi)
70	31.5	.5692	489	6.07	29.9
100	31.0	.5509	-	6.20	—
200	30.0	.5246	-	6.67	29.5
300	29.1	.4928	-	7.10	29.0
400	28.1	.4616	-	7.54	28.3
500	27.2	.4338	-	7.96	27.4
550	26.7	.4198	-	8.16	—
600	26.2	.4061	484	8.35	26.7

Table 4-3 Spectrum for Fatigue Crack Growth Analysis

TRANSIENT	N(cycles)	T_1(F)	T_2(F)	P_1(psi)	P_2(psi)
GRP1b[1]	29760	550	517	1005	764
GRP1b[1]	12480	550	517	1005	870
HSB[1]	25010	550	517	1005	764
LSPr[2]	12	550	205	764	12
HU/CD[3]	200	70	550	0	0
Hydro	50	70	70	0	1356

(1) THERMAL TRANSIENT; T_1 to T_2 in 1 sec; H = 90.5 BTU/HR-FT-F

(2) LSPr TRANSIENT; T_1 to T_2 in sec; H = 500.0 BTU/HR-FT-F

(3) HU/CD TRANSIENT; T_1 to T_2 100F/HR; H = 50.0 BTU/HR-FT-F

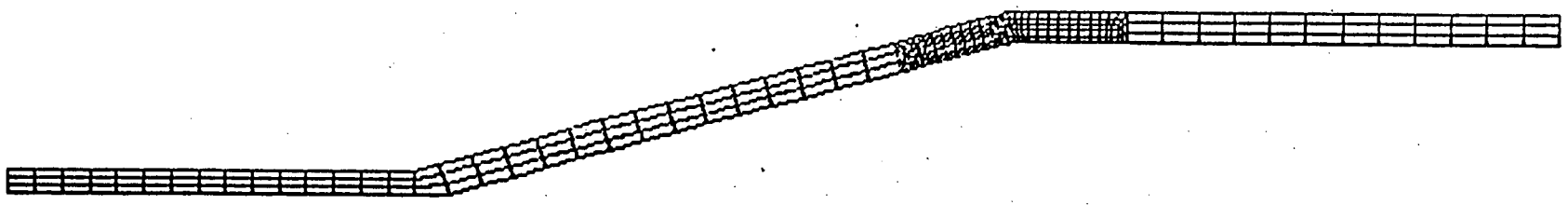

Figure 4-1 Finite Element Idealization of SG Girth Weld Region

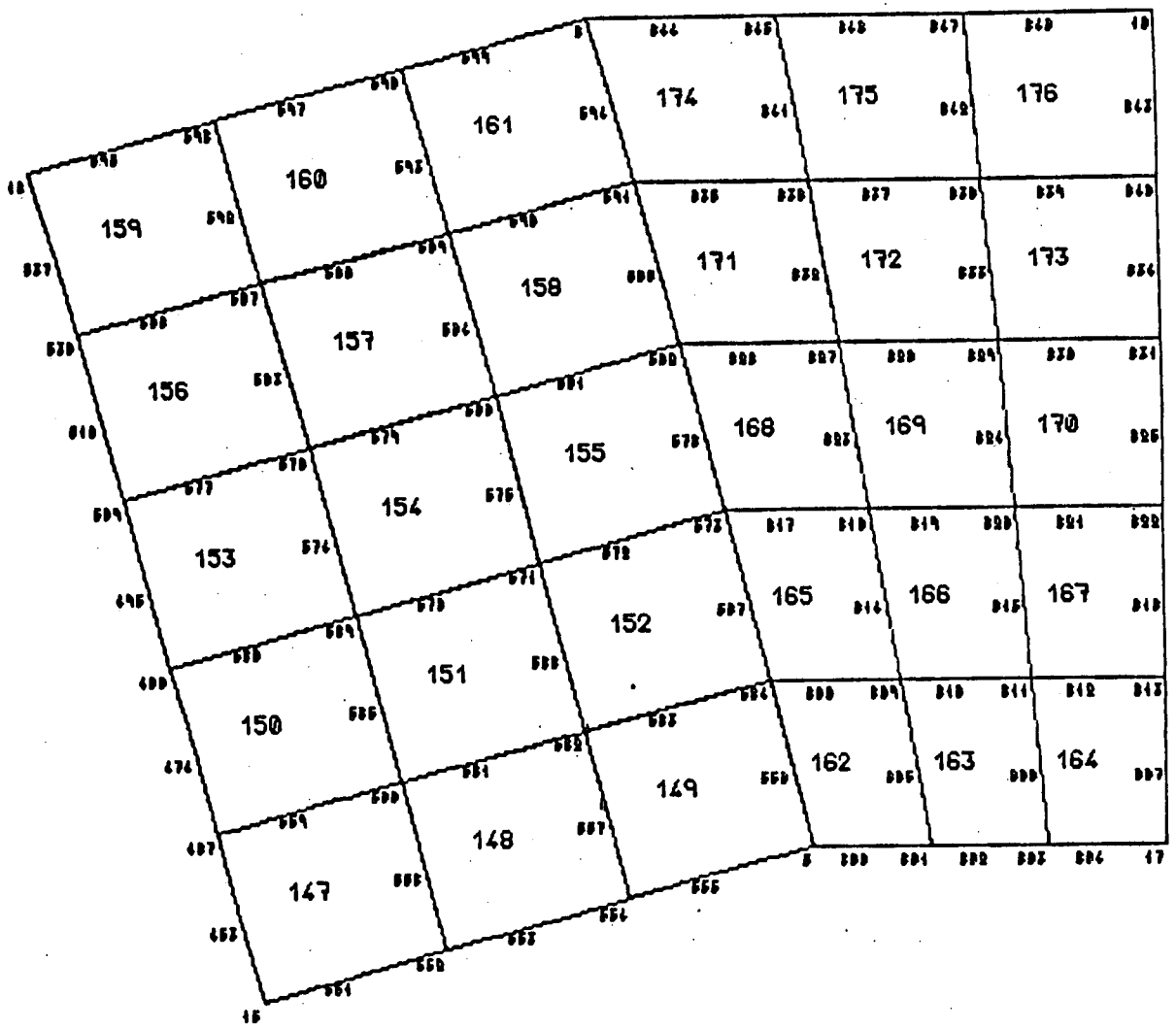

Figure 4-2 Detail of Girth Weld Region of Figure 4-1

Figure 4-3 Stresses for Girth Weld based on Figure 4-2 Idealization

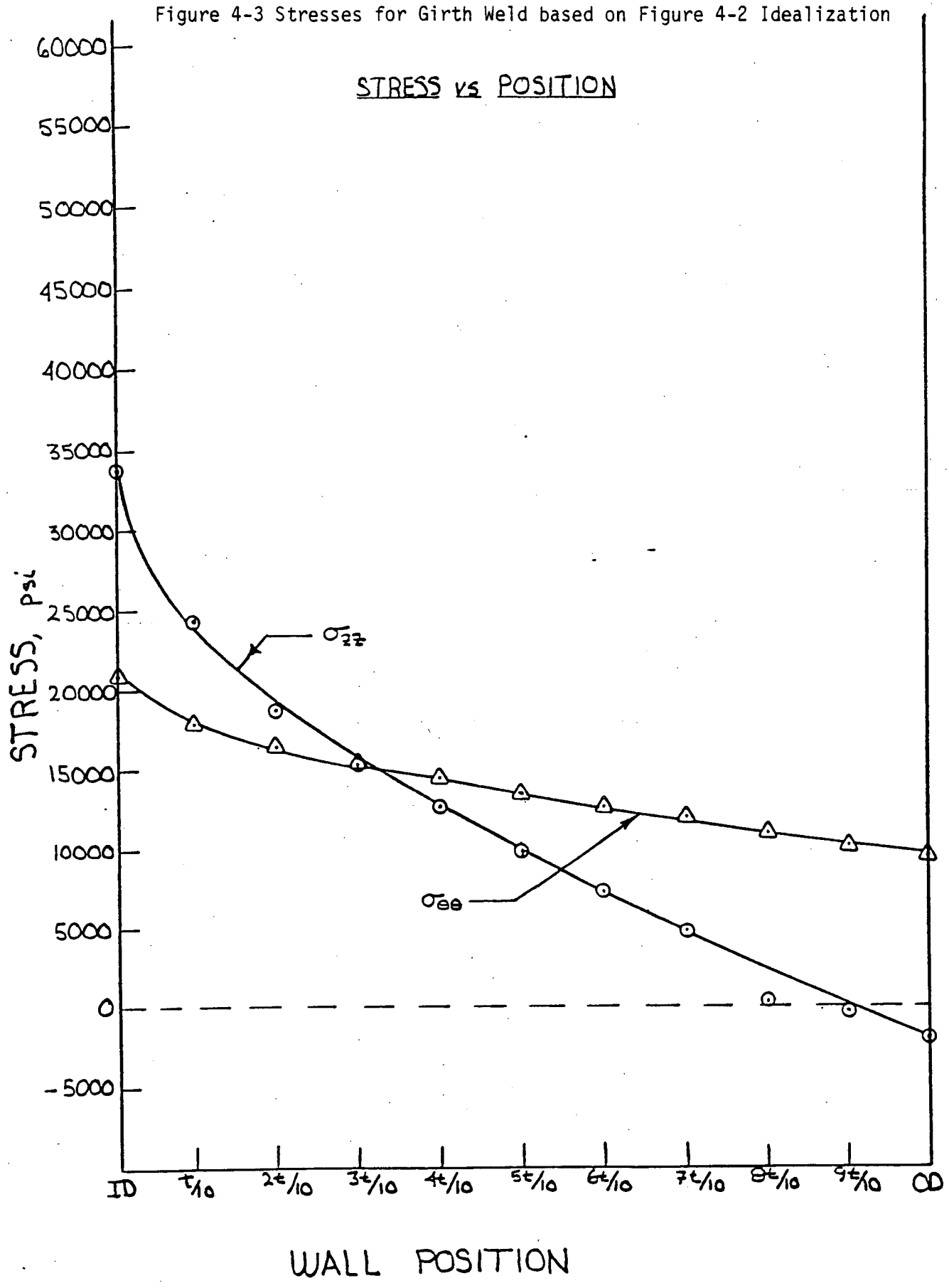

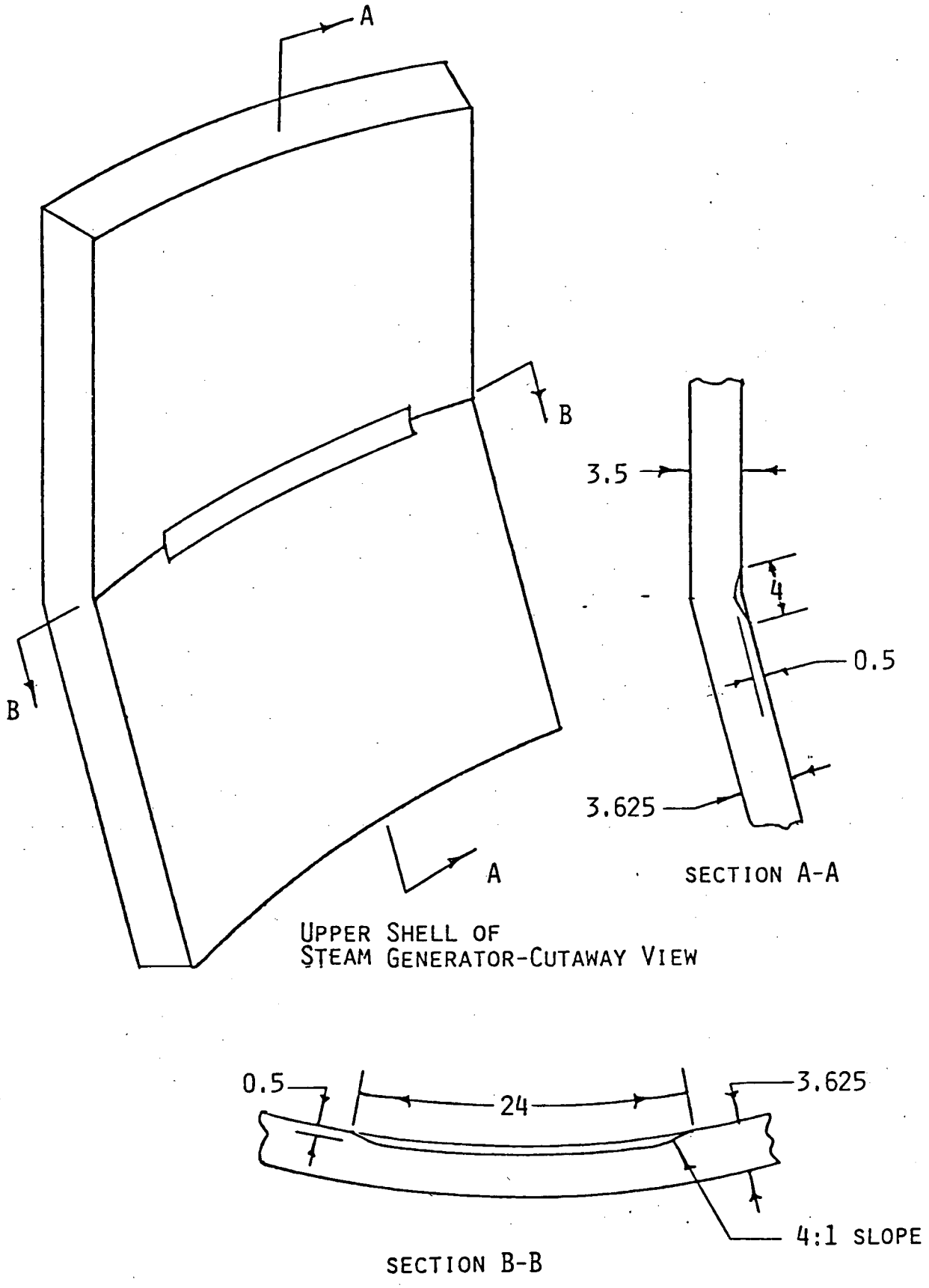
A
B
B
A
3.5
4
0.5
3.625
SECTION A-A
UPPER SHELL OF
STEAM GENERATOR-CUTAWAY VIEW
0.5
24
3.625
4:1 SLOPE
SECTION B-B

Figure 4-4

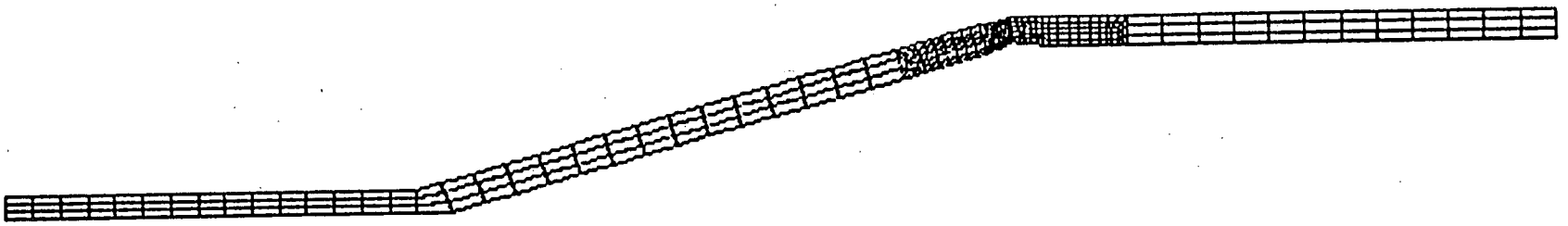

Figure 4-5 Finite Element Idealization of Local Thinning of SG Girth Weld Region

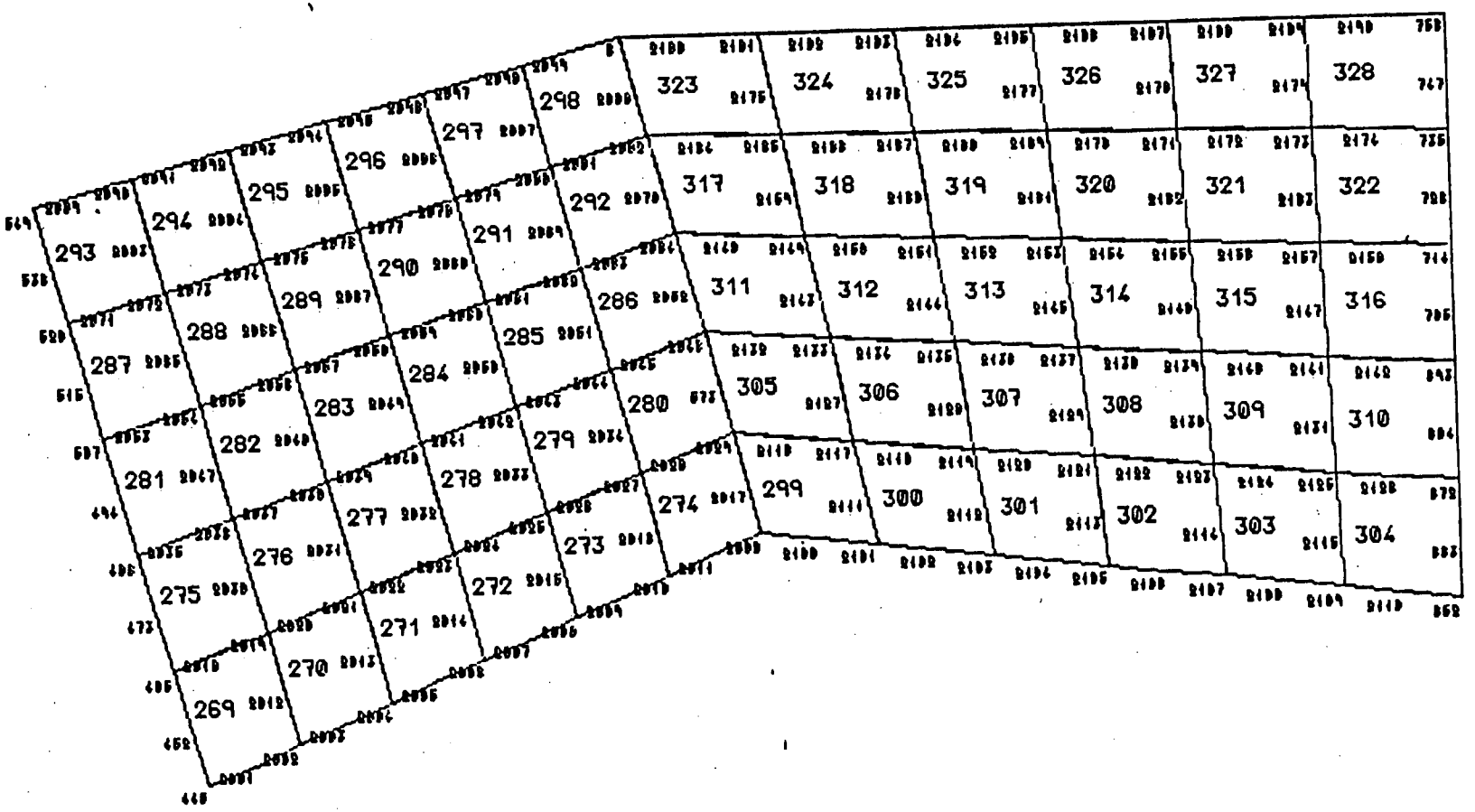

Figure 4-6 Detail of Girth Weld Region of Figure 4-5

Figure 4-7 Stresses for Girth Weld based on Figure 4-6 Idealization

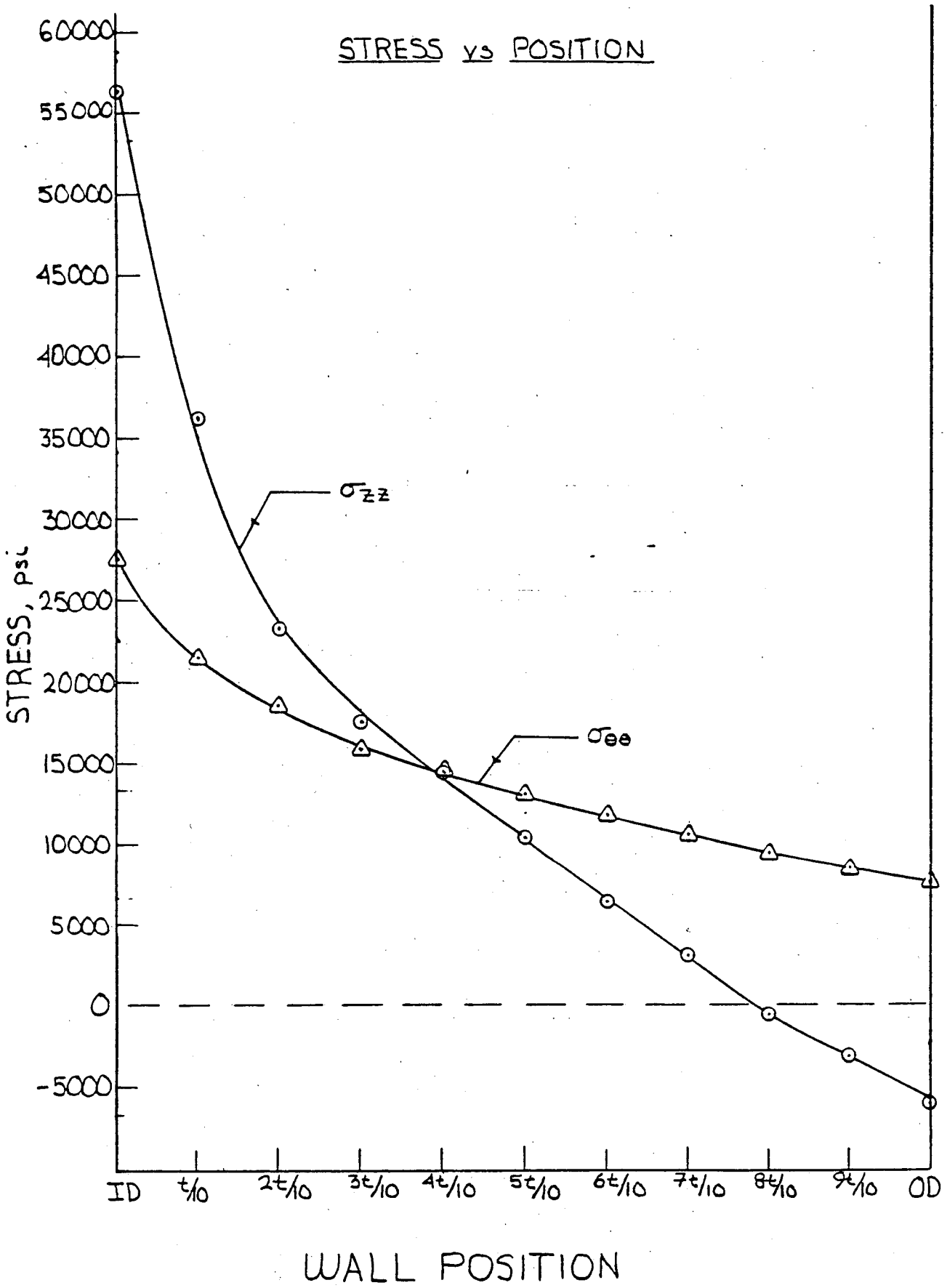

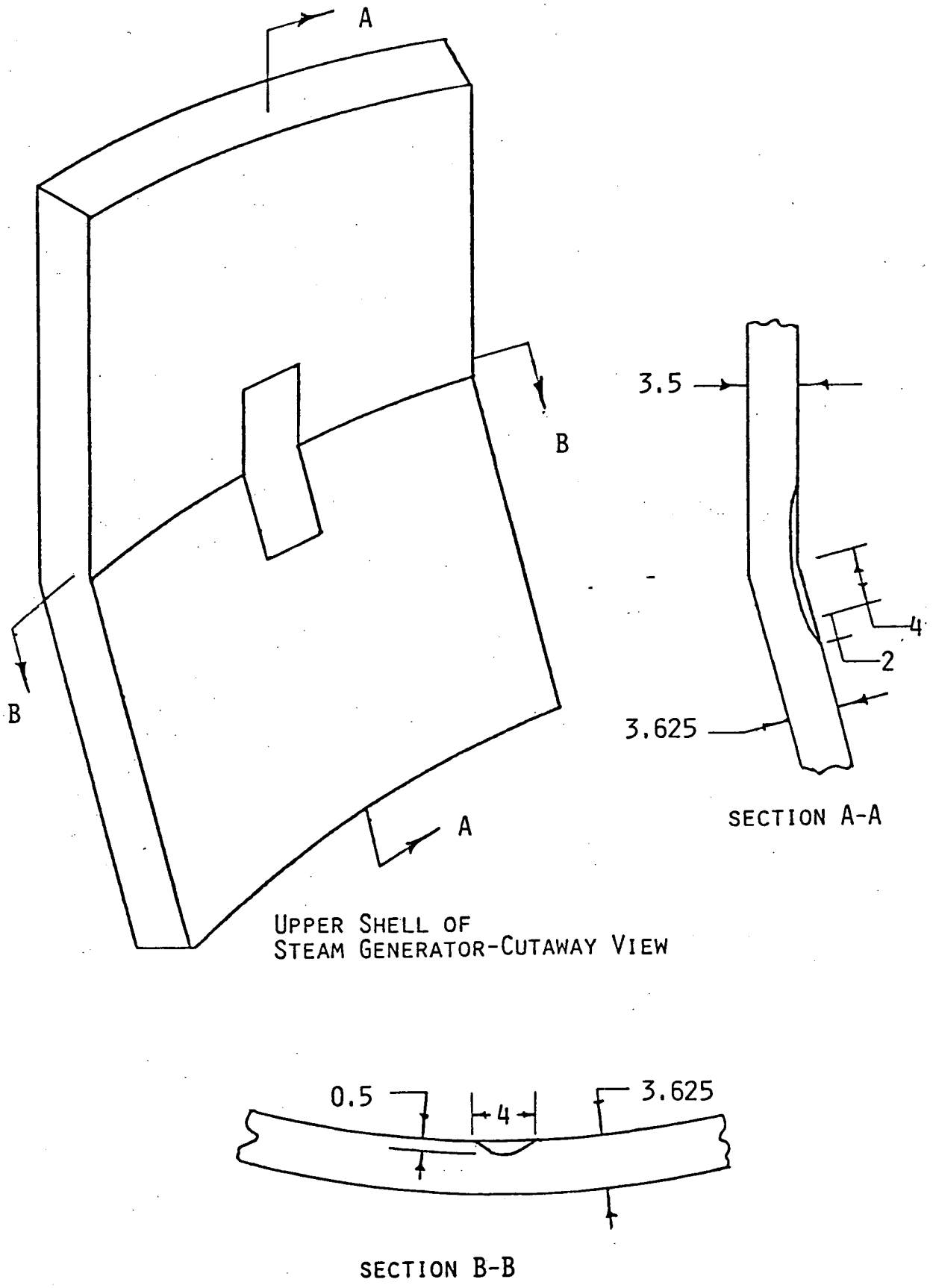

Fig. 4-8 Local Longitudinal Thinning

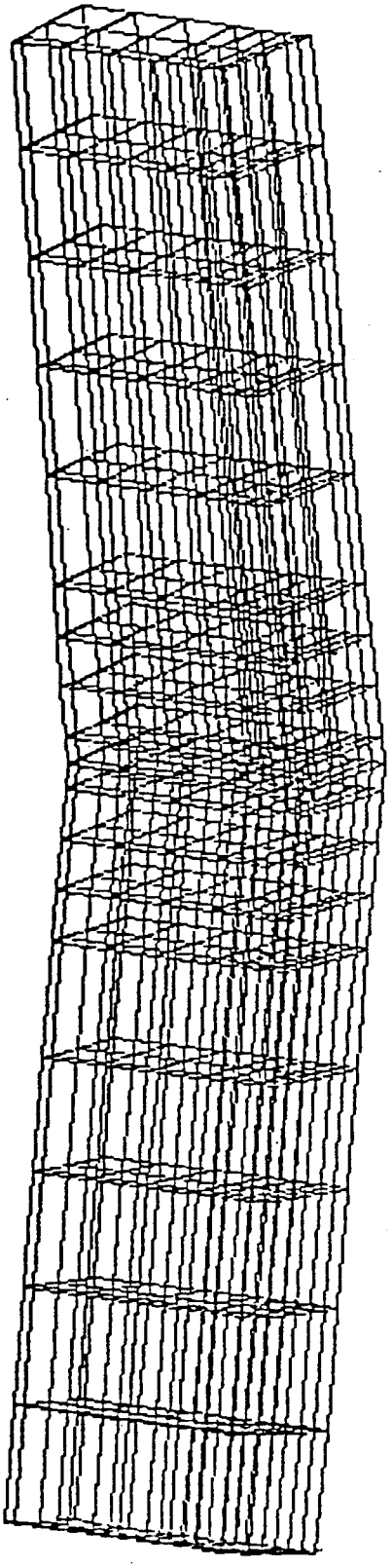

Fig. 4-9 3-d Idealization of Section Shown in Figure 4-8

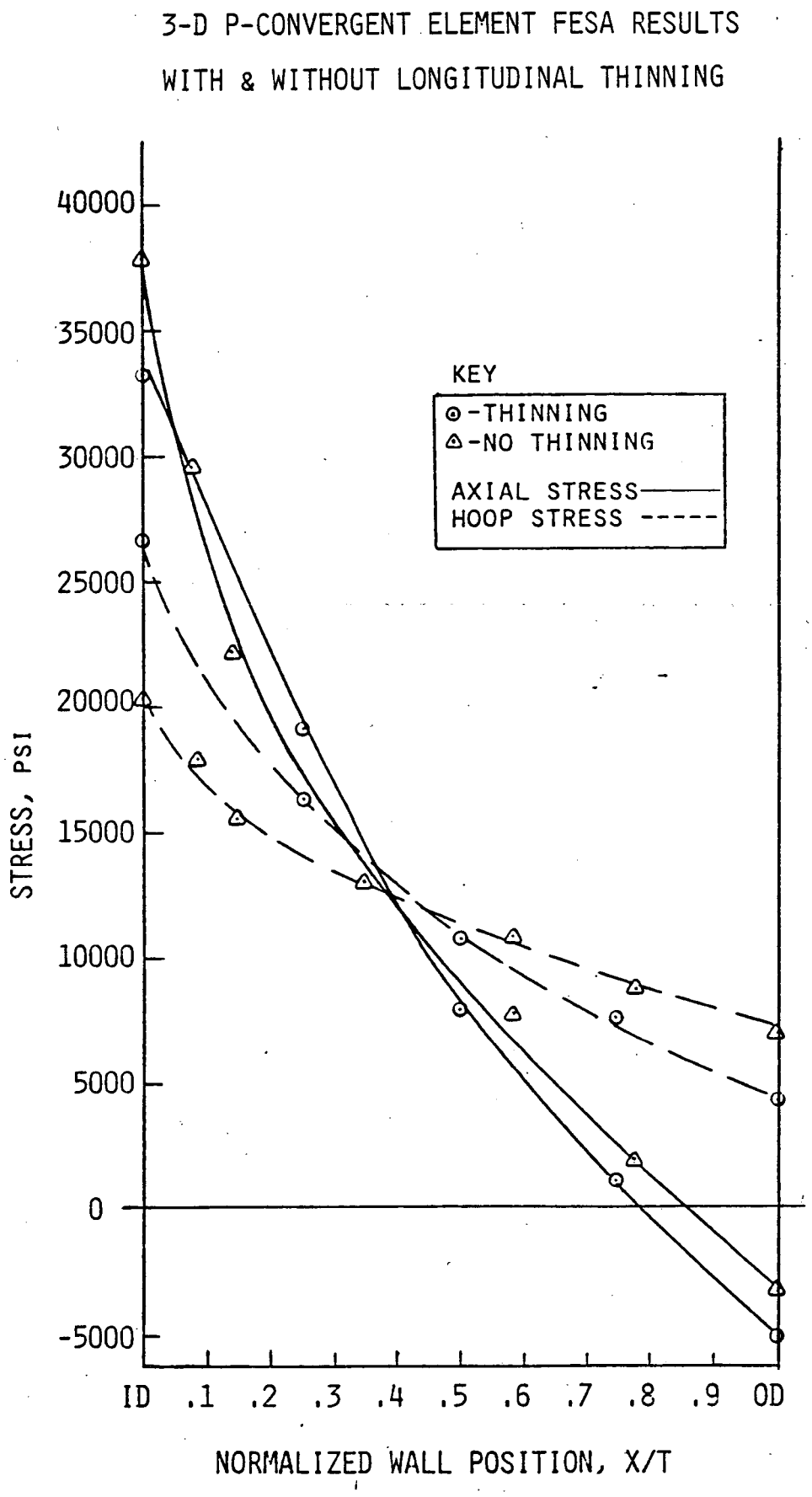

Fig. 4-10 Stresses from Idealization of Fig. 4-10, p=1000 psi

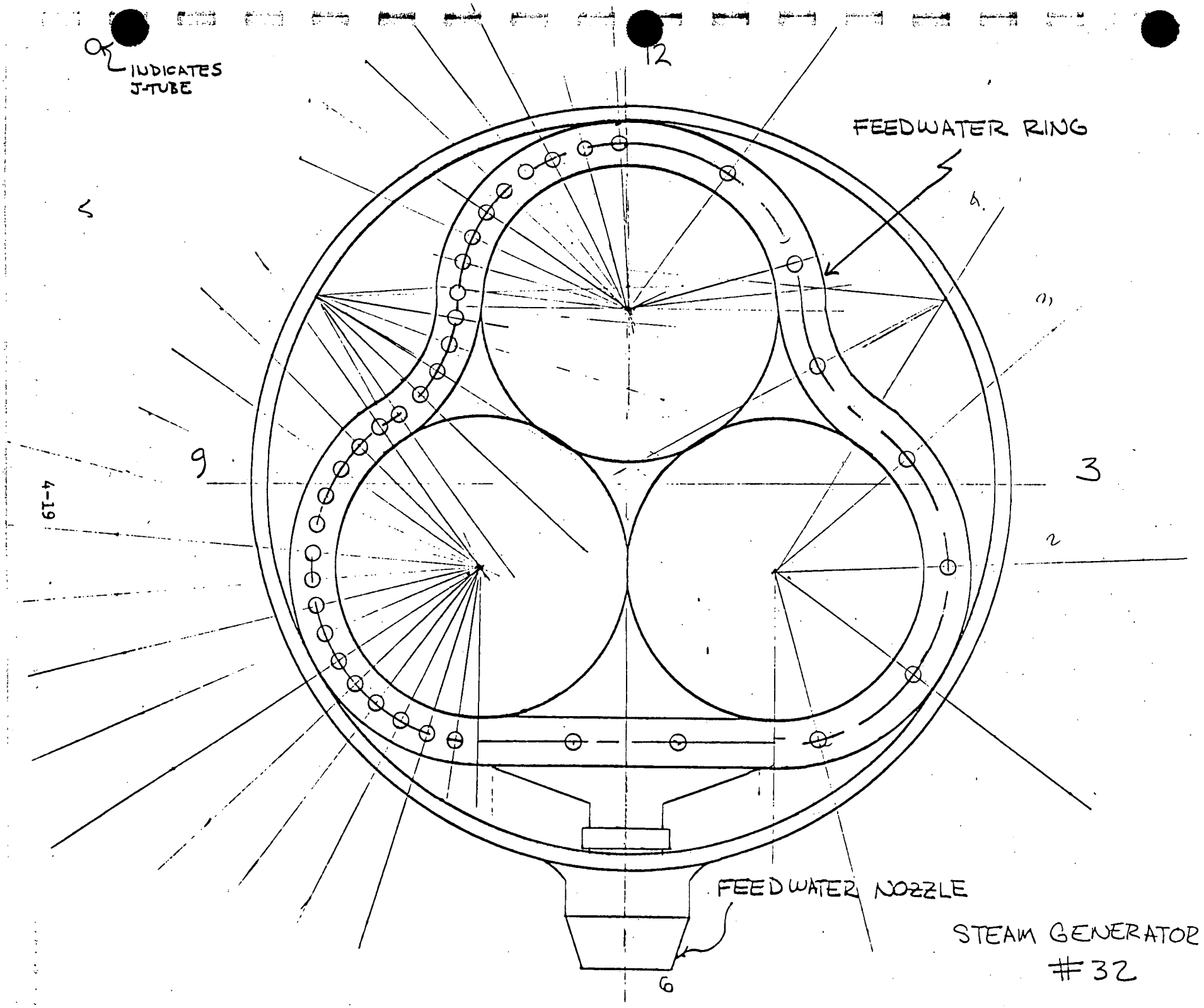

Figure 4-11 Plan view of SG Feedwater Ring

Figure 4-12 SUMMATION OF AXIAL STRESSES

(CIRCUMFERENTIAL CRACK)

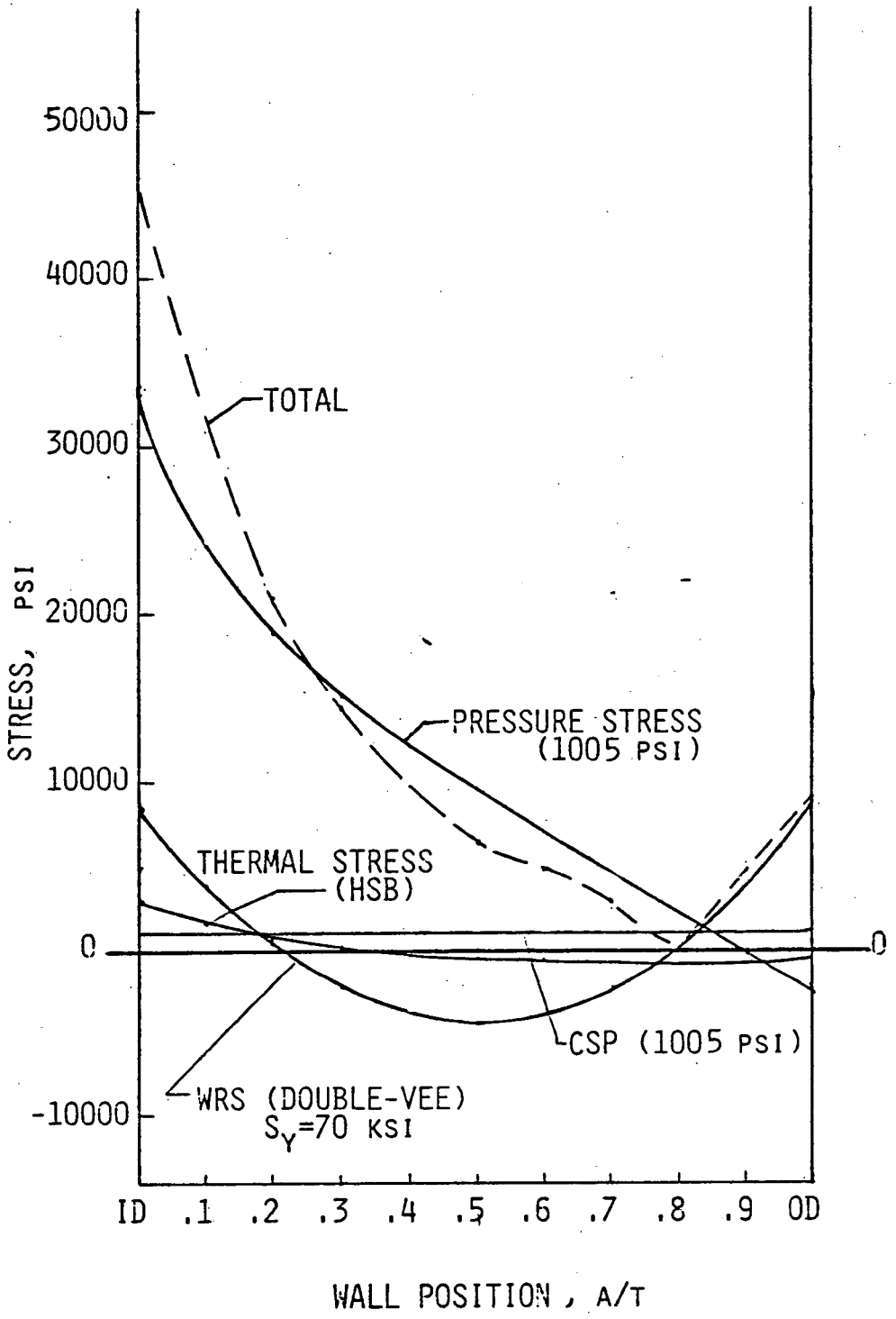

Figure 4-13 Combined Stresses, Circumferential Crack, No Thinning, GRP1a and HSB Transients

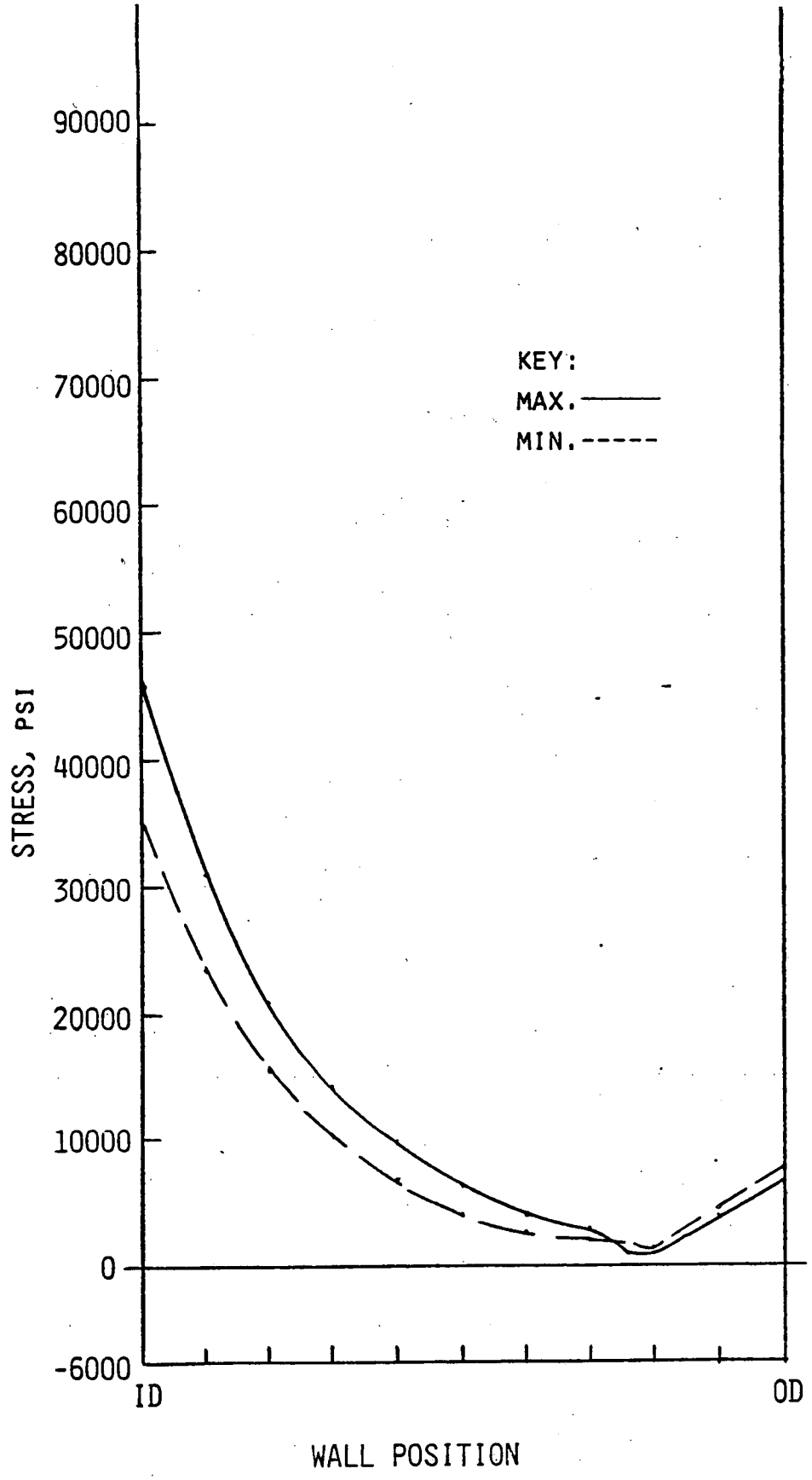

Figure 4-14 Combined Stresses, Circumferential Crack, No Thinning GRP1b Transient

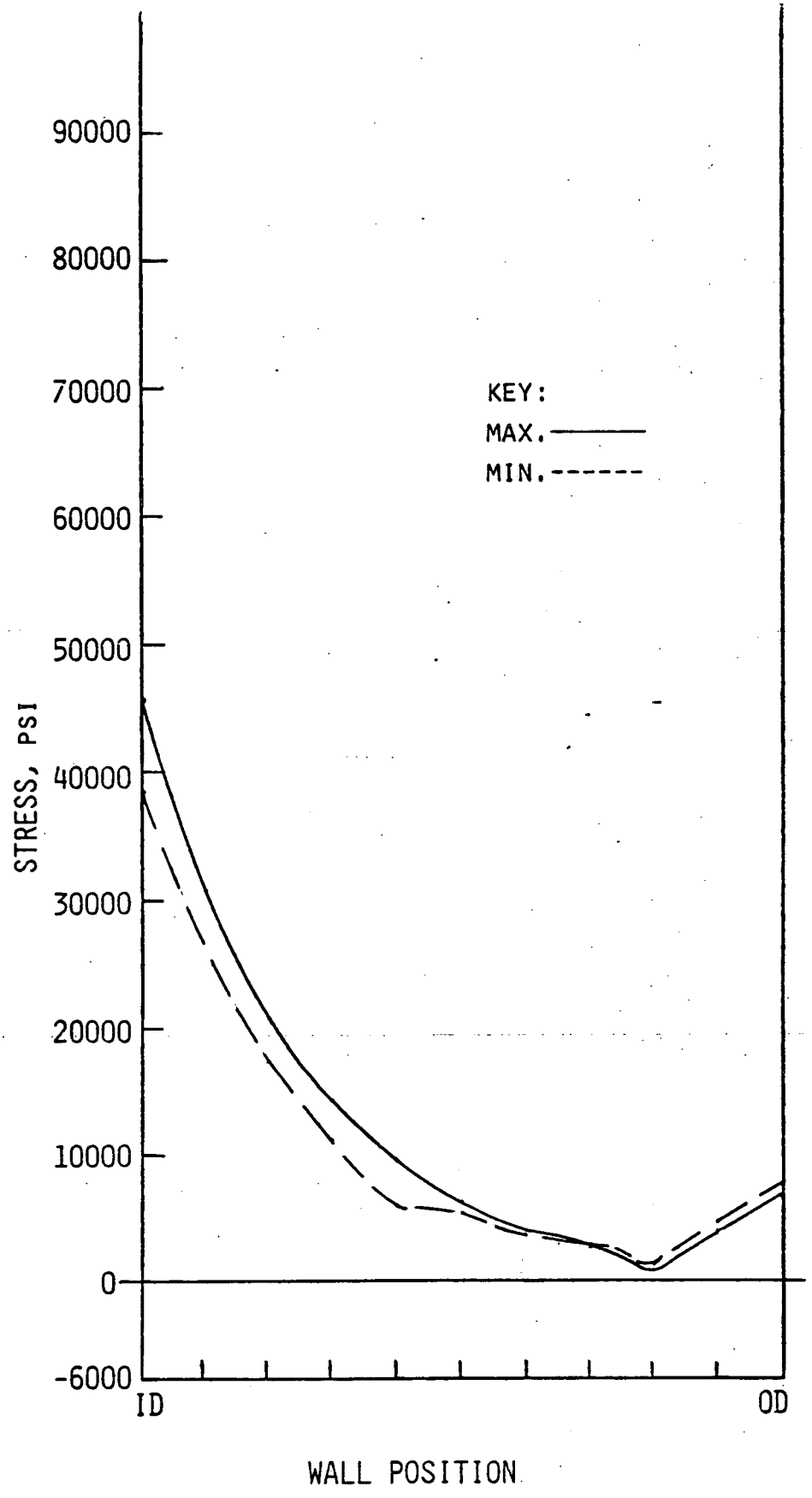

Figure 4-15 Combined Stresses, Circumferential Crack, No Thinning, LSPr Transient

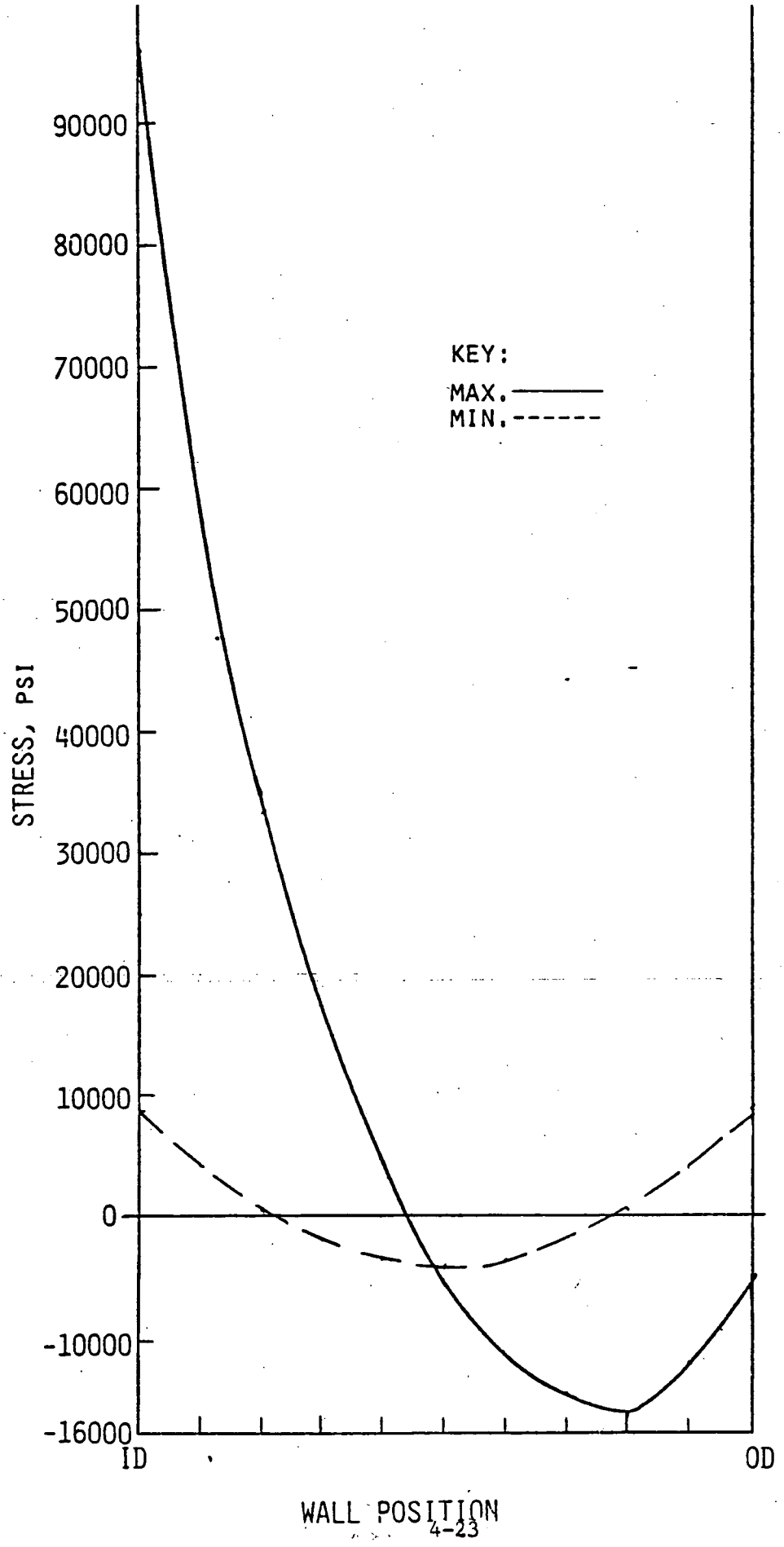

Figure 4-16 Combined Stresses, Circumferential Crack, No Thinning, HU/CD Transient

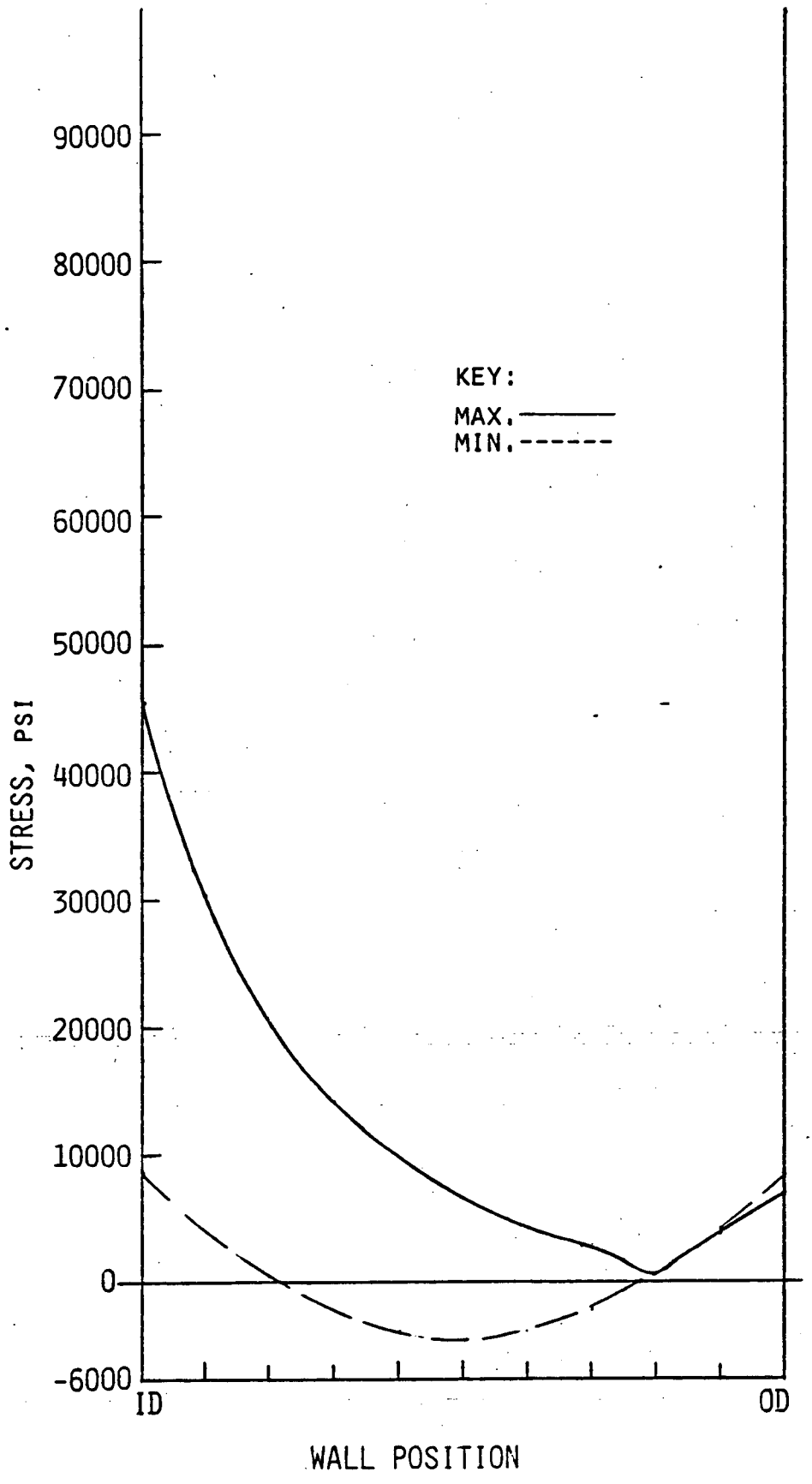

Figure 4-17 Combined Stresses, Circumferential Crack, No Thinning, Hydrotest Transient

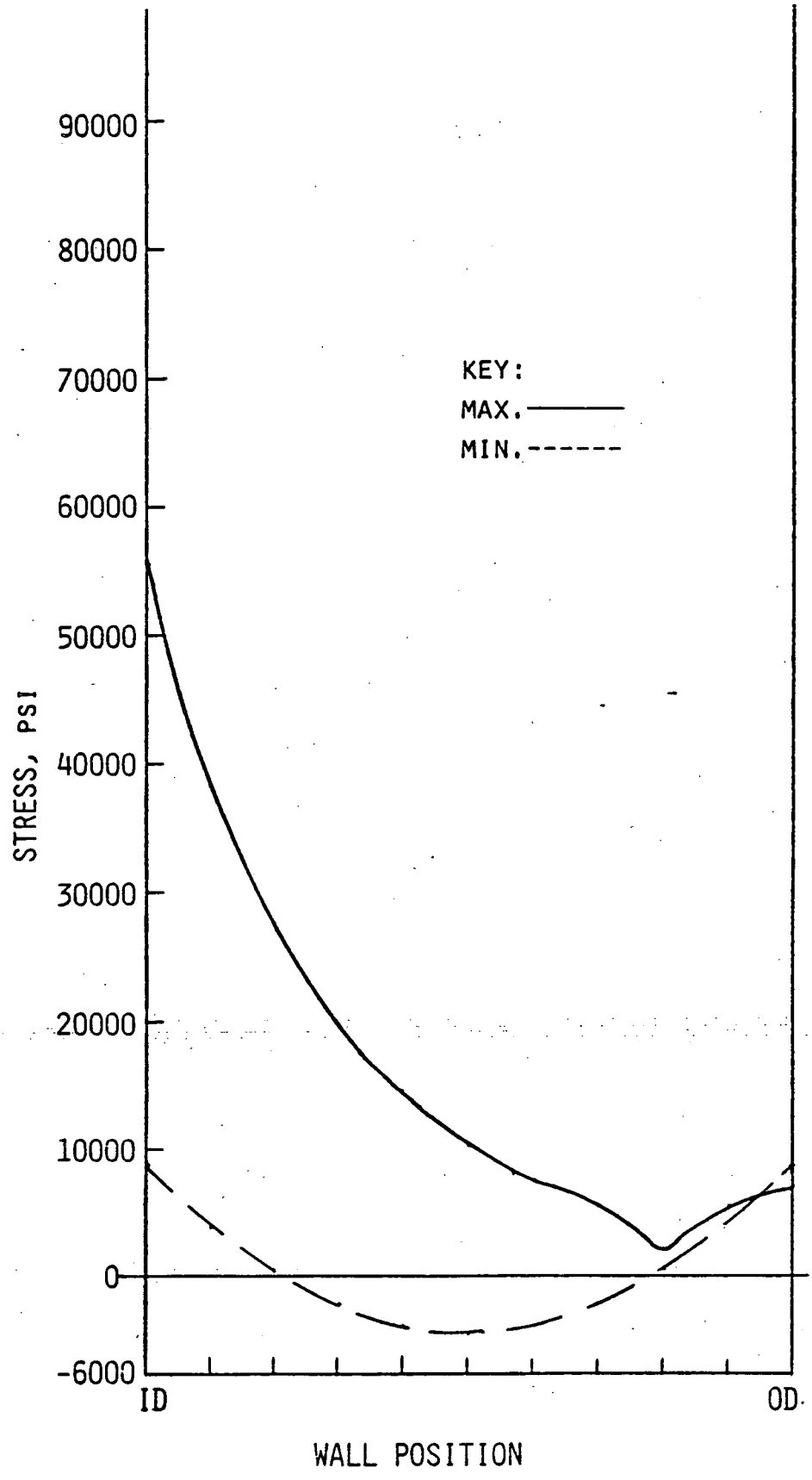

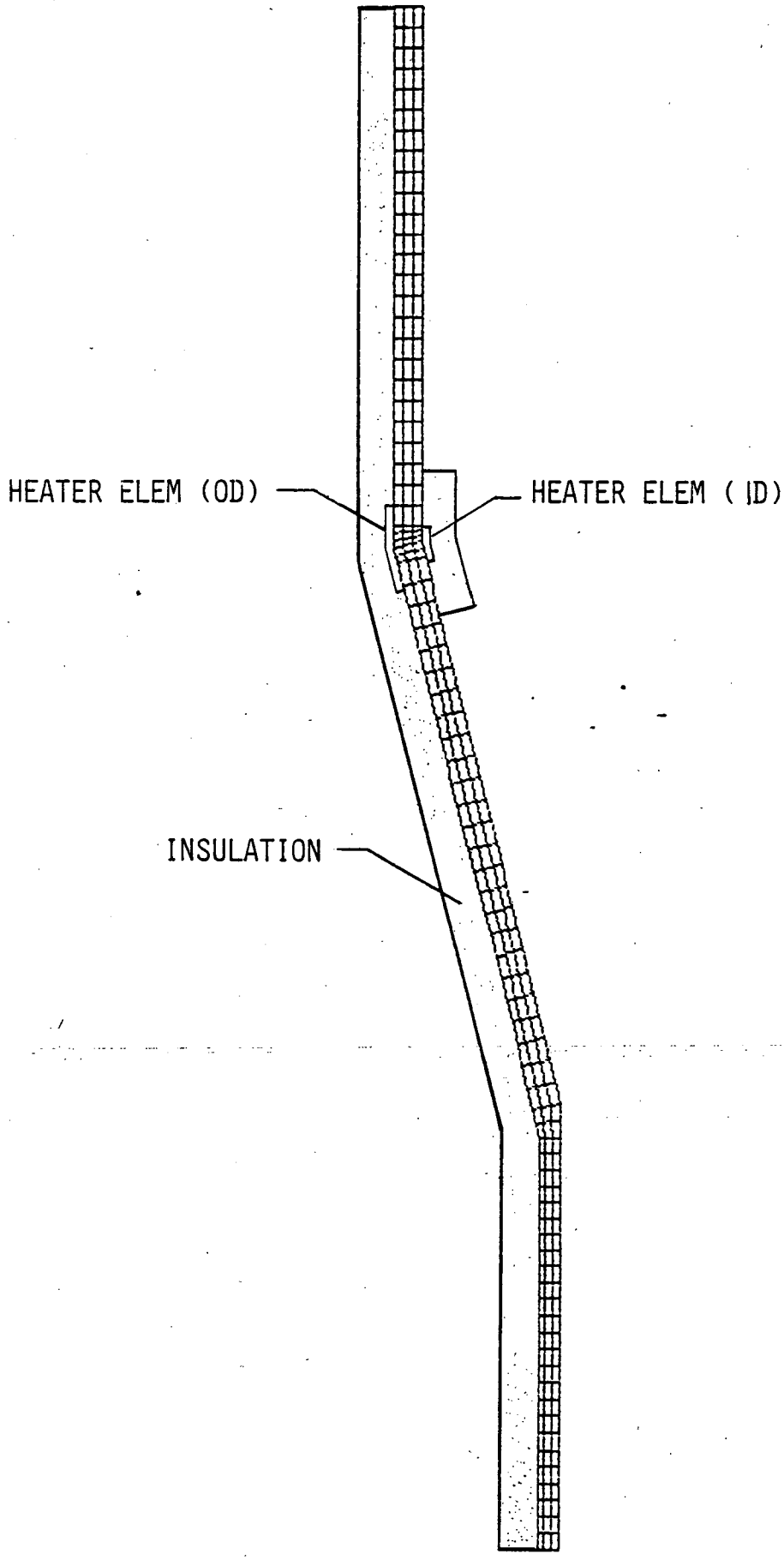

Fig. 4-18 Idealization for PWHT Thermal Analysis

Section 5

RESULTS

Fatigue crack growth computations, a generalized leak-before-break assessment and an evaluation of crack stability under pressurized thermal shock conditions were performed on the steam generator girth crack weld region and the results follow. 2

5-1 FATIGUE CRACK GROWTH

It is well known that the fatigue crack growth rate can be readily quantified in terms of stress intensity factor range ΔK. The ΔK parameter is determined using the computer program FPDSSM which also integrates the crack growth rate equation for specified material proprties. FPDSSM uses the slice synthesis method of determining stress intensity factors for an arbitrary stress gradient as more fully described in Appendix B. In the case of the steam generator, the stresses were determined based on a mapping of 77 stress points through the vessel wall. 1 This is shown schematically in Figure 5-1. Computation of crack growth rates under the spectrum of loads shown in Table 4-3 is accomplished by integrating a crack growth rate curve such as that shown in Figure 5-2. Figure 5-2 is taken from the 1974 ASME Section XI Code[12]. The growth rate curve for surface flaws in water reactor environment, as shown in Figure 5-2, was used for calculations. Based on an initial flaw aspect ratio of a/2c = 1/6 and the worst case stress, it was determined that the expected remaining life of the vessel with these typical postulated defects was between three and six times the design life. The aspect 2 ratio is adjusted after each increment of growth to account for variations in growth rate along the crack front. These results are shown in Table 5-1. It is noted that the generator design life is approximately 40 years.

5-2 LEAK-BEFORE-BREAK

Leak-before-break (lbb) logic is based upon the determination of the size of crack that produces a detectable leak under normal operating conditions. This is followed by demonstration that this size crack is stable under faulted conditions. 1

5-2.1 Material Properties

Because leak-before-break analyses are dependent on the fracture toughness and characteristic crack growth resistance curves, it is necessary to summarize the data contained in Appendix A. Material property curves are shown in Figures 5-3 to 5-5. Figure 5-3 is representative of the test results in the form of J-Δa resistance curves for samples taken from the Indian Point steam generator. It is noted that the curves shown in Figure 5-3 are conservative lower bounds to the actual test data. The specimen identified as CWLDS is from another source and is included to show the effect of specimen size. The specimens taken from the steam generator weld girth region were of .5T-CT type specimens. This means that the thickness of the specimen was 0.5 inch and its nominal overall dimensions were slightly over 1.0 inch. In contrast, the CWLDS specimen has a thickness of 1.0 inch and has overal dimensions in excess of 2.5 inches. The effect of size is readily apparent in Figure 5-3. The J-Δa curves of Figure 5-3 can be used to construct a family of J-T curves of these materials. These results are shown in Figure 5-4. It is noted in Figures 5-3 and 5-4 that the minimum J-Δa and J-T curves are for specimen US2JS. This specimen represents upper shell material, A302B, at 500F. As it is the minimum, it is obvious that it is a conservative representation of the material and will be used for the stability calculations. J-T data for specimen US2JS is shown in Figure 5-5. 2

Recent methodology permits analytical accounting for the effect of specimen size, in terms of $\Delta a/b$, on J. This analytical representation is in terms of a parameter called J_{mod} and is due to Ernst [18]. The results of converting the deformation theory J to J_{mod} are shown in Figure 5-5. It is noted that the J_m-T_m results indicated by a star give higher values for resistance to tearing. These are included for comparison. 2

5-2.2 Leak Rate Analysis

The estimate of the leak rate for various cracks was based upon the LEFM based methods given in Reference [17]. In general, the leak rate depends upon the applied stress and crack length. Thus, the calculation of leak rate necessitates the development of a fluid flow model for fluid leaking through a crack. It also requires consideration of the thermodynamics of the flow and the surface roughness of the crack. The simplest leak rate analysis[17] assumes that the opened area of the crack can be modeled as a rectangular slit of constant height. This idealization was used herein. 1

The typical presentation of the results of the leak-rate calculations is by a curve of leak rate vs. crack length, as shown in Figure 5-6. It is noted that the applied stress is a parameter. The higher the stress, the larger is the crack opening and the larger the corresponding leak rate. The estimated leak rate behavior for longitudinal and circumferential cracks under normal operating conditions, at the girth weld, is shown in Figure 5-6. These computations were performed using 'LKRATE'[17] and an estimated effective average membrane stress. 2

5-2.3 Crack Stability for LBB

1

Taking results from Figure 5-6, at leak rates of approximately 10 gpm, it is found that the corresponding circumferential crack, herein called $2c_{10}$, has a length of approximately 14 inches and the longitudinal crack has a length of approximately 10 inches. Then, following typical lbb logic, 2t is added to $2c_{10}$. Using the methodology developed in Section 3-1.1, the values for J can be computed for cracks of $2c_{10}$+2t and longer, and the results are shown in Figure 5-7 for the circumferential through-the-wall crack. For the case of the crack in Figure 5-7, should the value of J exceed J_{Ic}, then the tearing stability methodology of Section 3-1.3 is required. The results of such an approach are shown in Figure 5-8. For the case of a circumferential through-wall crack at a location with localized thinning, then the results in Figures 5-9 and 5-10 are applicable.

2

2

2

In the case of longitudinal cracks, the analytical methodology is slightly different than that for circumferential cracks. This was previously discussed in Section 3-1.2 and 3-1.4. The results of postulated longitudinal cracks are shown in Table 5-2.

5-3 PRESSURIZED THERMAL SHOCK

Under certain postulated accident conditions, operation of the steam generators could result in a low water level. This event is associated with an interruption of feedwater flow followed by introduction of auxiliary feedwater at 70F. The flow of auxiliary feedwater manifests itself as a jet of cold water impinging on the hot steam generator wall. In the limiting case, this can cause very large stresses and could cause crack instability should a large crack be present.

2

Crack stability calculations were conducted [21] under conditions of pressurized thermal shock and the results are presented in Figure 5-11. Details of this methodology are PROPRIETARY and only those persons authorized to have access to the referenced report [21] shall be privy to the methodology. 1

5-4 DISCUSSION

The stress analysis methods used for local thinning and circumferential orientation rely on an axisymmetric idealization. This approach results in stresses that are very conservative because the actual "notch" associated with the local thinning is limited to 20 inches in length. For the actual case, load transfer would occur and the stresses would be much lower and the stress-gradient through-the-wall, less steep.

Fatigue crack growth computations were based on the representative [12] data which is assumed to be that of the typical "water reactor environment" shown in Figure 5-2. This approach does not take into account any previous adulteration of the steam generator water chemistry. If good water chemistry control is maintained throughout the remaining operating life, this growth rate is valid. Should the water become contaminated, then these rates may be unconservative. 2

At present, fatigue crack growth tests are being performed using test specimens fabricated from material taken from the girth weld region. These tests are to be conducted in an environment that is typical of that expected to be present in the generator during its remaining service life. Results obtained therefrom shall be factored into this analysis in the form of an Addendum.

The development of estimates of leak rates for circumferential and longitudinal through-wall cracks is hampered by the complexity of determining general crack opening areas for complex shell geometries. Rather than undertake a large developmental effort, suitable estimates were made. These relied on limiting crack lengths to cracks having lengths over 5t and developing the concept of an "effective" membrane stress that produces the crack opening. In all cases, the estimation approach is conservative for cracks longer than 5t. 2

Table 5-1 Fatigue Crack Growth Results

a_i, in(1)	N, Lifetimes
.250	6^+
.875	3^+

(1) a/2c = 1/6, worst stress case

Table 5-2 Stability of Longitudinal Cracks

$\dot{Q}$, gpm(1)	2c(in)	2c + 2t,(in)	$J_{app}^{(2)}$, lb/in	J_{pzif}, lb/in
0.1	3.2	10.2	163	5579
1.0	6.5	13.5	234	6649
10.0	14.3	21.3	475	8387

(1) Based on 1000 psi

(2) Based on 1085 psi; $J = K^2(c+r_y)/E'$, $K = \sigma_h\sqrt{\pi c}\ F(\lambda)$

COMPUTE K USING 2-D MAP OF STRESS
S = S(X,Y), S(X,Y) IS HIGH ORDER POLY.

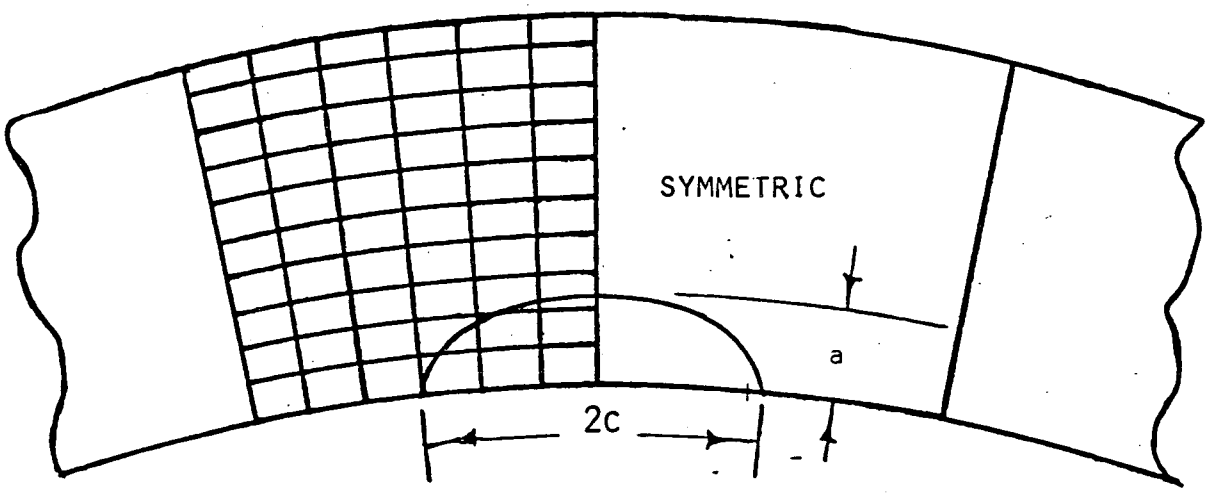

MAPPING USES:

11 POINTS THRU THICKNESS
7 POINTS CIRCUMFERENTIALLY

Fig. 5-1 Stress Mapping for FPDSSM K Computation

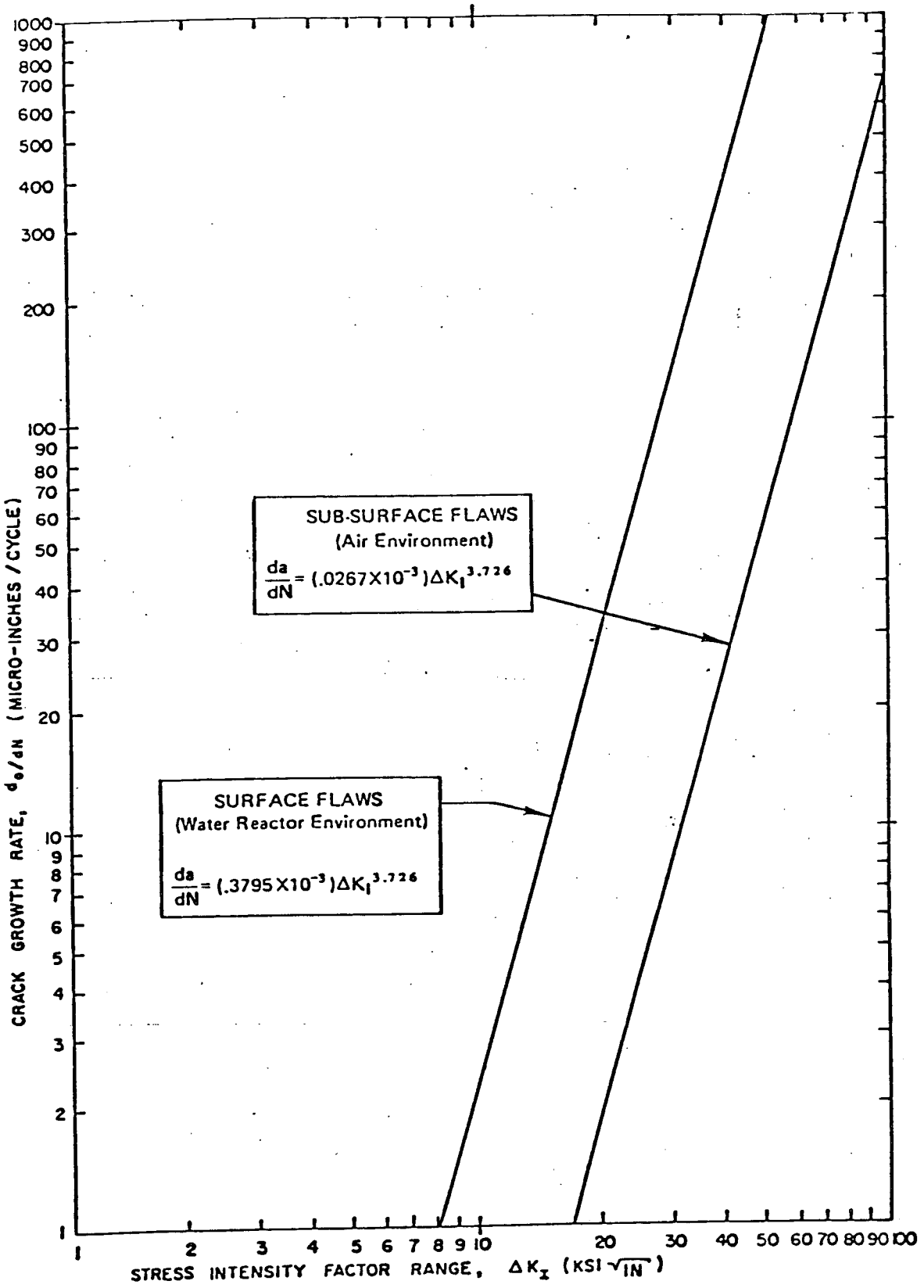

Fig. 5-2 UPPER BOUND FATIGUE CRACK GROWTH DATA FOR REACTOR VESSEL STEELS, Ref.[12]

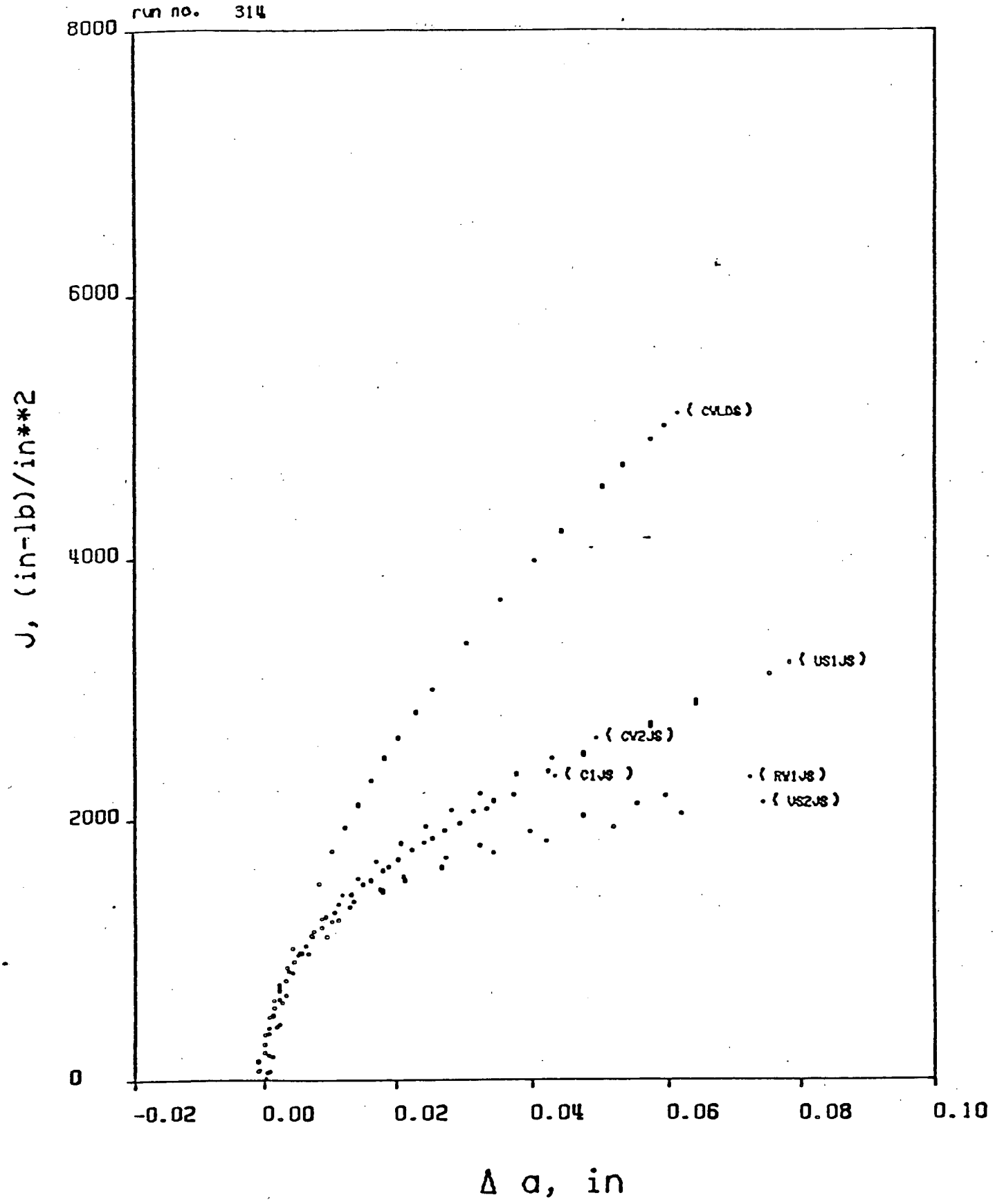

Fig. 5-3 IP3 SG J-Δa Test Results from Figure A-19

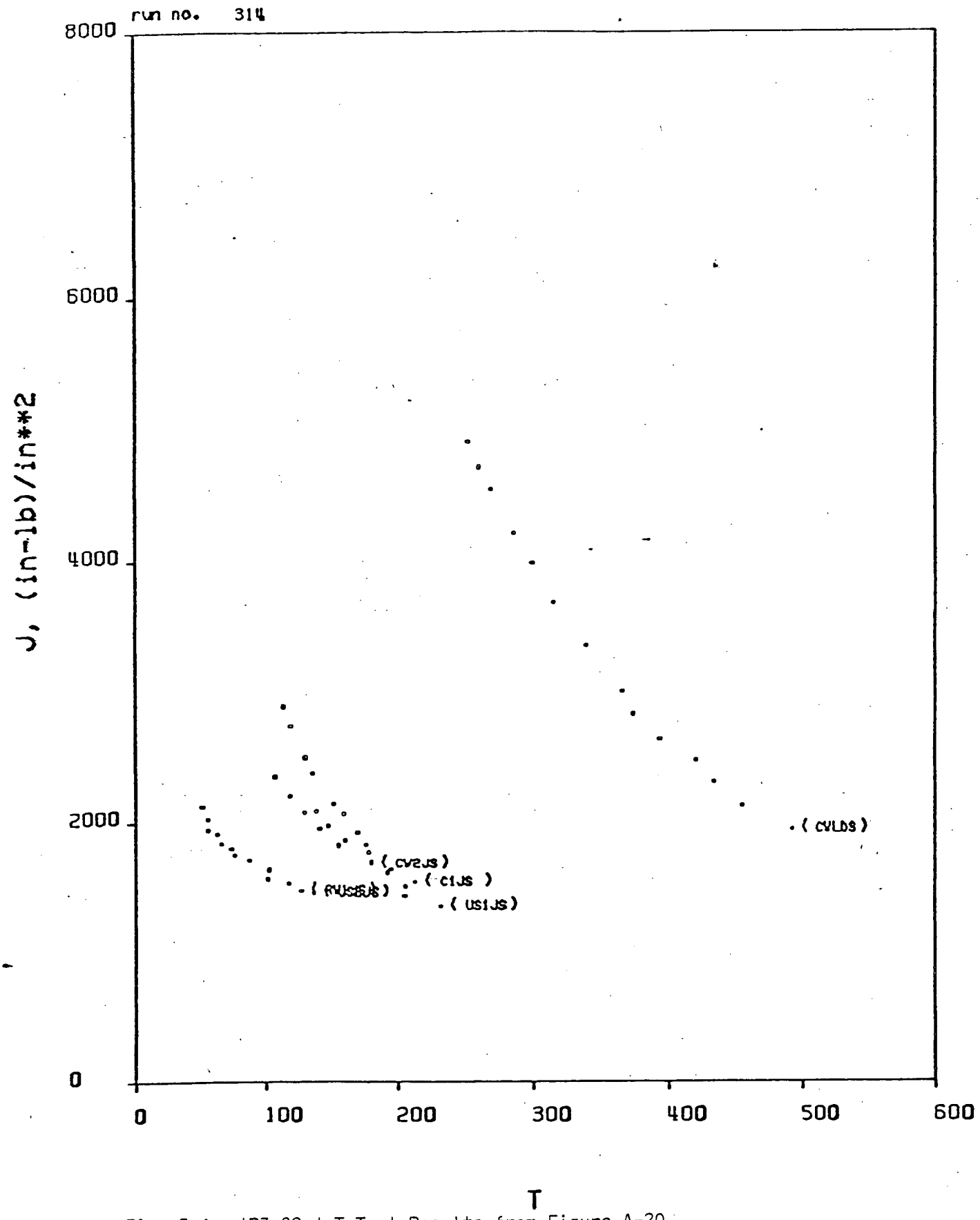

Fig. 5-4 IP3 SG J-T Test Results from Figure A-20

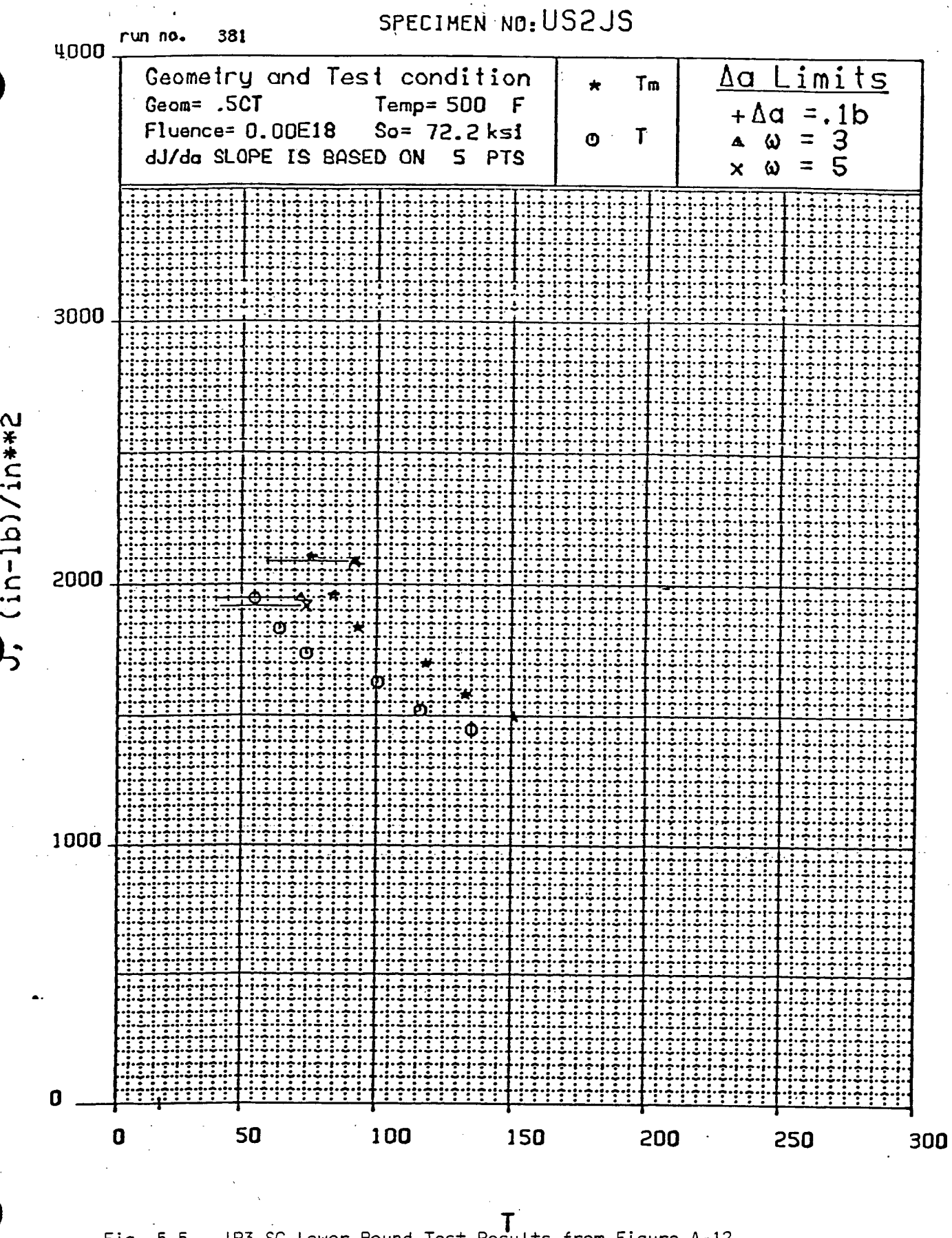

Fig. 5-5 IP3 SG Lower Bound Test Results from Figure A-12

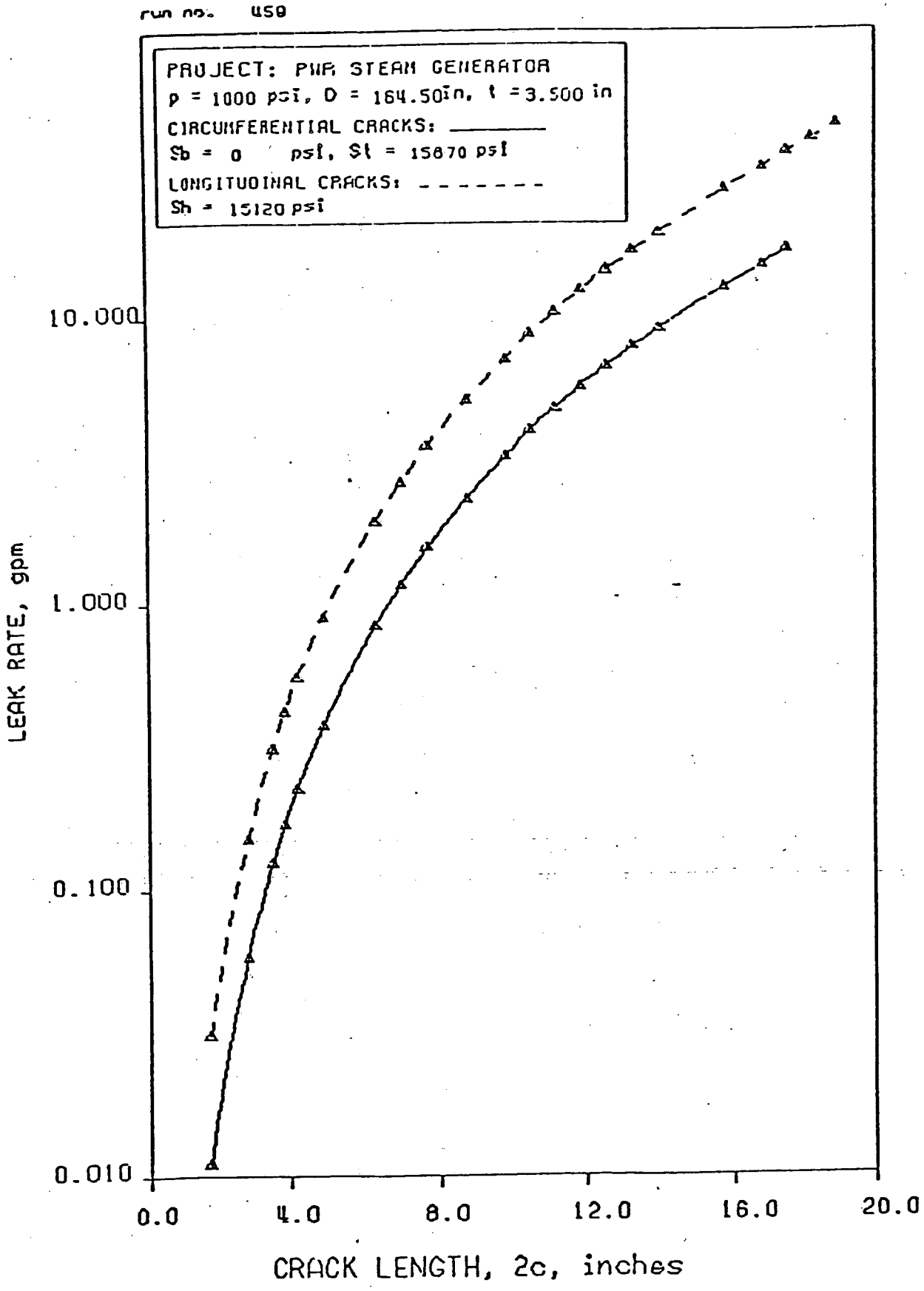

Fig.5.6 Leak Rates for Circumferential and Longitudinal Cracks at the Girth Weld Under Normal Operating Conditions

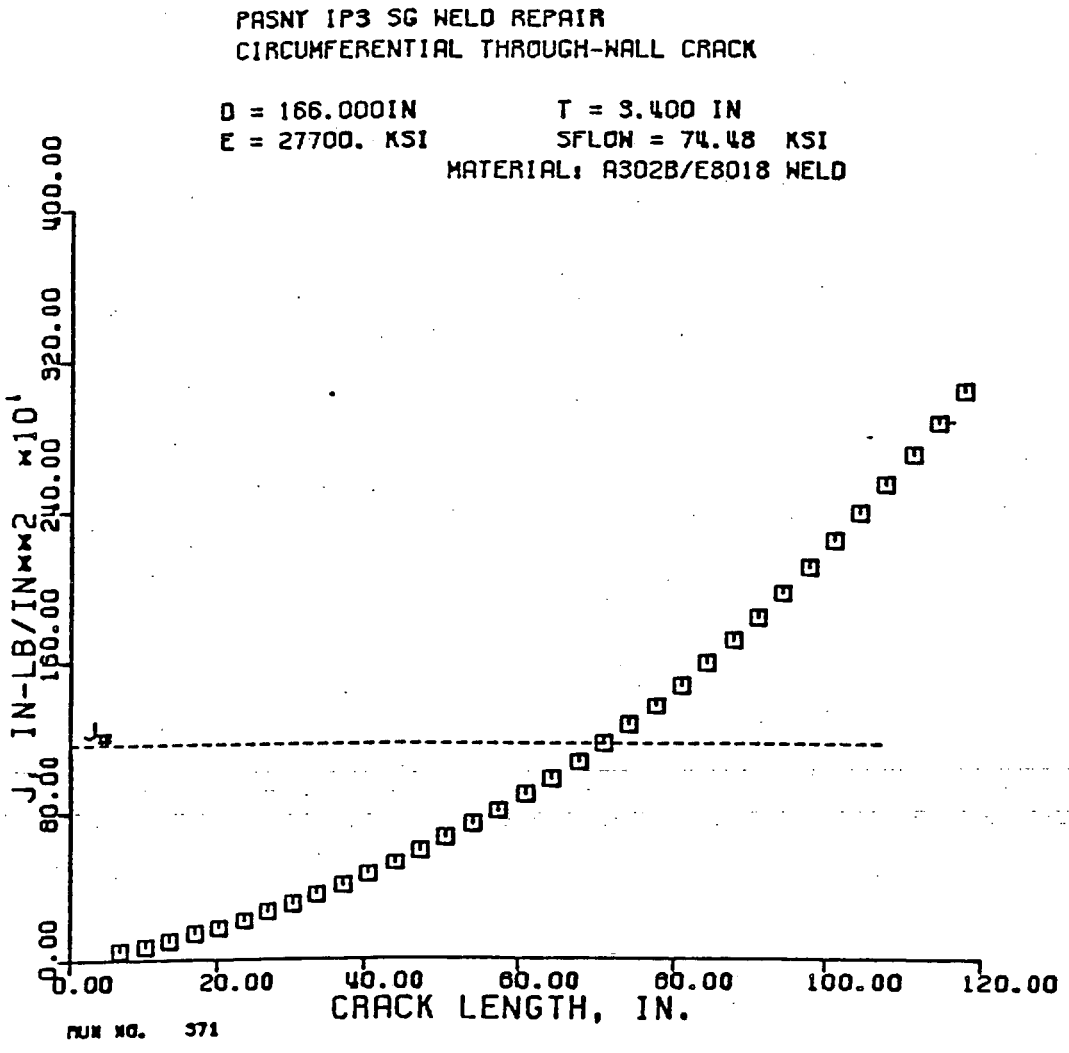

Fig. 5-7 Determination of Circumferential Through-Wall Crack Stability for LBB

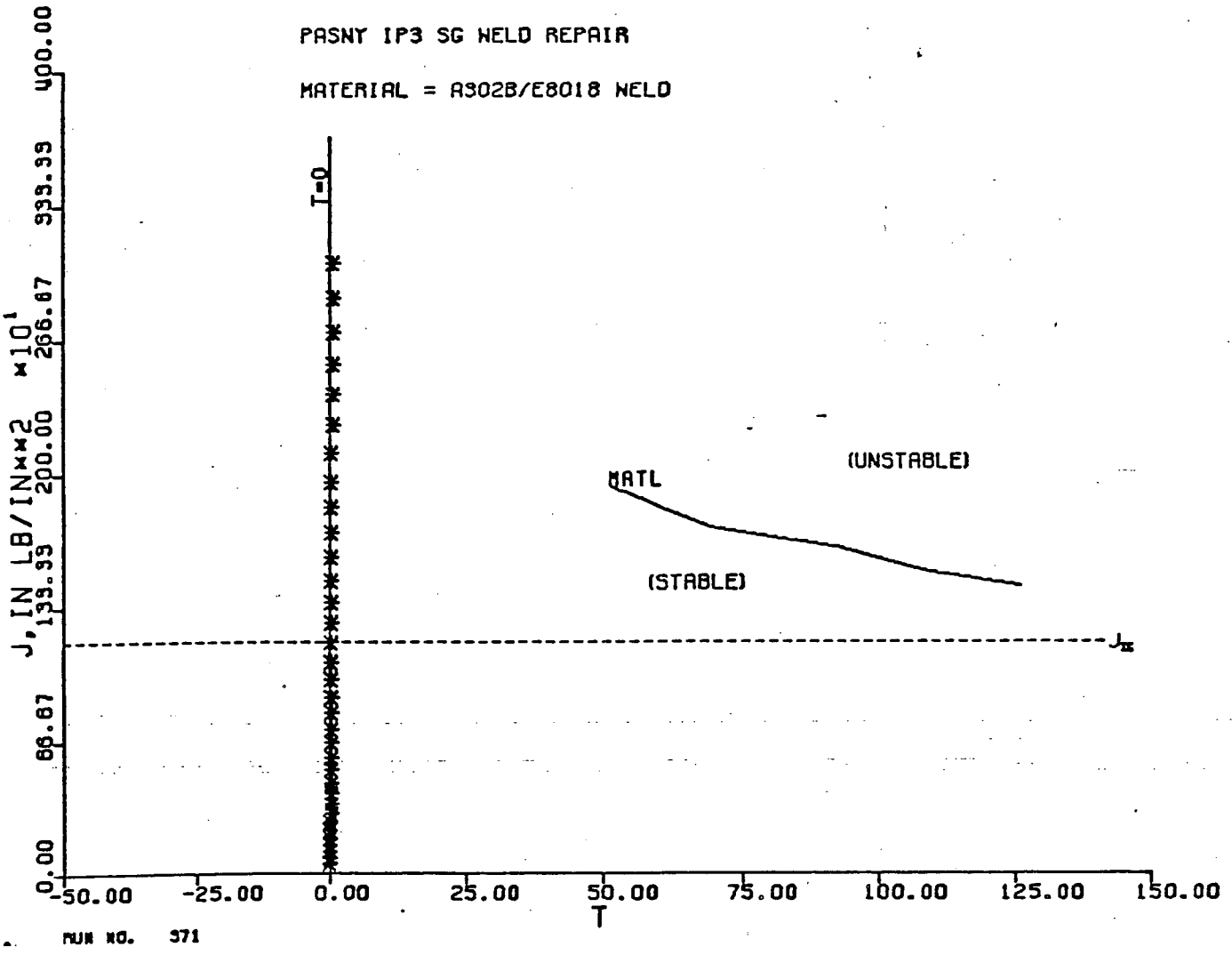

Fig. 5-8 J-T Stability Diagram for Figure 5-7

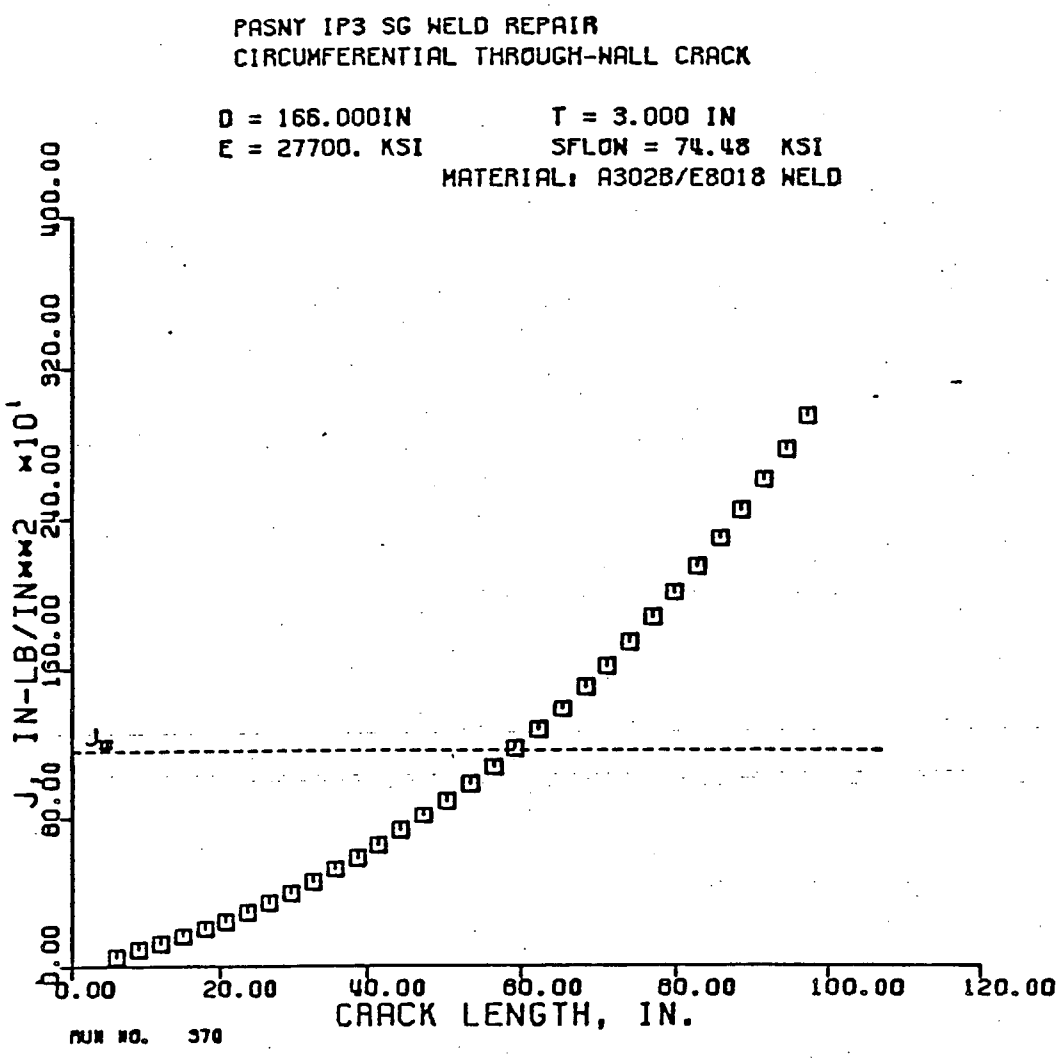

Fig. 5-9 Determination of Effect of Local Thinning on Circumferential Through-Wall Crack Stability for LBB

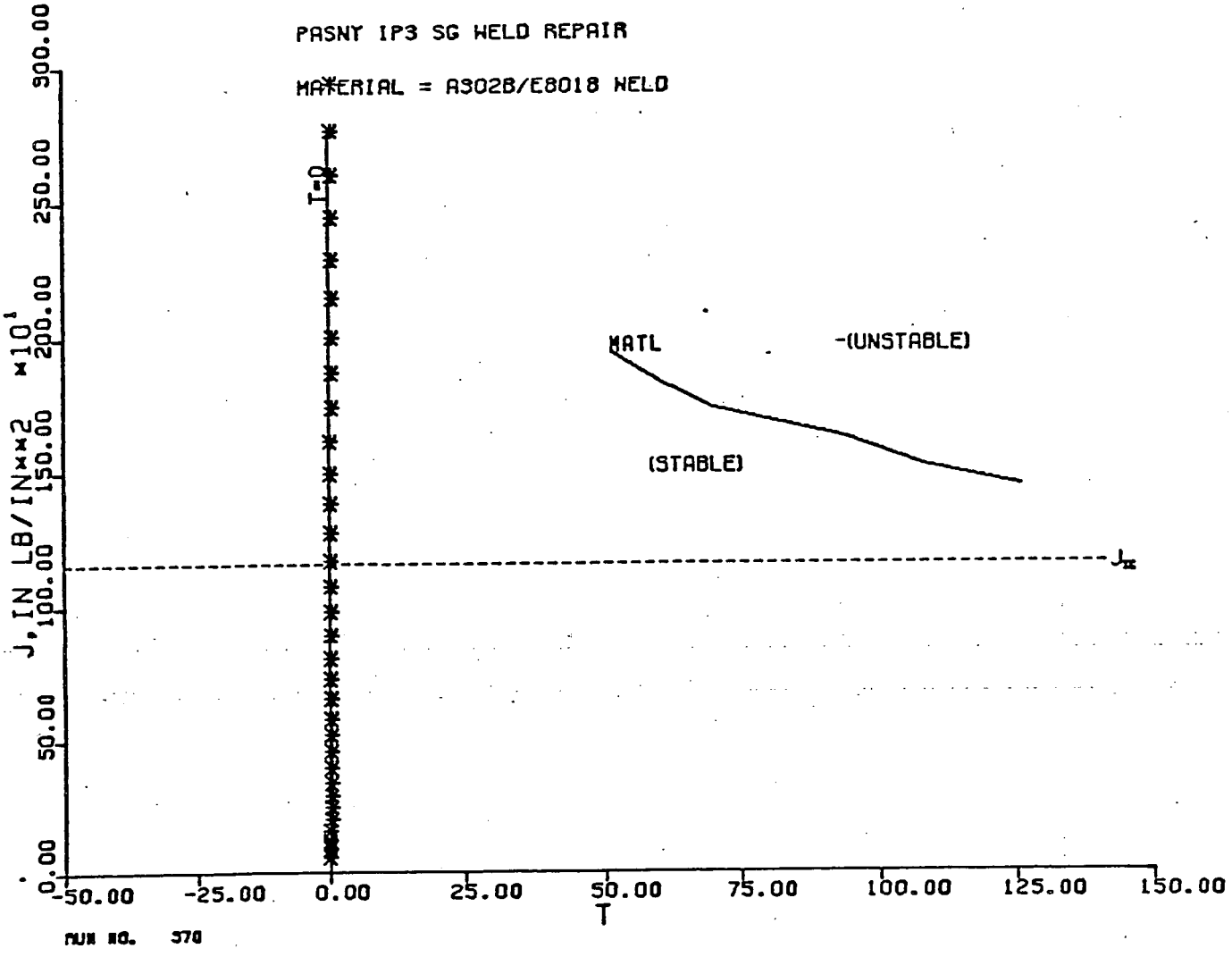

Fig. 5-10 J-T Stability Diagram for Figure 5-9

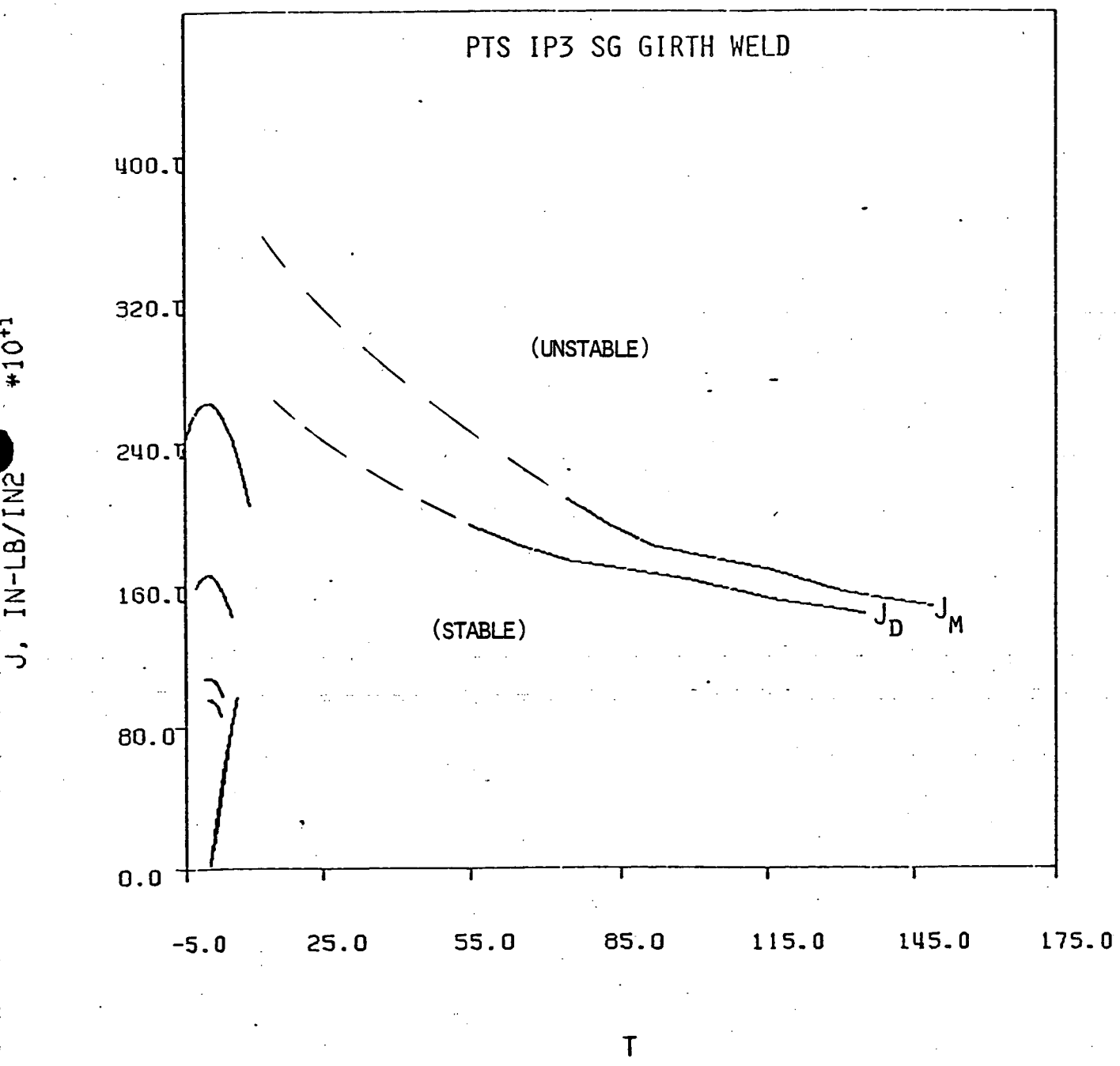

Fig. 5-11 J-T Stability Diagram for PTS Condition (21)

Section 6

CONCLUSIONS

Part-through surface cracks were postulated to exist in the worst location of the girth weld and fatigue crack growth computations were performed, using representative growth rate data. It was determined that cracks having an aspect ratio of 6:1 and a depth of .25 inches would take more than six times the remaining operating life (37 years) to propagate through-the-wall of the vessel. Similarly, for cracks having a depth of one-quarter of the wall thickness (.875 inches), it required over three times the remaining operating life to propagate through the vessel wall. 1,2 2

A generalized leak-before-break criteria was evaluated based on cracks that extended through-the-thickness of the vessel wall. This involved determining the longitudinal and circumferential crack lengths, $2c_{10}$, corresponding to leak rates of 10 gpm under normal operating loads. Then, the stability of cracks having a length equal to $2c_{10}$ plus 2t was examined under Level D conditions. It was demonstrated that both longitudinal and circumferential cracks, that cause such leak rates, have excellent margins of stability. In fact, cracks having lengths in excess of 20 inches were shown to be stable. 1

Lastly, consideration was given to a postulated accident condition under which 70F feedwater is introduced into a hot steam generator having a low water level. This event, commonly known as pressurized thermal shock, was analyzed and it was concluded that excellent stability for a conservatively sized (large) crack could be expected.

Section 7

REFERENCES

1. Paris, P.C., et al., 'A Treatment of the Subject of Tearing Instability,' NUREG-0311, Aug. 1977.

2. Paris, P.C. and Tada, H., 'Further Results on the Subject of Tearing Instability - I,' NUREG/CR-1220, Vol. I, Jan. 1980; and Zahoor,A. and Paris, P.C., 'Further Results on the Subject of Tearing Instability - II,' NUREG/CR-1220, Vol. II, Jan. 1980.

3. Tada, H. and Paris, P.C., 'Tearing Instability Analysis Handbook,' NUREG/CR-1221, Jan. 1980.

4. Paris, P.C., 'A Method of Application of Elastic-Plastic Fracture Mechanics to Nuclear Vessel Analysis', USNRC Report NUREG-0744, App. A, April 1981.

5. Johnson, R.E., et al., 'Resolution of the Reactor Vessel Materials Toughness Safety Issue,' USNRC Report NUREG-0744, April, 1981.

6. Paris, P.C., Tada, H. and Baldini, S.E., 'Fracture Proof Design,' in 'CSNI Specialists Meeting on Plastic Tearing Instability,' USNRC Report, NUREG/CP-0010, Jan. 1980.

7. ASME Boiler and Pressure Vessel Code, Section III, 1974 ed.

8. Rice, J.R., Jour. Appd. Mech., Vol. 35, 1968, pp. 379-388.

9. Hutchinson, J.W. and Paris, P.C., 'Stability Analysis of J-Controlled Crack Growth,' ASTM STP-668, 1979, pp. 37-64.

10. Zahoor, A. and Kanninen, M.F., 'A Plastic Fracture Mechanics Prediction of Fracture Instability in a Circumfrentially Cracked Pipe in Bending', July 1980, ASME Paper 80-WA/PVP-3, Accepted for Publication in the ASME J. of P. Vessel and Technology, 1981.

11. Gudas, J.P. and Joyce, J.A., 'Degraded Pipe Experimental Program', HSST Review - VIRG Meeting, 23 and 24 July 1980, Silver Spring, MD.

12. ASME Boiler and Pressure Vessel Code, Section XI, 1974 ed.

13. Ferril, Juhl and Miller,'Measurement of Residual Stress in Heavy Weldment', Weld Journal WRG Supp, 45, H, 1966.

14. Westinghouse Report, Vertical Steam Generator Stress Report, April 20,1969; Prepared by: R.P. Wedler.

15. Folias, E.S., 'A Circumferential Crack in a Pressurized Cylindrical Shell,' Intl. J. of Fracture Mechanics, Vol. 3, pp. 1-11, 1967.

16. Erdogan, F. and DeLale, F., 'Ductile Fracture of Pipes and Cylindrical Containers with a Circumferential Flaw,' ASME J. of Pressure Vessel Technology, Vol. 103, May 1981, pp. 160-168.

17. 'LKRATE', USNRC computer code for determining leakage rates through cracks in piping and pressure vessels. Transmitted by M. Boyle, USNRC/SEP to FPDC, 9 Sept. 1982.

18. Ernst, Hugo, 'Material Resistance and Instability Beyond J-Controlled Crack Growth', Elastic-Plastic Fracture: Second Symposium, ASTM STP 803, C.F. Shih and J.P. Gudas, Eds., American Society for Testing and Materials, 1983, Appendix. 1

19. PASNY Letter; J.V. Brunetti to FPDC, January 5, 1983. Transmittal of IP3 Steam generator drawings, metallurgical reports, material properties and structural analysis.

20. Vasquez, J. and Paris, P.C., 'The Application of the Plastic Zone Instability Criterion to Pressure Vessel Failure,' Journadas Metalurgicas, Sociedad Argentina de Metales, Cordoba, Argentina, Nov. 1970., (also in NUREG/CP-0010, Sept. 1979.)

21. FPDC Report 83-155, 'Analysis of the Indian Point 3 Steam Generator Girth Weld Under Pressurized Thermal Schock Conditions', April 1982, PROPRIETARY.

22. FPDC Report 83-104, 'Development of J-Resistance Curves for Stainless Steel Plate and Welds at High J Levels', in preparation for The Power Authority of the State of New York, 1983.

23. Private communication, J.W. Hutchinson to P.C. Paris, February 17, 1983, St. Louis, MO. 1

24. Peano, A. et al., 'Adoptive Approximations in Finite Elements Structural Analysis', ISMES Report 114, November 1978.

APPENDIX A

MATERIAL PROPERTIES

Appendix A describes the methods used for transforming test results or data into J-Δa and J-T plots to be used as material properties for the crack stability calculations. The reduction of the data and the plotting of the extrapolated J-Δa and J-T curves was accomplished by using the computer program JTPLOT [6]. It also summarizes other available data from the literature that is relevant to the subject of this report.

A-1 SOURCE OF TEST DATA

The data base included nine J-Δa curves from two sources. The source for six of the J-Δa curves was the report 'J-Integral Fracture Toughness Testing of Indian Point #3 Steam Generator Material' [2]. This report [2] included both A302B steel and A302B/E8018 weld metal taken from the steam generator (SG). The other J-Δa data was taken from 'EPRI Report NP-304' [5]. This latter set of data [5] was A533B/E8018 weld metal. Tensile properties were taken from Ref.[1,3,4and5]. A detailed discussion of the method of data reduction and the QA procedures utilized follows.

A-2 DATA REDUCTION

For the specimens from Ref.[2], the yield, ultimate and flow stresses were calculated according to whether they were A302B steel or weld metal material types. For the A302B steel, the flow stress was computed from the tensile properties determined from tests on the material taken from the SG [3]. This value of flow stress is valid for a temperature of 70°F. However, specimen US2J was tested at a temperature of 500°F. To obtain flow stress estimates at 500°F, interpolation was required. The ratio of the flow stress at 500°F compared with that at 70°F based on Ref.[4] data was used to extrapolate the 70°F flow stress obtained from on Ref.[3] data to 500°F. For the weld metal, the values of the yield and the ultimate stresses at 70°F and 500°F were determined by interpolating the yield and the ultimate stress data given in Ref.[4]. These tensile properties
1| have been summarized in Table-A1. Values for the modulus of elasticity, E, were taken directly from the ASME B+PV Code, Section 3 [1], corresponding to the test temperature.

1| TABLE A-1 TENSILE PROPERTIES EVALUATION

MATERIAL TYPE	TEMP °F	REF.	METHOD OF EVALUATION OF FLOW STRESS	AVERAGE STRESS YIELD (ksi)	ULTIMATE (ksi)	FLOW (ksi)
A302B	70	3	straight average	67.0	86.3	76.65
A302B	500	3,4	interpolation between references	na	na	72.24
Weld A302B/E8018	70	4	interpolation	80.35	92.63	86.49
Weld A533/E8018	70	2	average of sum of specimen data	na	na	77.30

na - data not available

J-Δa and load data from References [2] and [5] was transferred to a computer

input data sheet and then entered into the computer for storage on a disk file. The data from Ref.[5] was taken from three groupings, CMM, CNM and COM. These groups were combined into one data set and renamed CWELD. The values of temperature, flow stress, thickness, and initial and final crack lengths used for CWELD represented an average of all data points within groups CMM, CNM, and COM. After performing standard FPDC QA procedures, the data entered into the computer was graphically displayed on a computer terminal screen for comparison with the original J-Δa plots given in Ref.[2] and [5].

Any abnormal points were investigated and, if necessary, corrected. The corrected values were then re-checked by re-plotting and comparing as described above. Next, the data files were printed out and checked digit by digit against the original data.

The single specimen test procedure used for developing the J-Δa curves for the SG material involved heat-tinting at the end of the test to compare computed Δa with actual Δa. Some errors in computed vs. actual were noted [2]. In order to remove these errors in computed vs. actual Δa, based on heat-tint after testing, an extrapolation at the data was performed for each specimen in Ref.[2]. The extrapolation involved shifting the Δa computed to correspond with the value of Δa based on heat-tint. This shifting involved a visual estimation of the shape of the J-Δa curve that brought the computed Δa into correspondence with the Δa
1| from heat-tinting. The solid curve shown in Figures A-1 through 6 represents the adjusted Δa values used for developing the J-T plots. The values of Δa from this adjusted curve (hand drawn) were then entered into the computer. Again, QA procedures were followed in the same manner as for the first data reduction. After this adjusted curve data had been verified, the appropiate J-Δa and J-T

curves were plotted, using JTPLOT [6]. All adjusted data and plots have been identified by appending the letter 'S' to the specimen number.

The data used for the CWELD group was developed during the multi-specimen J test era. Thus, adjusting the Δa to correspond with the heat-tint value was not required. But, the data did exhibit considerable scatter. To eliminate the scatter, a smooth curve was drawn (by hand) through the lower bound of the data points as shown in Figure A-6. From this curve, the same method of data reduction
1 and QA verification used for Figures A-1-5 was used to develop the 'adjusted' J-Δa and J-T plots. These results are tabulated in Tables A-2 through 8.

Using the results from the adjusted data plot, combination plots of J-Δa, J_{mod}-Δa and J-T, J_{mod}-T_{mod} for each specimen (except CWELD), were plotted using the JTPLOT [6]. For CWELD only J-Δa and J-T are given. The purpose of incorporating the modified values of J and T in the J-Δa and J-T material evaluation was to yield a better correlation of material property data and a higher factor of safety, for the crack stability analysis. A description of the method used to determine J_{mod} follows below.

As a final note, Specimen CW1J did not have a sufficient number of data points to develop a valid J-T plot. Thus, it is not shown. Specimen CW1J exhibited intermittent crack instability during testing[2], causing the material to behave in an erratic manner. The J-Δa data so obtained was not included because of the abnormal behavior. The abnormality can be attributed to the presence of large residual stress and possibly, pre-existing cracks.

A-3 PROCEDURE FOR CALCULATING T_{mat}

The value of T_{mat} or T is computed by fitting a second order polynomial through m data points where m is an odd and user selectable number. Starting with the first data point, i, for which $J_i > J_{1c}$, and using the next m-1 data points, i.e., J_i, J_{i+1}, ..., J_{i+m-1} for curve fitting, the slope at the mid-point was calculated. The mid-point corresponds to J_p where $p = i+(m-1)/2$. The next step is to evaluate the slope at J_{p+1}, J_{p+2}, ..., J_{last}. The process stops when i+m-1 exceeds the number of data points. T is computed from the slope of the fitted J-Δa curve, dJ_p/da, from $T_p = (dJ_p/da)(E/\sigma^2)$, where E and σ are the modulus and flow stress respectively for the temperature of interest. Typically, the evaluation starts with m = 5, and if the J-T plot has excessive scatter, m is increased to m = 7, 9, or 11.

On each J-Δa and J-T plot, the J and T values corresponding to Δa=0.1b, ω = 3 and ω = 5 (where $\omega = (dJ/da)(b/J)$) were identified. If these values exceeded the upper or lower limits of the data points, the marks were drawn at the last data point for the 0.1b limit or at the first data point for either ω limit.

A-4 PROCEDURE FOR CALCULATING J_{mod}

The process of calculating J_{mod} was based upon the method proposed by Ernst [7]. The value of J_{mod}, at the data point (i+1) was determined by ultilizing the following incremental expression: $J_{m(i+1)} = J_{d(i+1)} + \Delta J_{(i+1)}$; where $J_{d(i+1)}$ denotes the value of the deformation theory J at that level. The term $\Delta J_{(i+1)}$ was calculated using the expression $\Delta J_{(i+1)} = \Delta J_i + [(m/b)(J_{pl})]_i (a_{i+1} - a_i)$ under the

condition $\Delta J=0$ when $i=0$. The term $[\ ]_i$ designates that the parameters inside the brackets were evaluated at stage i.

For the CT specimen type the value of m, in the equation for $\Delta J_{(i+1)}$, was determined from the expression $m_i=(1+0.76b/W)_i$; where the remaining ligament b_i= width-initial crack-Δa_i. The plastic component of J, J_{pl}, is determined from $J_{pl}=J-J_e$, where $J_e=K^2/E$. The expression for K [8,9] that was chosen was:

$$K_i = \frac{P_i(2+\alpha)}{BW^{1/2}(1-\alpha)^{3/2}}(0.886 + 4.64\alpha - 13.32\alpha^2 + 14.72\alpha^3 - 5.6\alpha^4)$$

where α_i= a/W. The expression for α was considered to be valid for the condition $\alpha_i > 0.2$.

A-5 RESULTS

By using the previously discussed curve fitting procedure and with the aid of 'adjusted' data, J-Δa, J_m-Δa and J-T, J_m-T_m were plotted for each specimen as shown in Figures A-7 through 18. Figures A-7 and 8 are for CWELD for which J_m could not be calculated. In addition, all J-Δa and J-T data was plotted in Figures A-19 and 20 to compare the material properties. Similarly, Figures A-21 and A-22 involved plotting a family of curves of all specimens (excluding CWLDS), for the modified J-Δa and J-T curves, to provide a basis for comparison. Comparative J_{ic}, T_{mat} and CVN data is also included from literature sources as shown in Figures A-23 through 25.

A-6 REFERENCES

1. 'ASME Boiler and Pressure Vessel Code', Section 3, ASME, 1974.

2. 'J-Integral Fracture Toughness Testing of Indian Point #3 Steam Generator Material', Del Research Division, PSG, Inc., Hellertown, PA, September 1982.

3. 'Metallurgical Examination of Shell Girth Weld Coupon from Steam Generator 32, Indian Point #3 Nuclear Power Plant', Report No. 7164,

4. 'Nuclear Pressure Vessel Steel Data Base', EPRI Report NP-933, Fracture Control Corporation, Goleta, California, December, 1978.

5. 'Subcritical Crack Growth in Ferritic Materials for Light Water Nuclear Reactor Vessels', EPRI Report NP-304, Combustion Engineering, Inc., Chattanooga, Tennessee, August 1976.

6. 'JTPLOT' Computer Code, Version 2, Level 3, Fracture Proof Design Corporation, St. Louis, MO.

7. 'Material Resistance and Instability Beyond J-Controlled Crack Growth', Ernst, Hugo A., Elastic-Plastic Fracture: Second Symposium, ASTM STP 803, C.F. Shih and J.P. Gudas, Eds., American Society for Testing and Materials, 1983.

8. 'Stress Analysis of the Compact Specimen Including the Effects of Pin Loading', Fracture Analysis, ASTM STP 560, 1974, pp. 105-121.

9. 'Wide Range Stress Intensity Factor Expressions for ASTM E399 Standard Fracture Toughness Specimens', International Journal of Fracture, Vol. 12, June 1976, pp. 415-476.

SPECIMEN NO: CWELD

FIGURE A-1

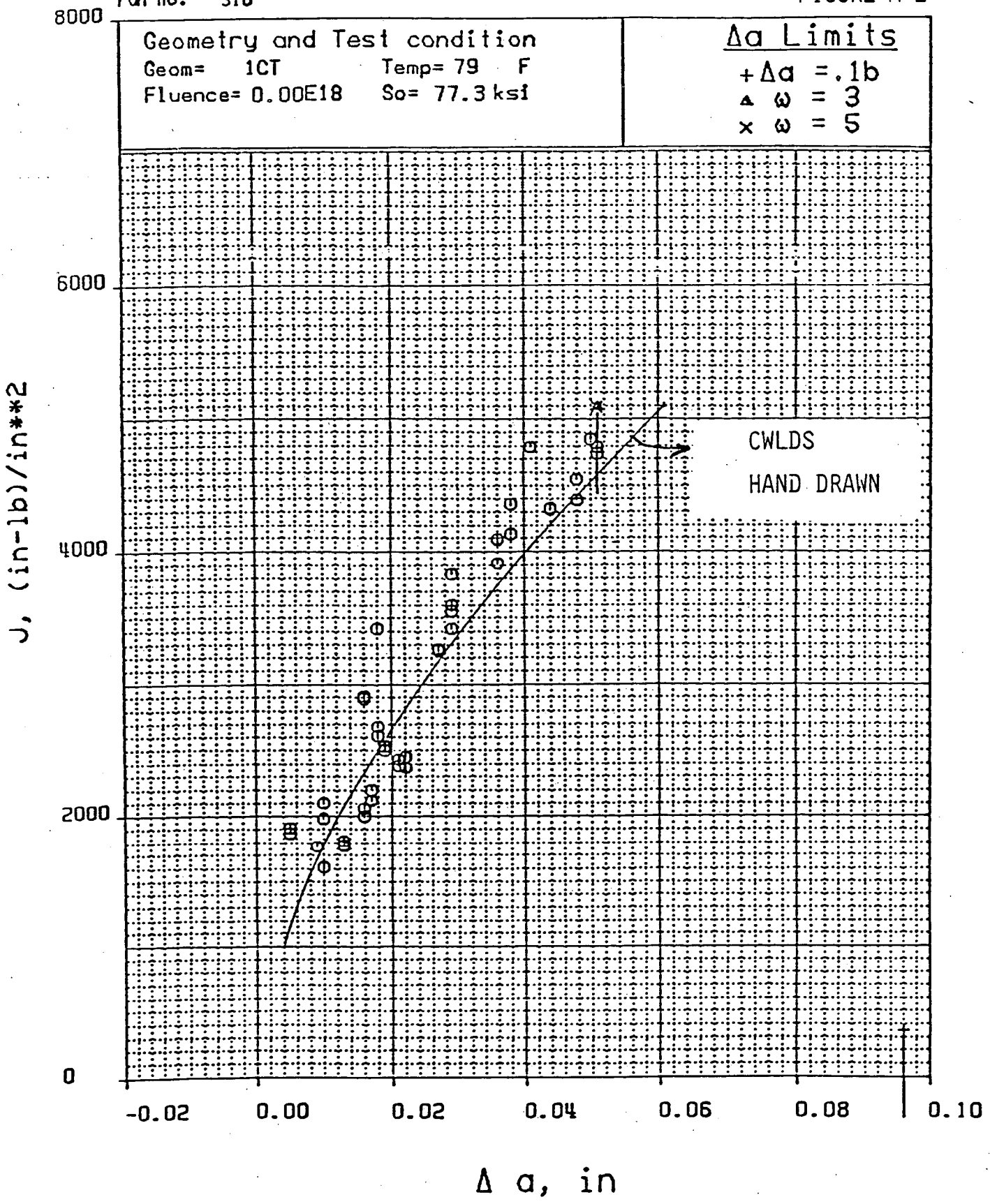

run no. 310

SPECIMEN NO: US1J

FIGURE A-2

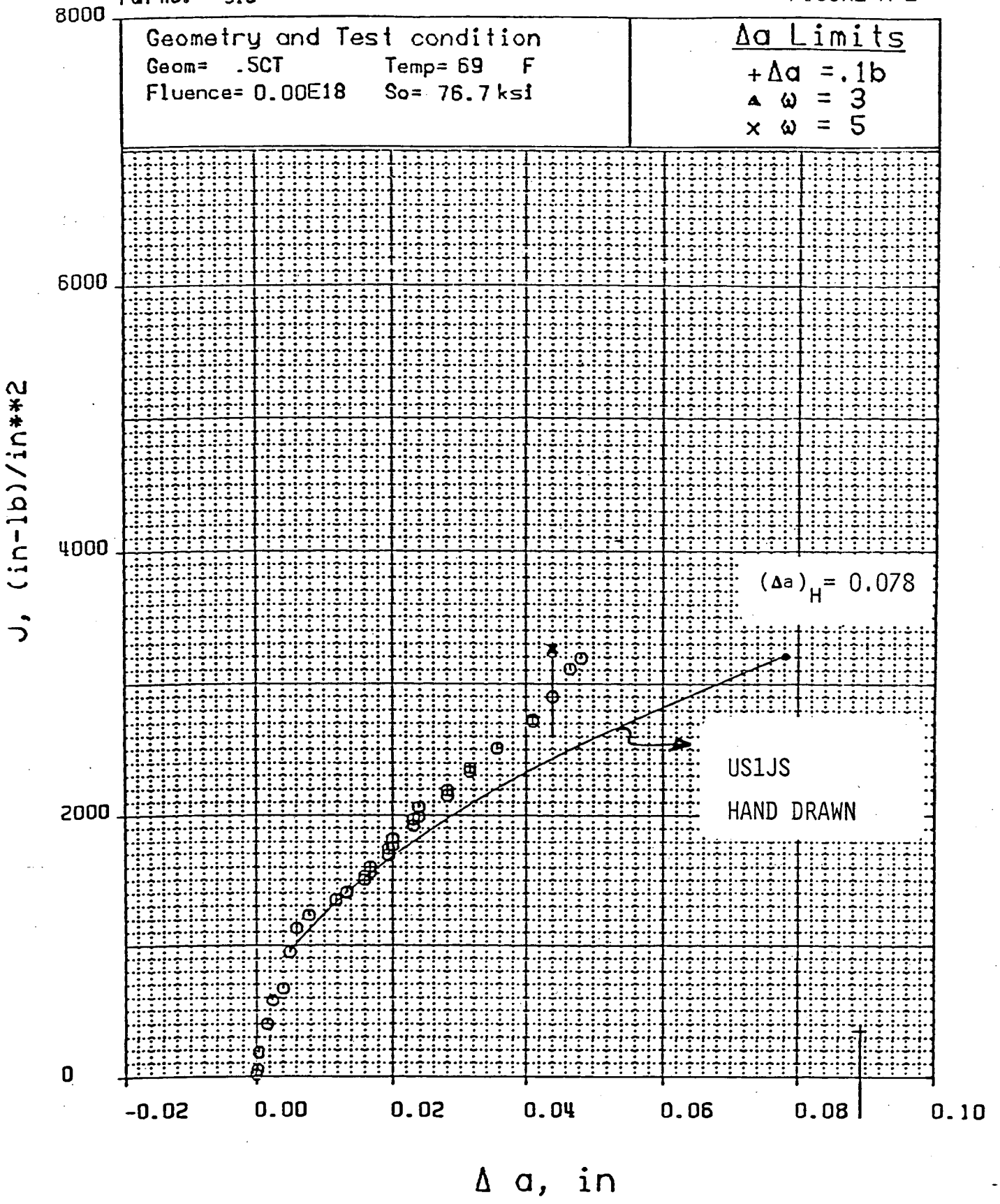

SPECIMEN NO: US2J

run no. 310

FIGURE A-3

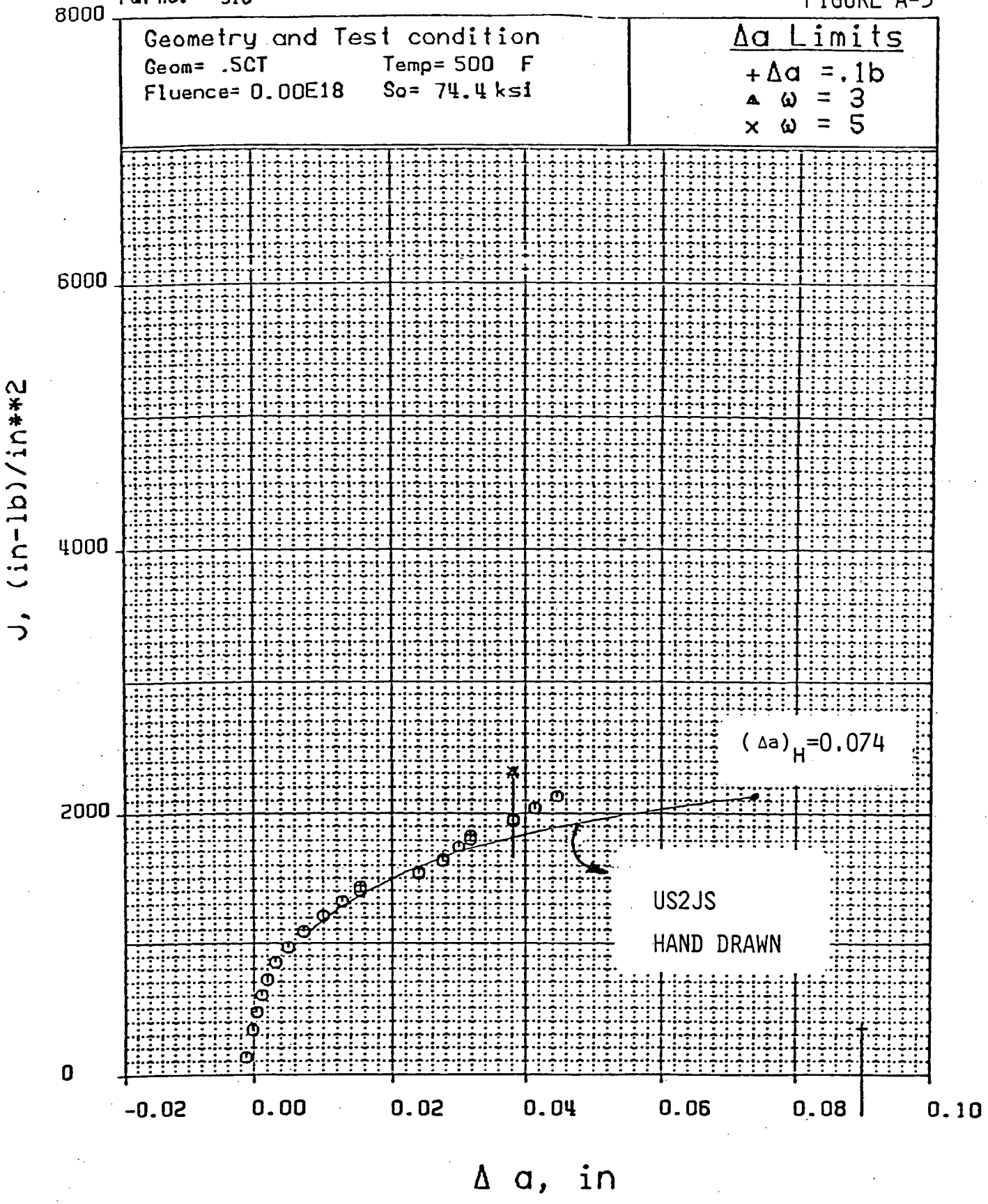

run no. 310

SPECIMEN NO: C1J

FIGURE A-4

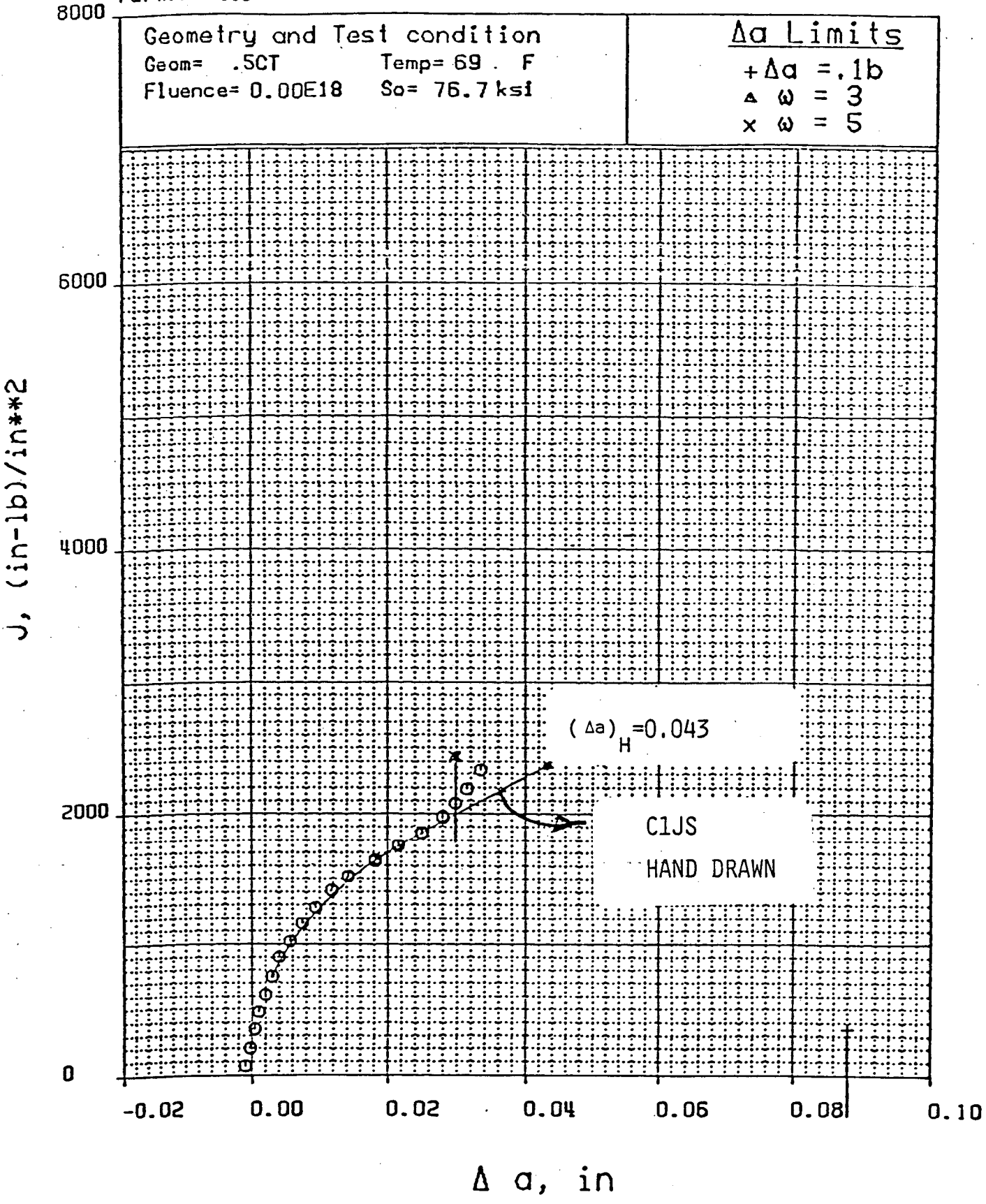

SPECIMEN NO: CW2J

FIGURE A-5

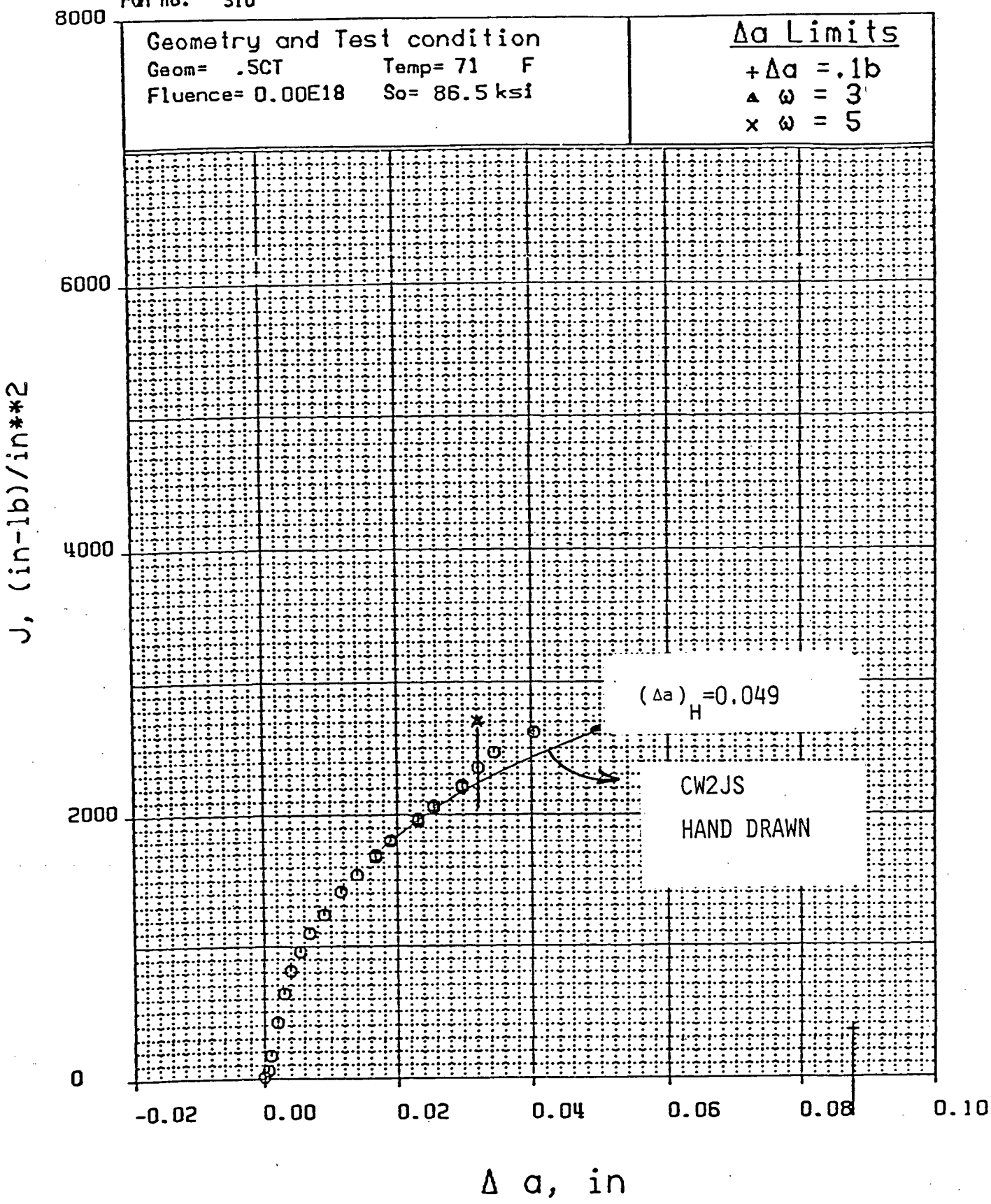

SPECIMEN NO: RW1J

FIGURE A-6

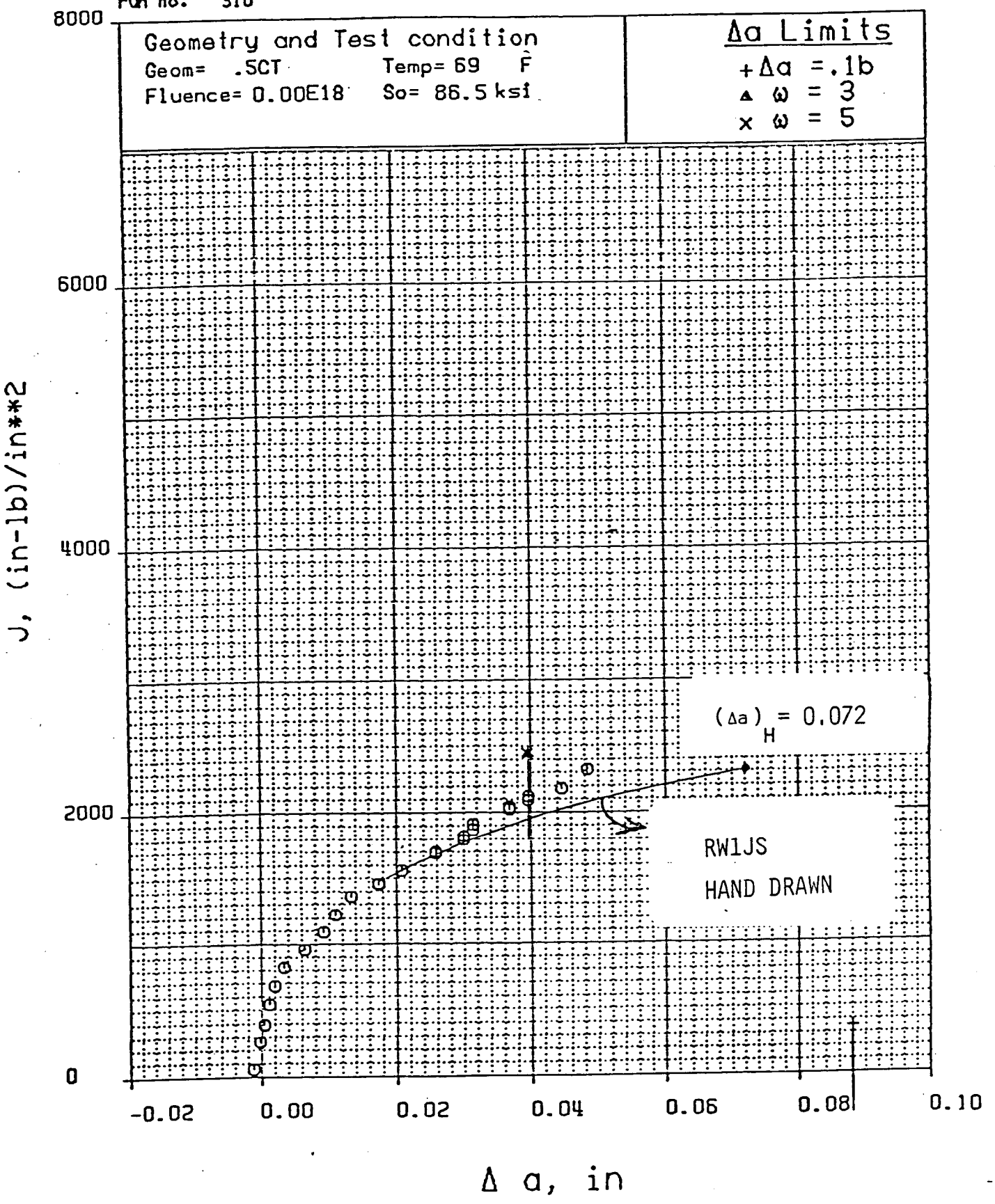

SPECIMEN NO: CWLDS

FIGURE A-7

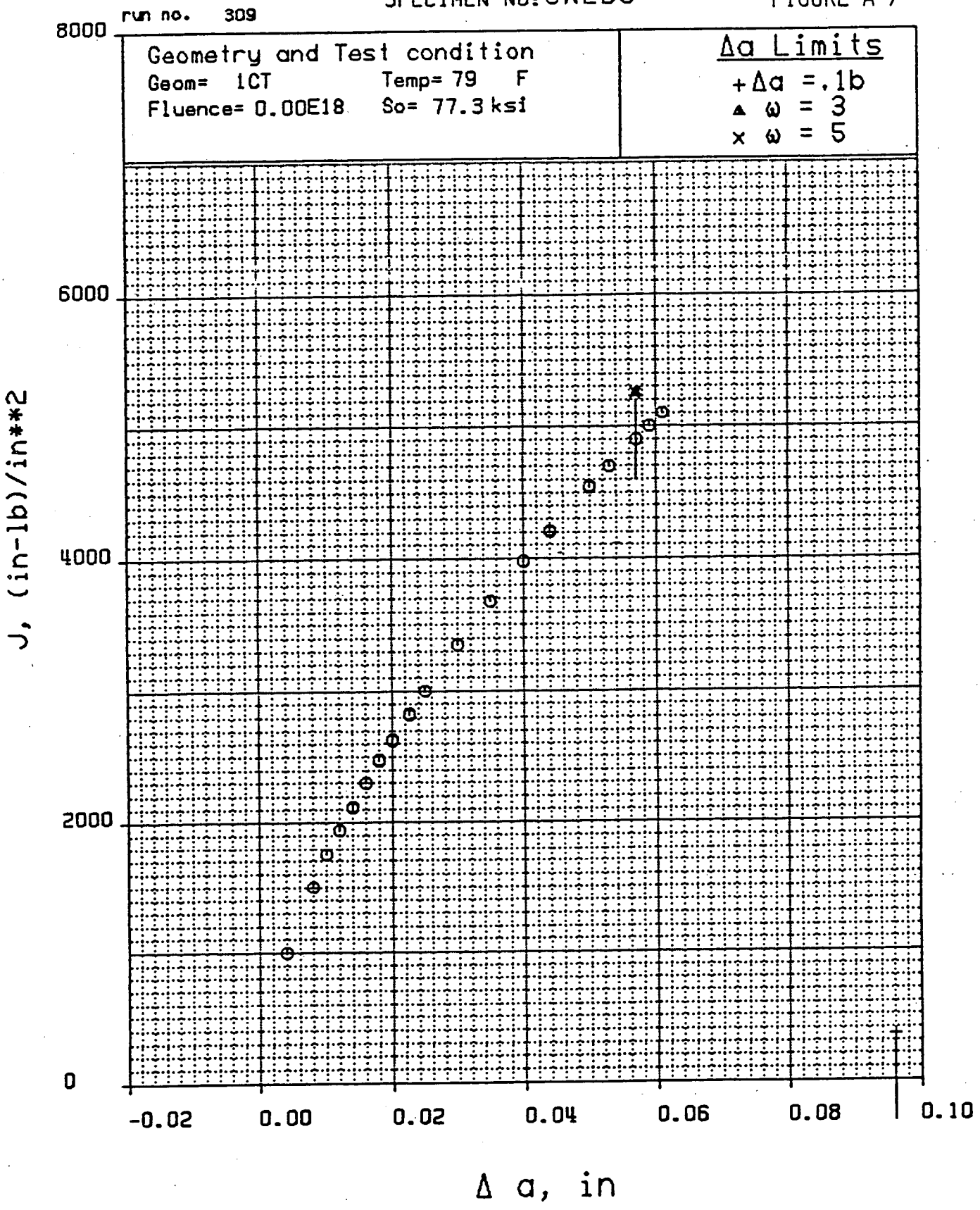

SPECIMEN NO: CWLDS

FIGURE A-8

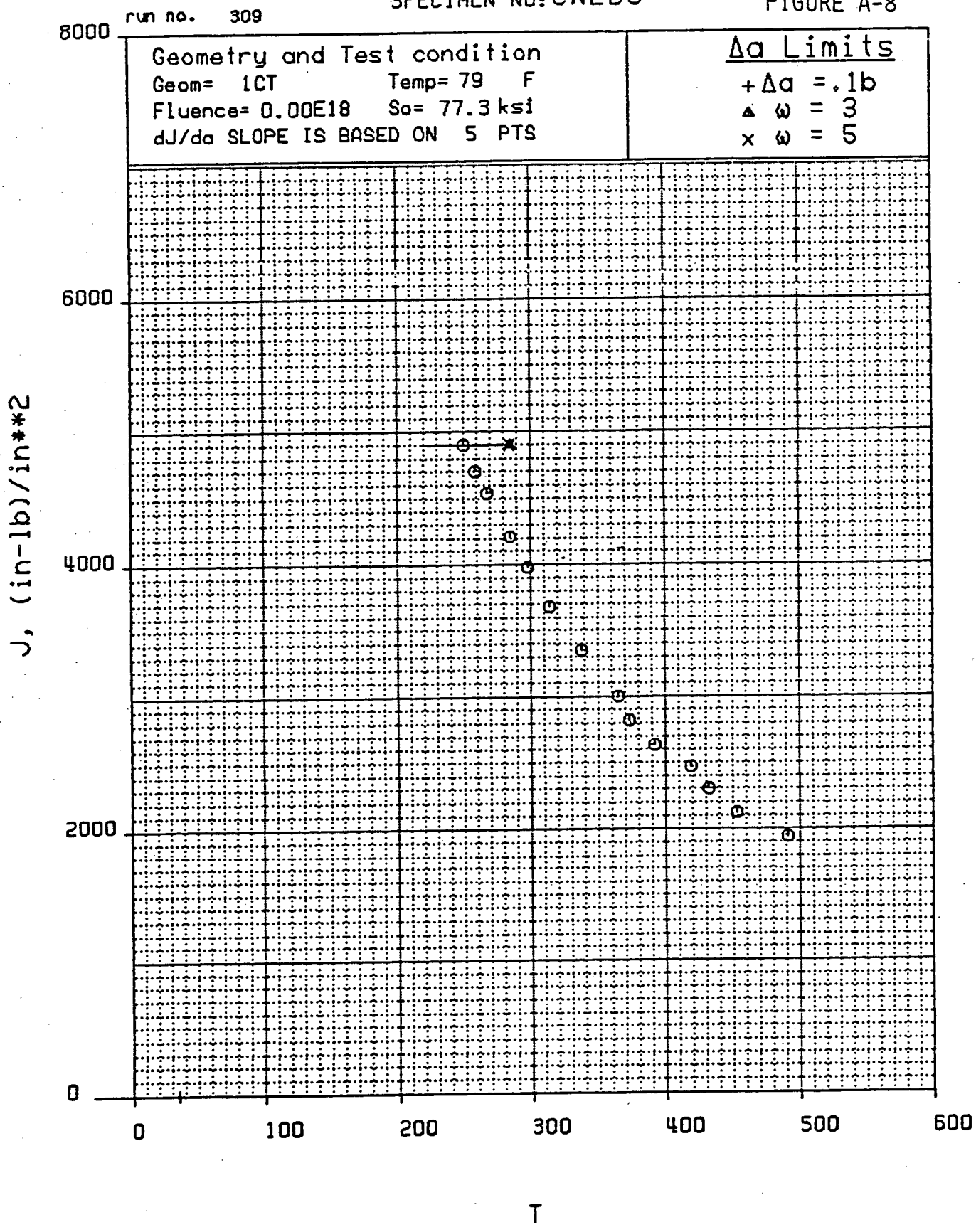

SPECIMEN NO: US1JS

FIGURE A-9

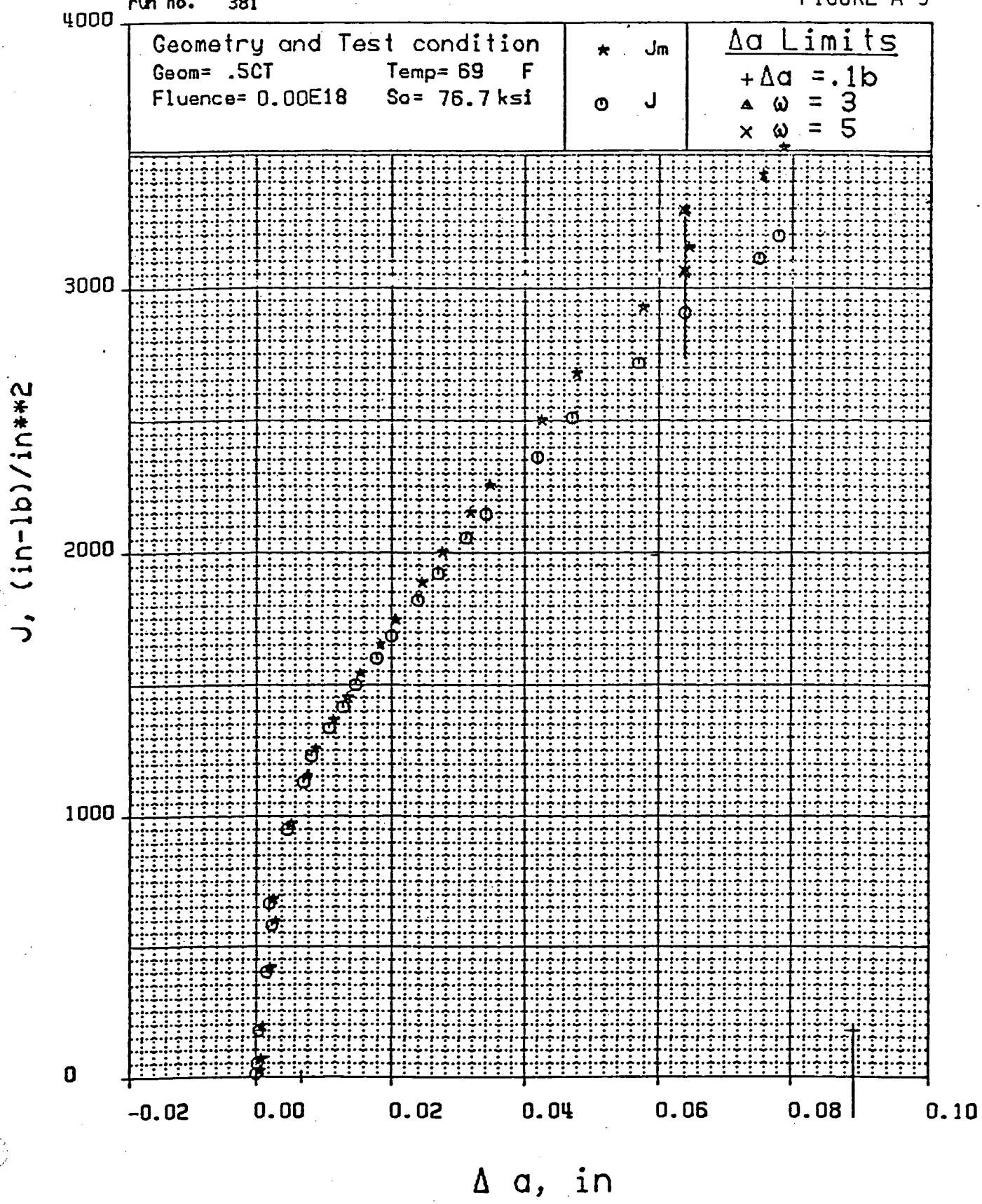

SPECIMEN NO: US1JS

FIGURE A-10

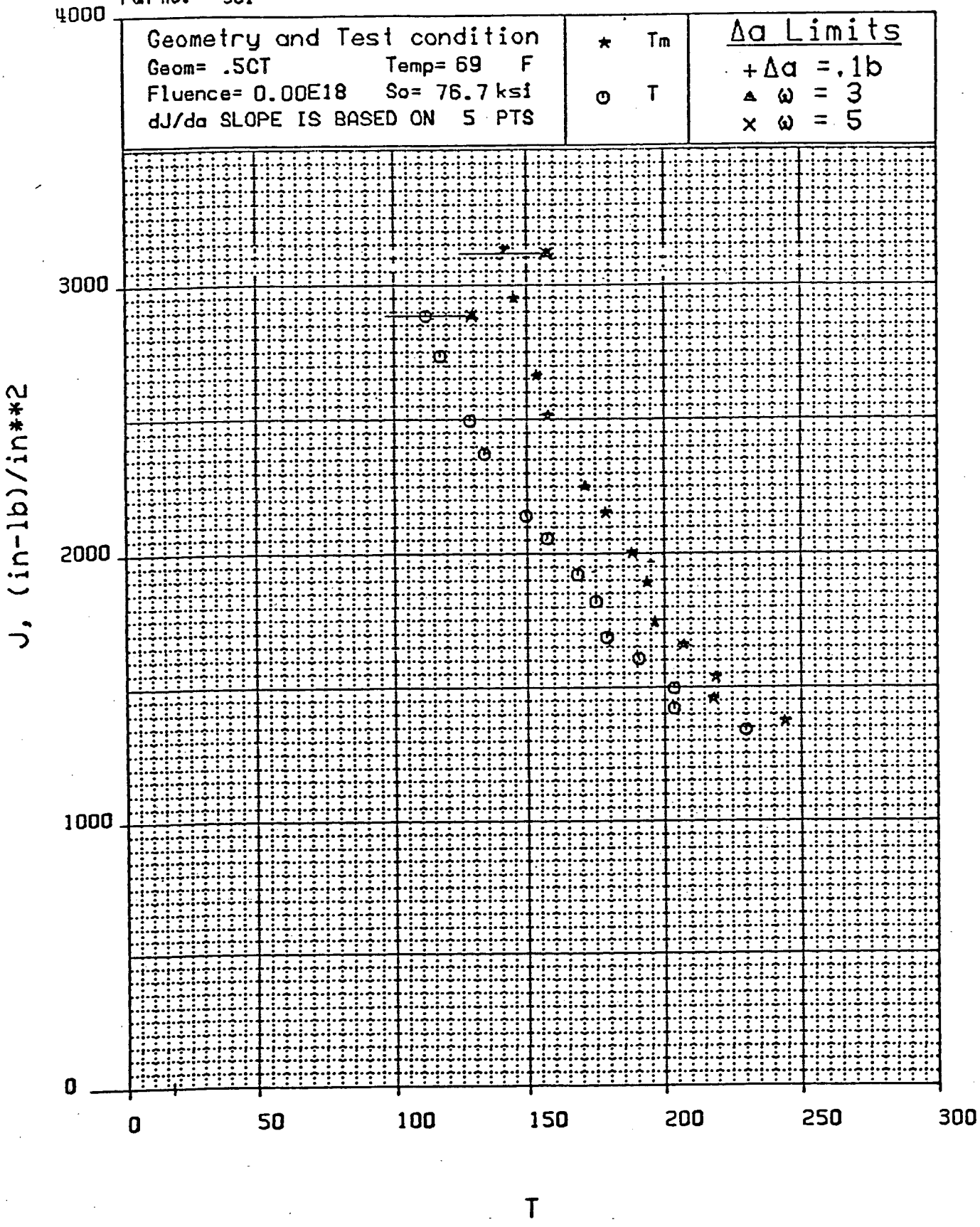

SPECIMEN NO: US2JS

FIGURE A-11

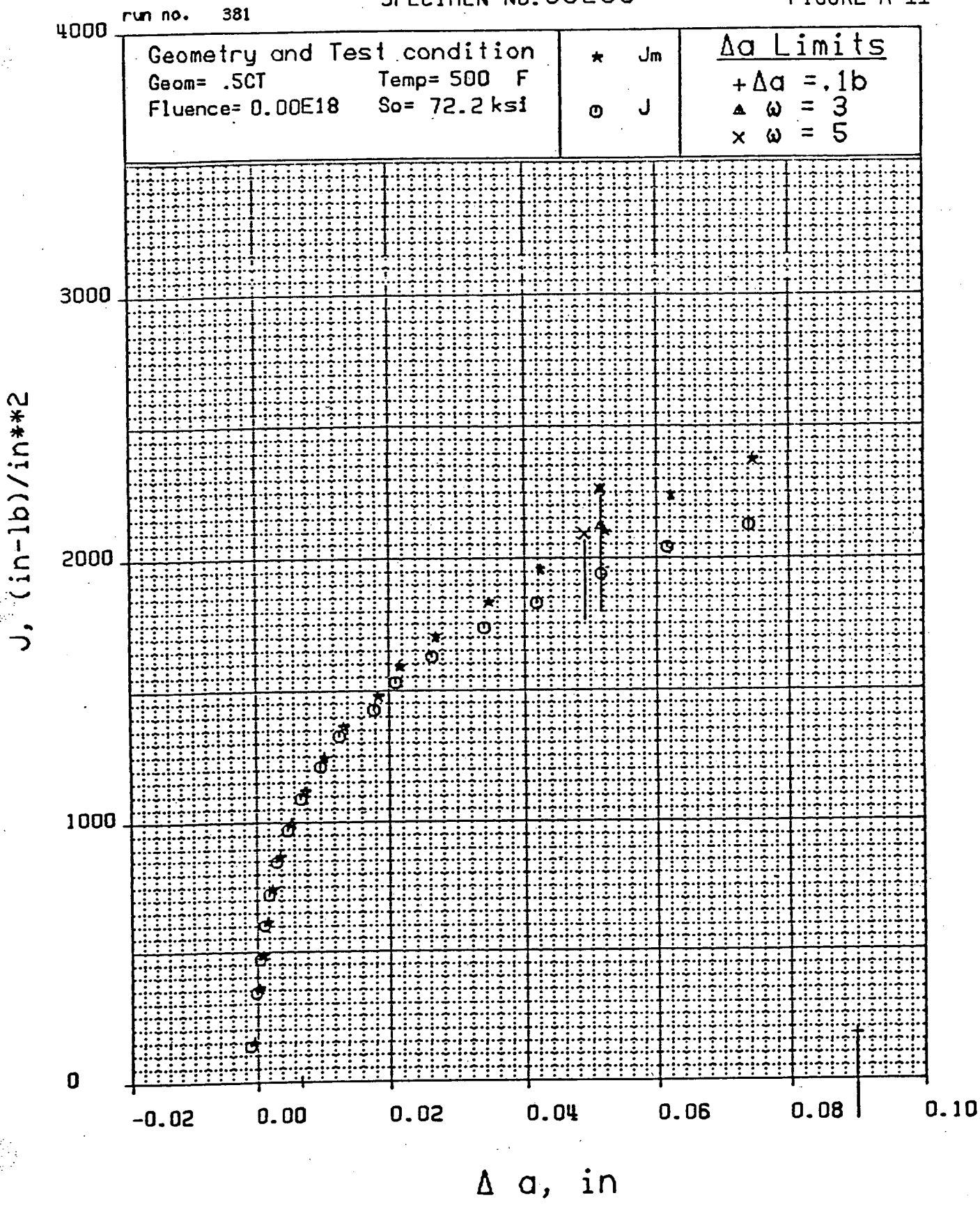

SPECIMEN NO: US2JS

FIGURE A-12

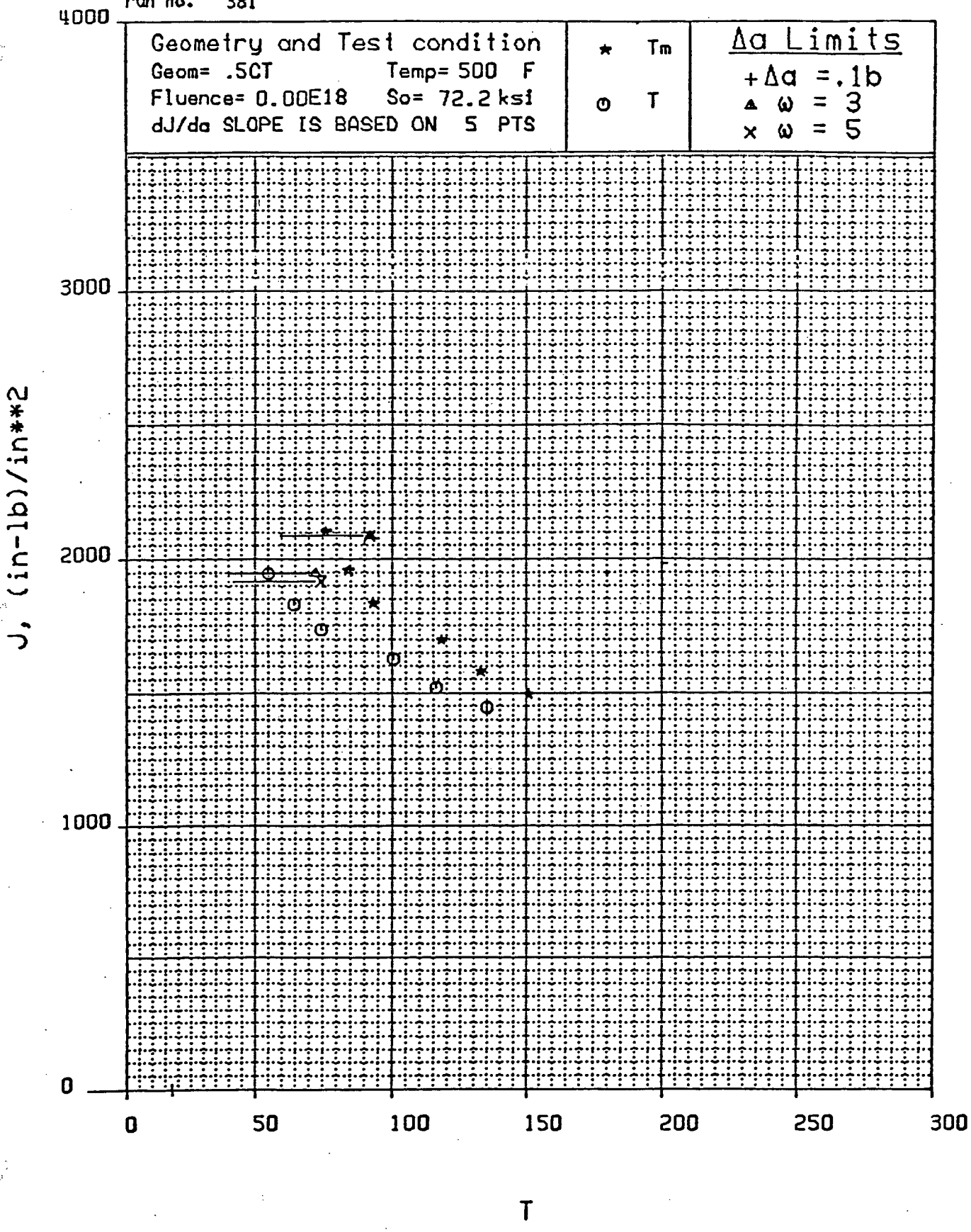

SPECIMEN NO: C1JS

FIGURE A-13

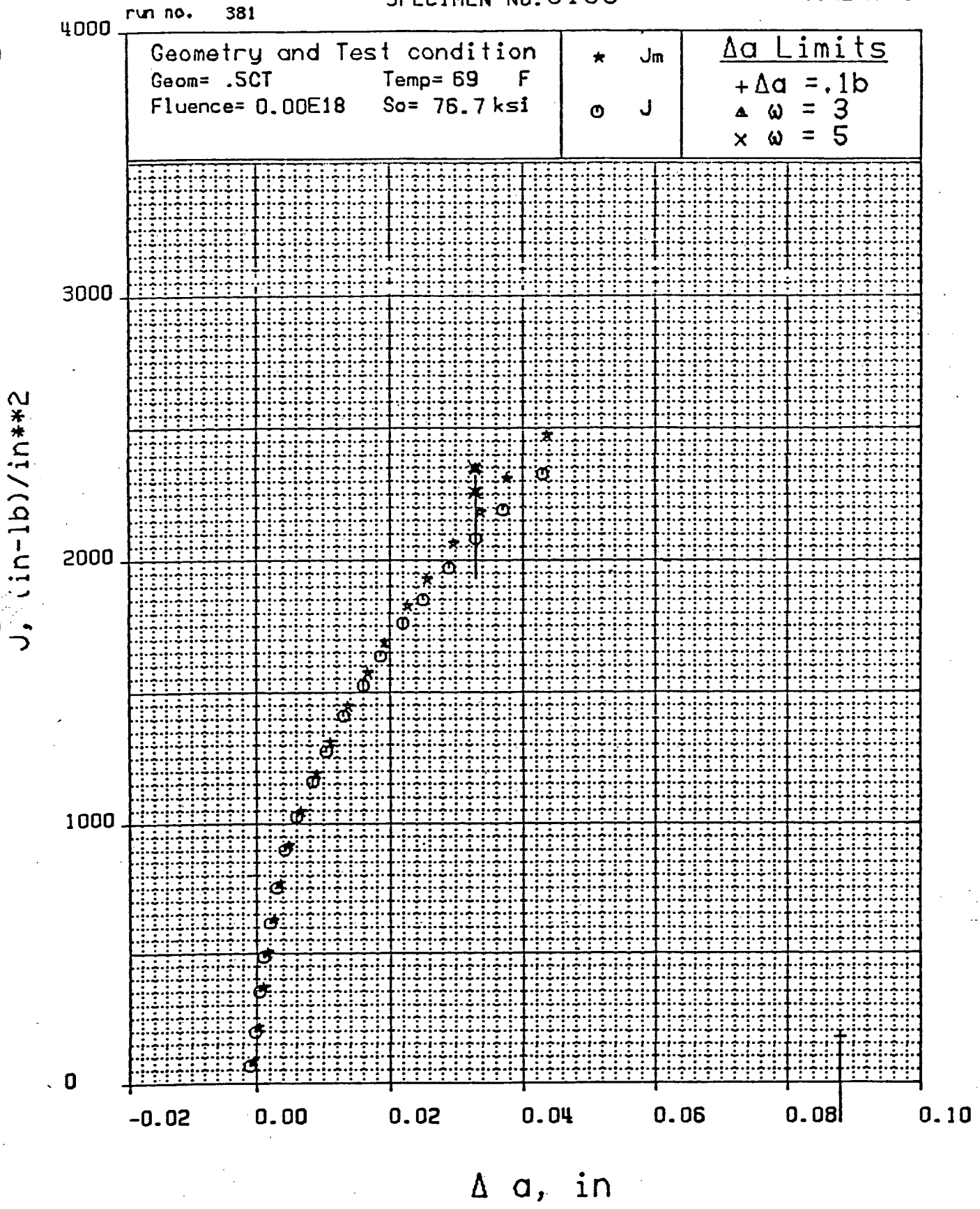

SPECIMEN NO: C1JS

FIGURE A-14

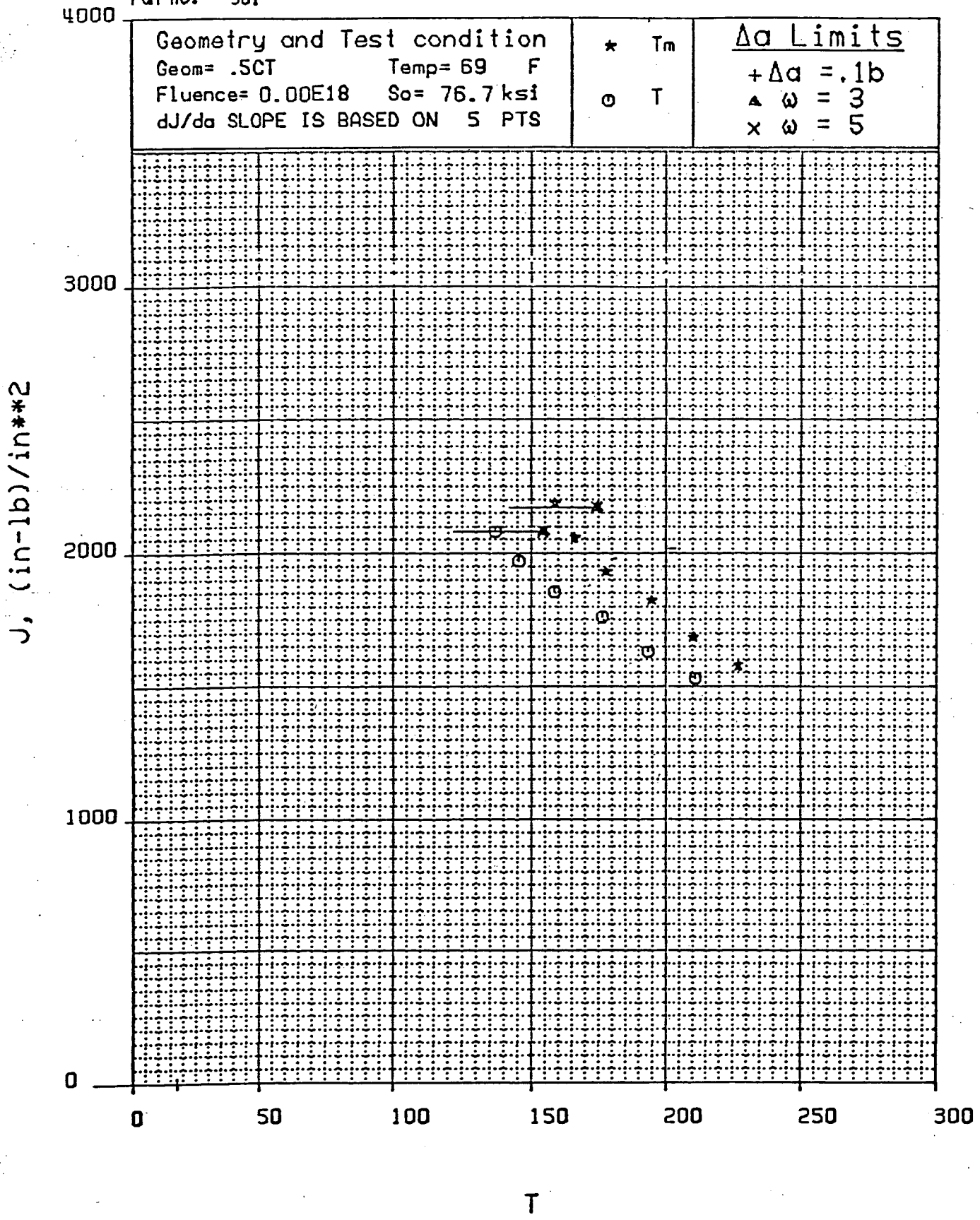

SPECIMEN NO: CW2JS

FIGURE A-15

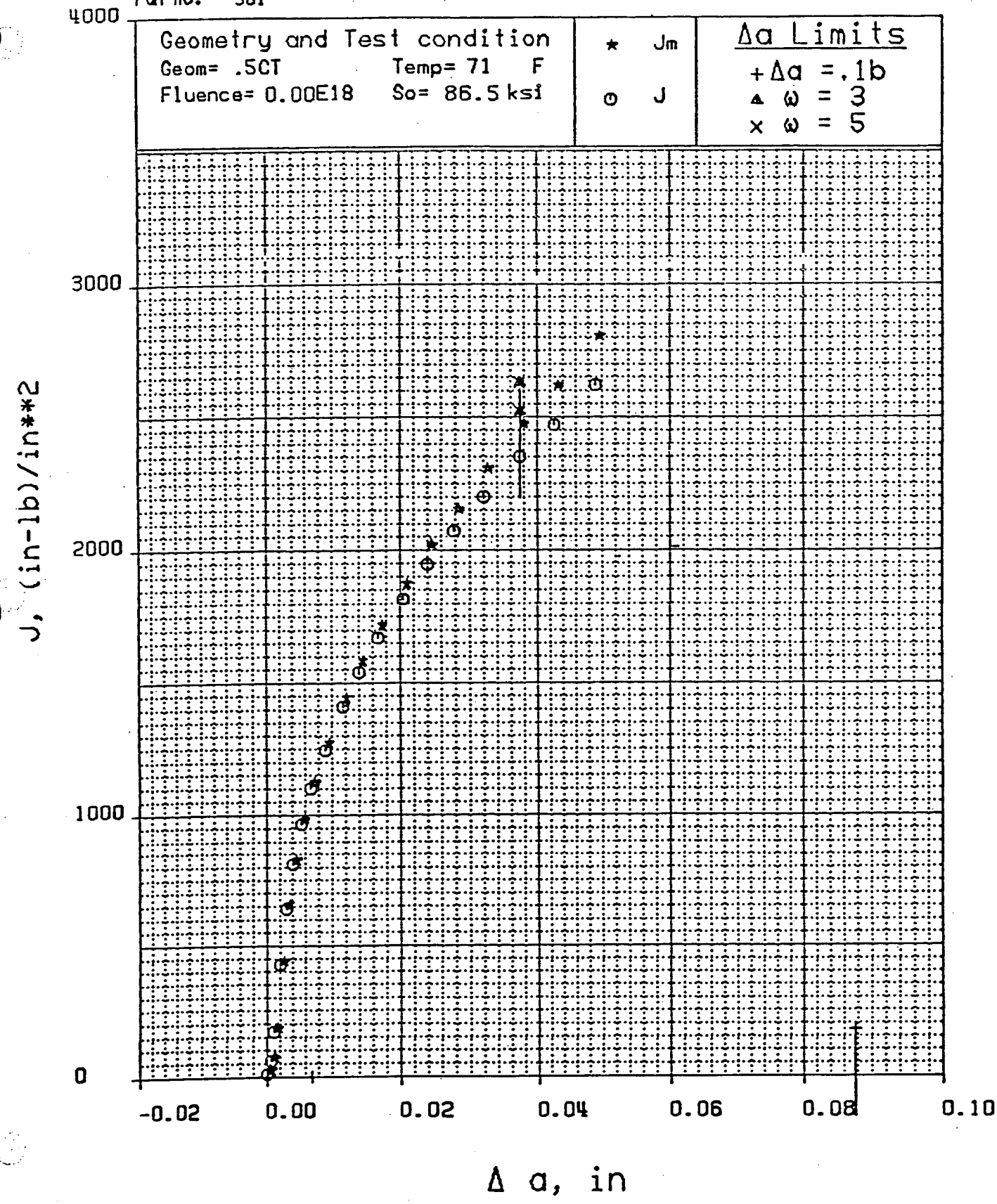

SPECIMEN NO: CW2JS

FIGURE A-16

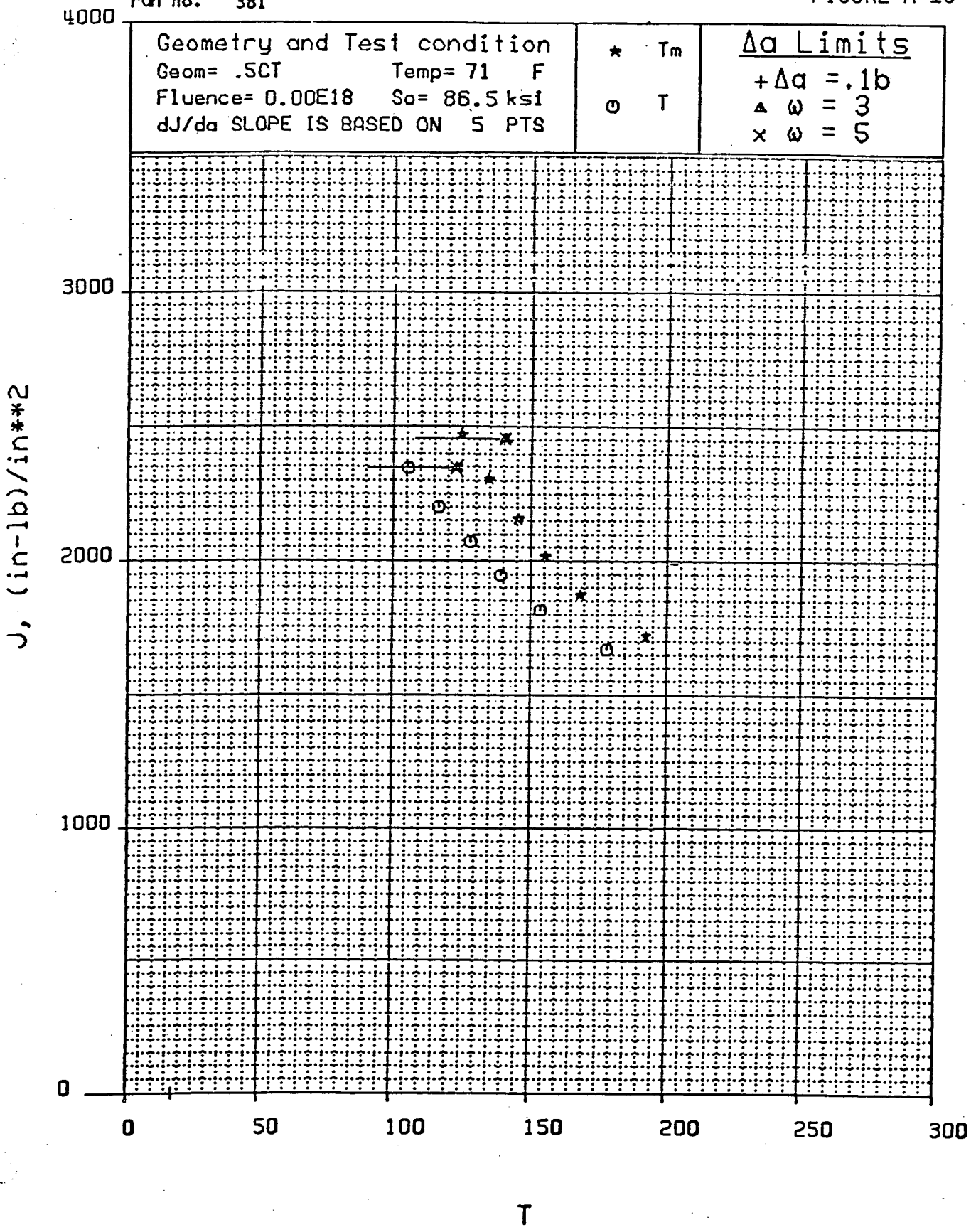

SPECIMEN NO: RW1JS

FIGURE A-17

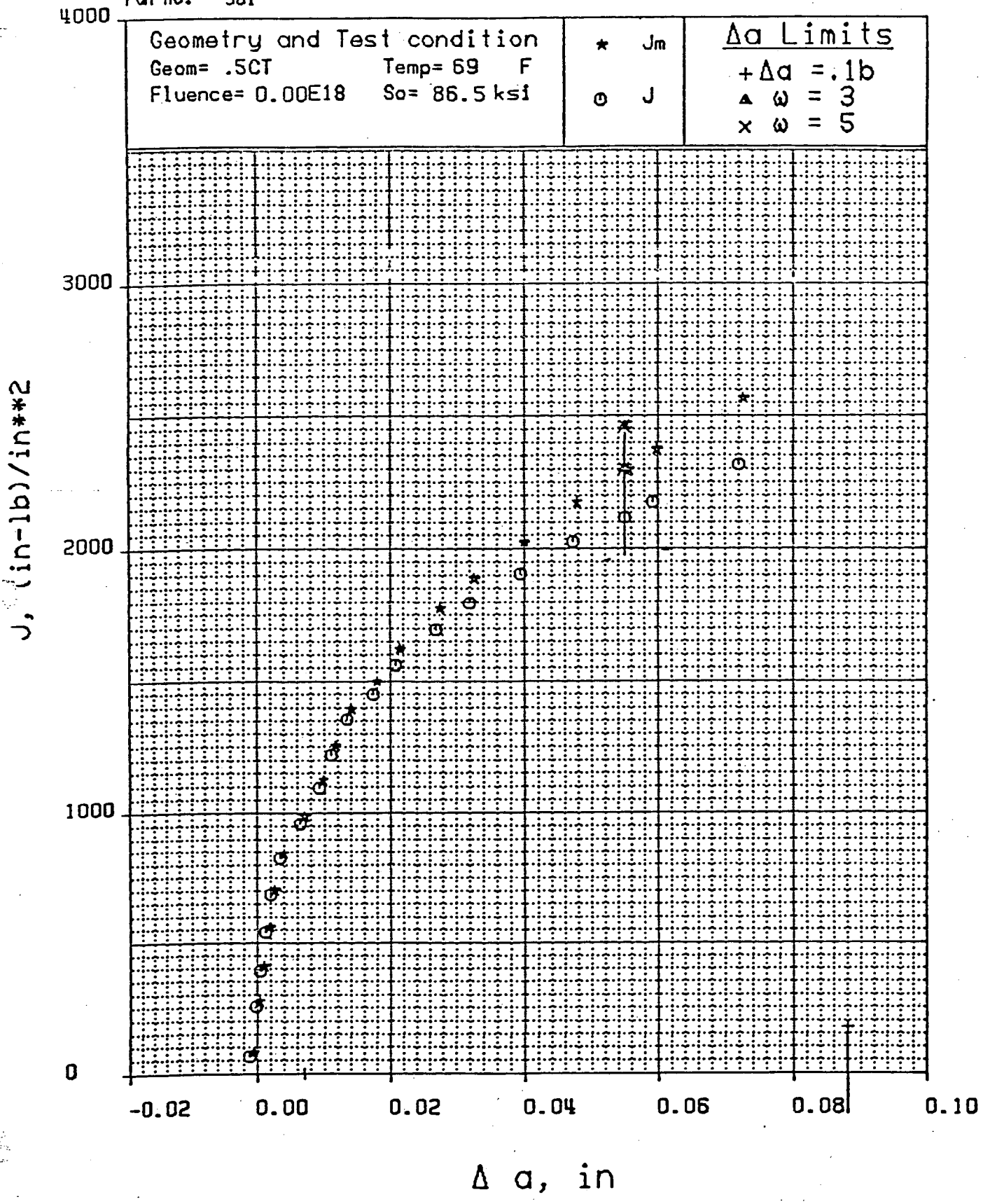

SPECIMEN NO: RW1JS

FIGURE A-18

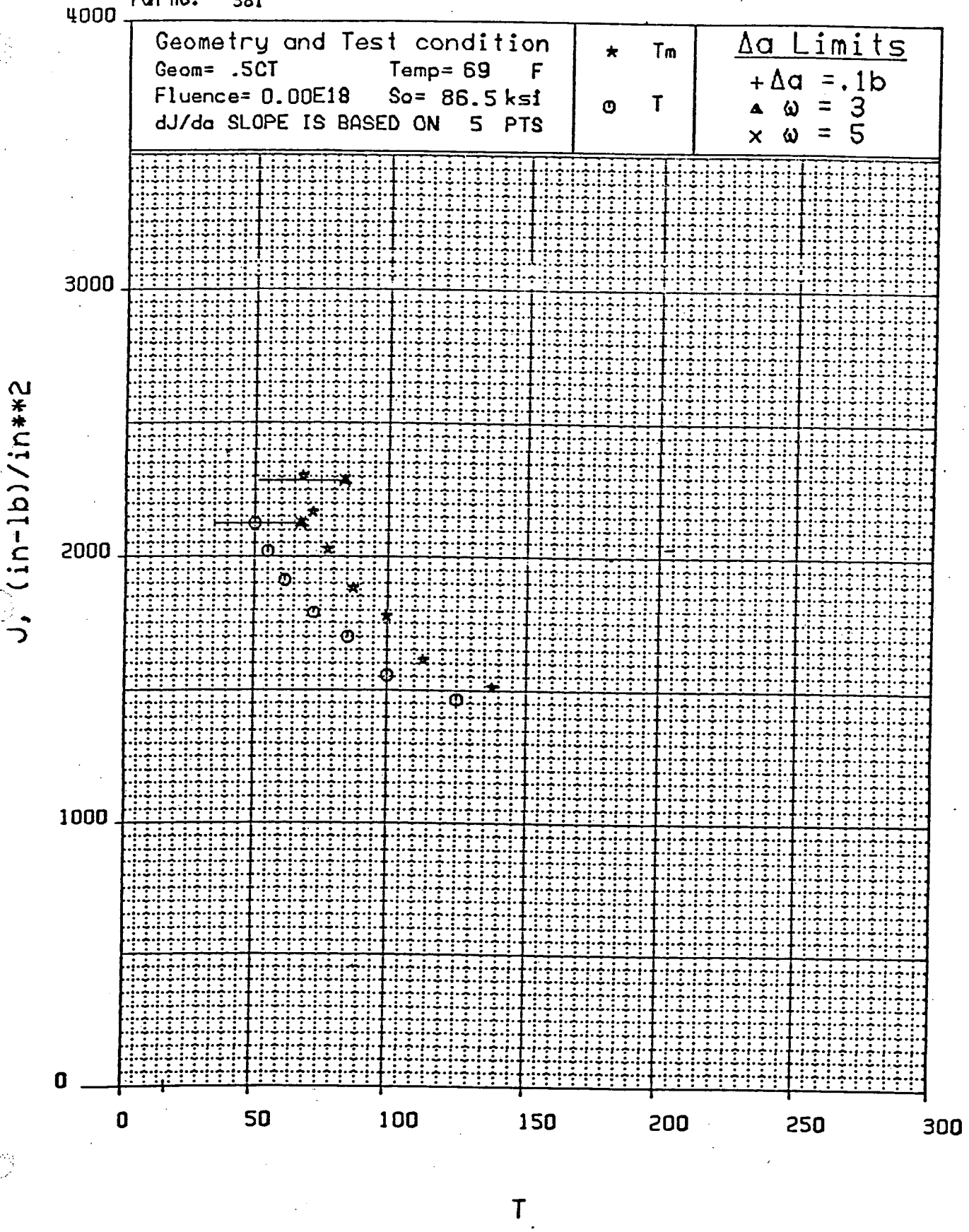

FIGURE A-19

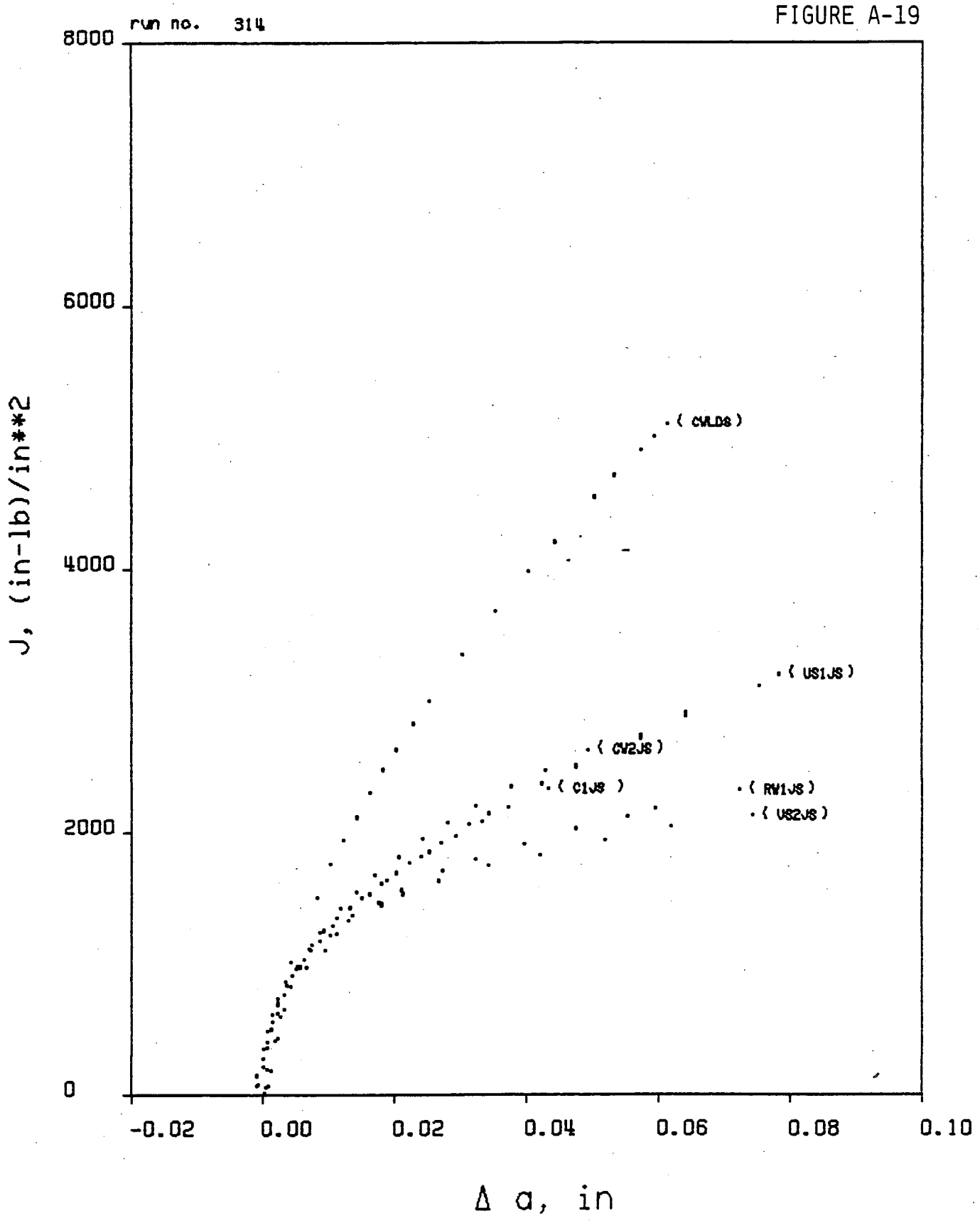
run no. 314
8000
6000
4000
2000
0
J, (in-lb)/in**2
-0.02
0.00
0.02
0.04
0.06
0.08
0.10
Δ a, in
(CWLDS)
(US1JS)
(CW2JS)
(C1JS)
(RW1JS)
(US2JS)

FIGURE A-20

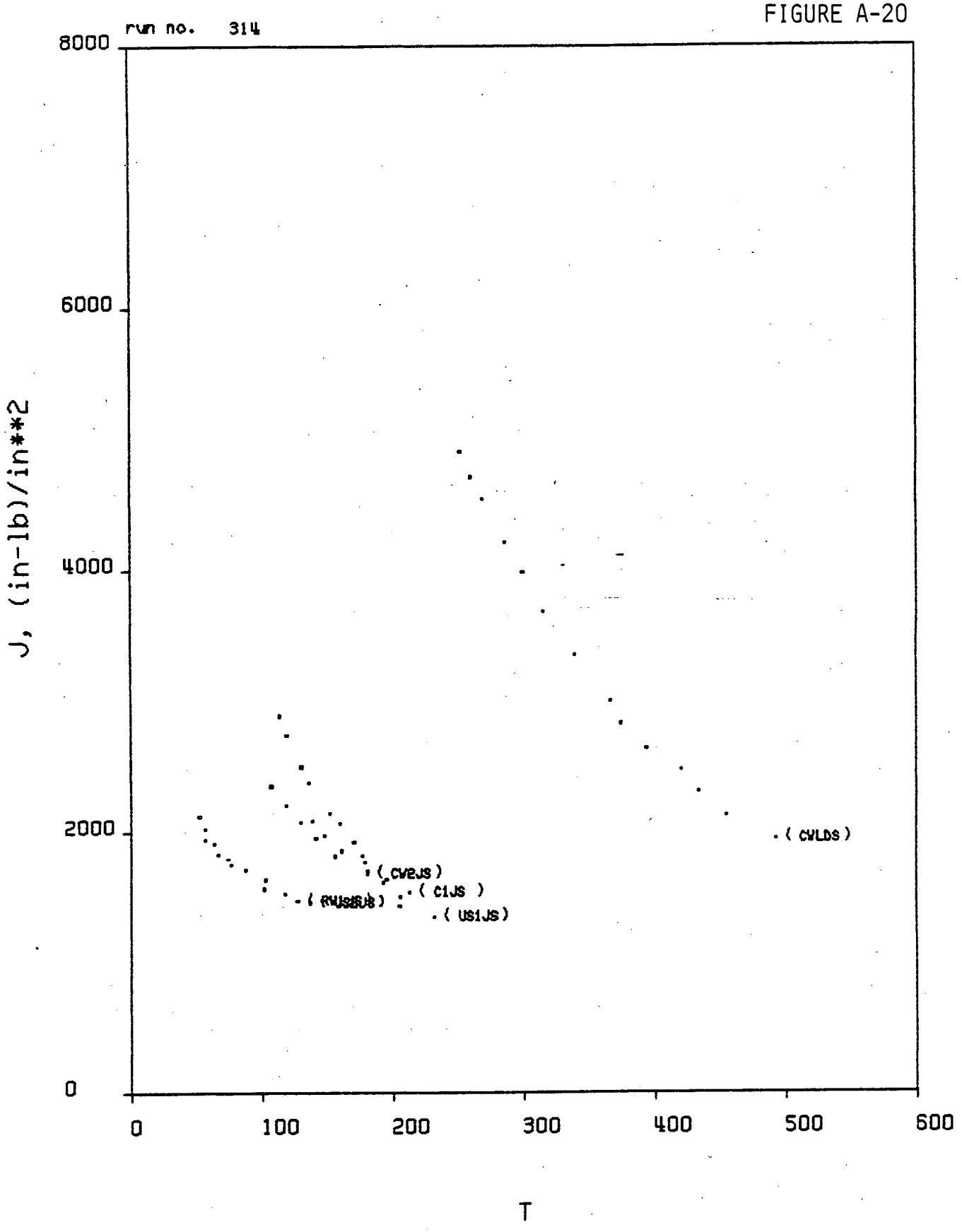
run no. 314
8000
6000
4000
2000
0
J, (in-lb)/in**2
0
100
200
300
400
500
600
T
(CV1DS)
(CV2JS)
(C1JS)
(RWUS&US)
(US1JS)

FIGURE A-21

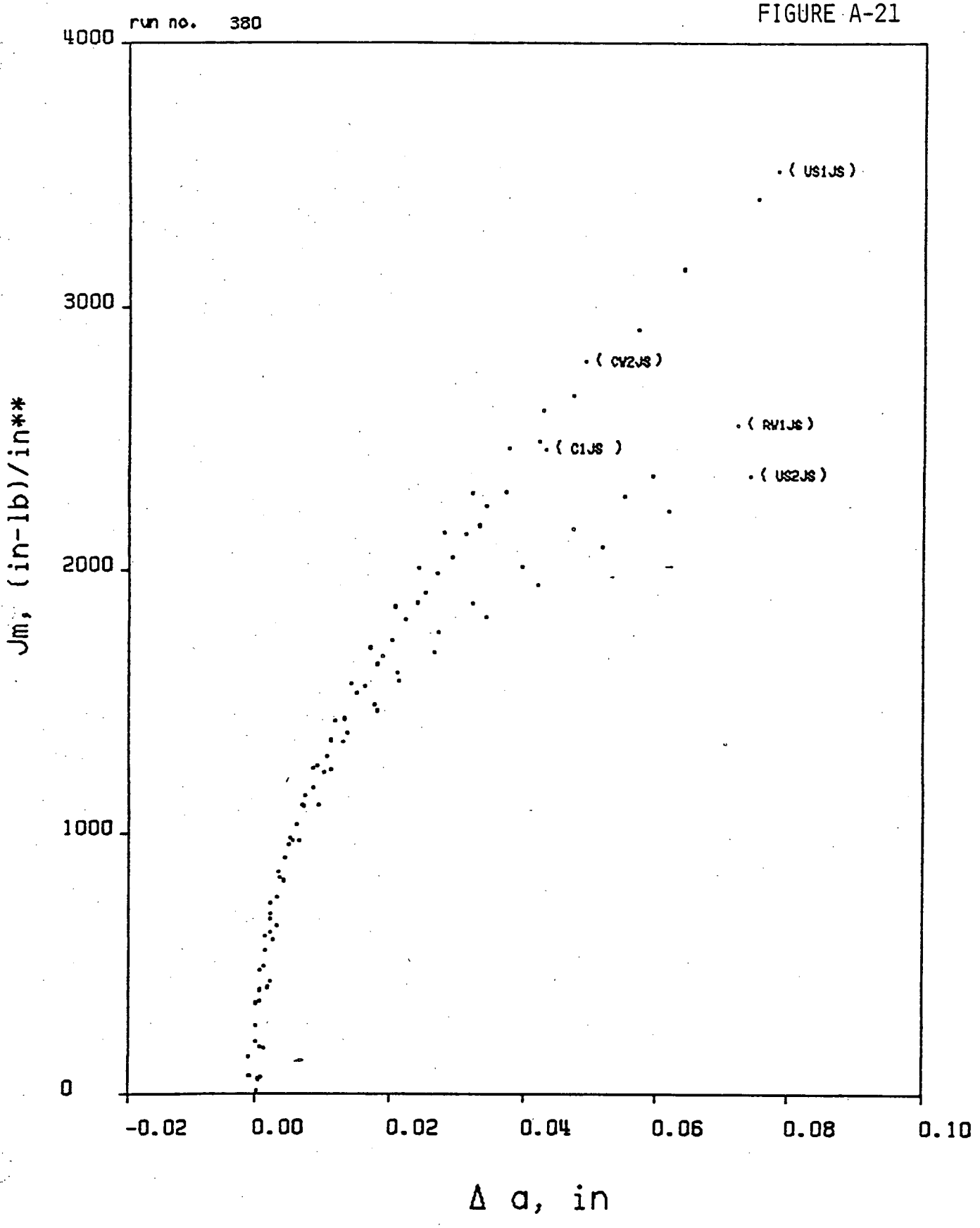
run no. 380
4000
3000
2000
1000
0
Jm, (in-lb)/in**
(US1JS)
(CV2JS)
(RV1JS)
(C1JS)
(US2JS)
-0.02
0.00
0.02
0.04
0.06
0.08
0.10
Δ a, in

FIGURE A-22

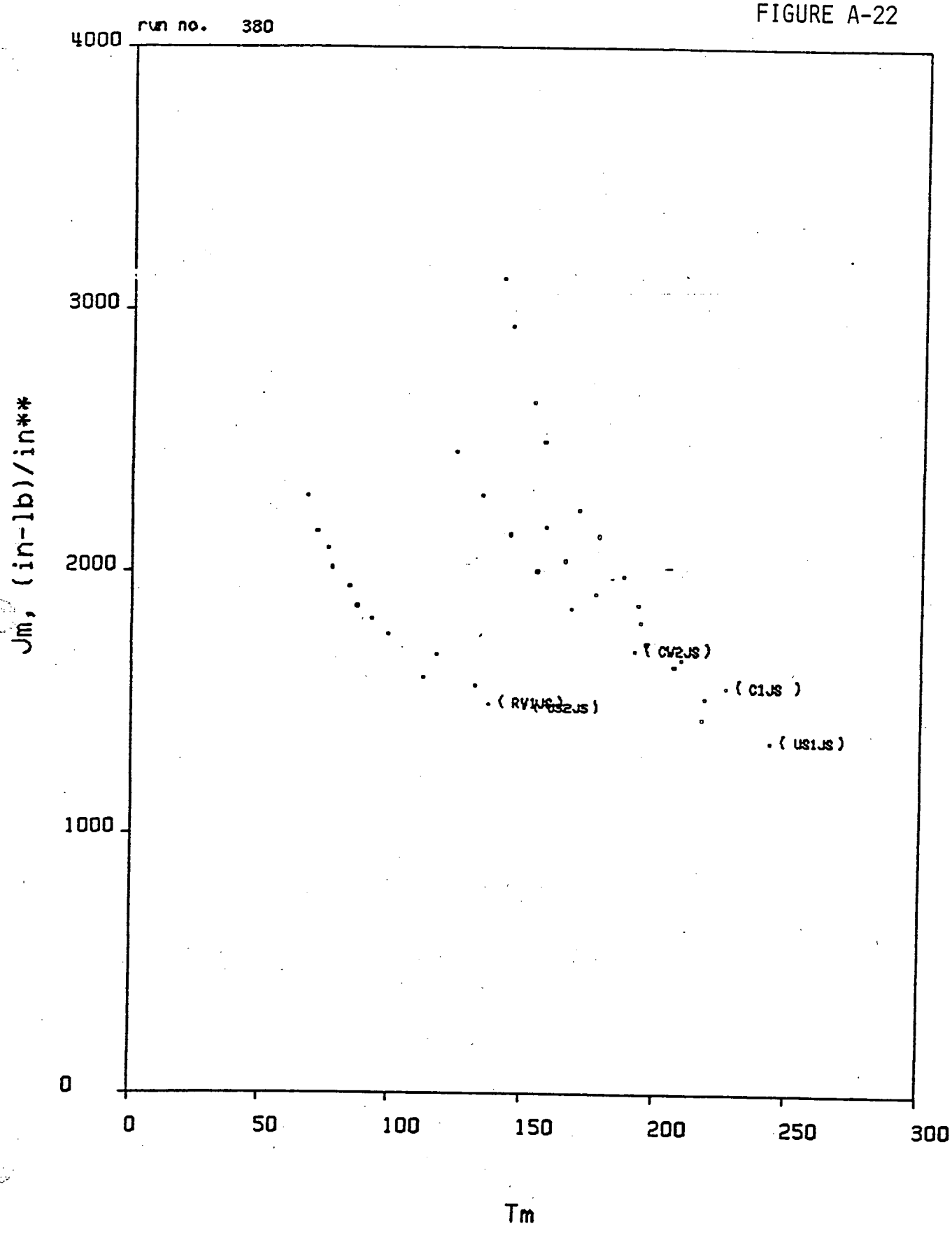
run no. 380
4000
3000
2000
1000
0
Jm, (in-lb)/in**
0
50
100
150
200
250
300
Tm
(CV2JS)
(C1JS)
(RV1JS)
(US2JS)
(US1JS)

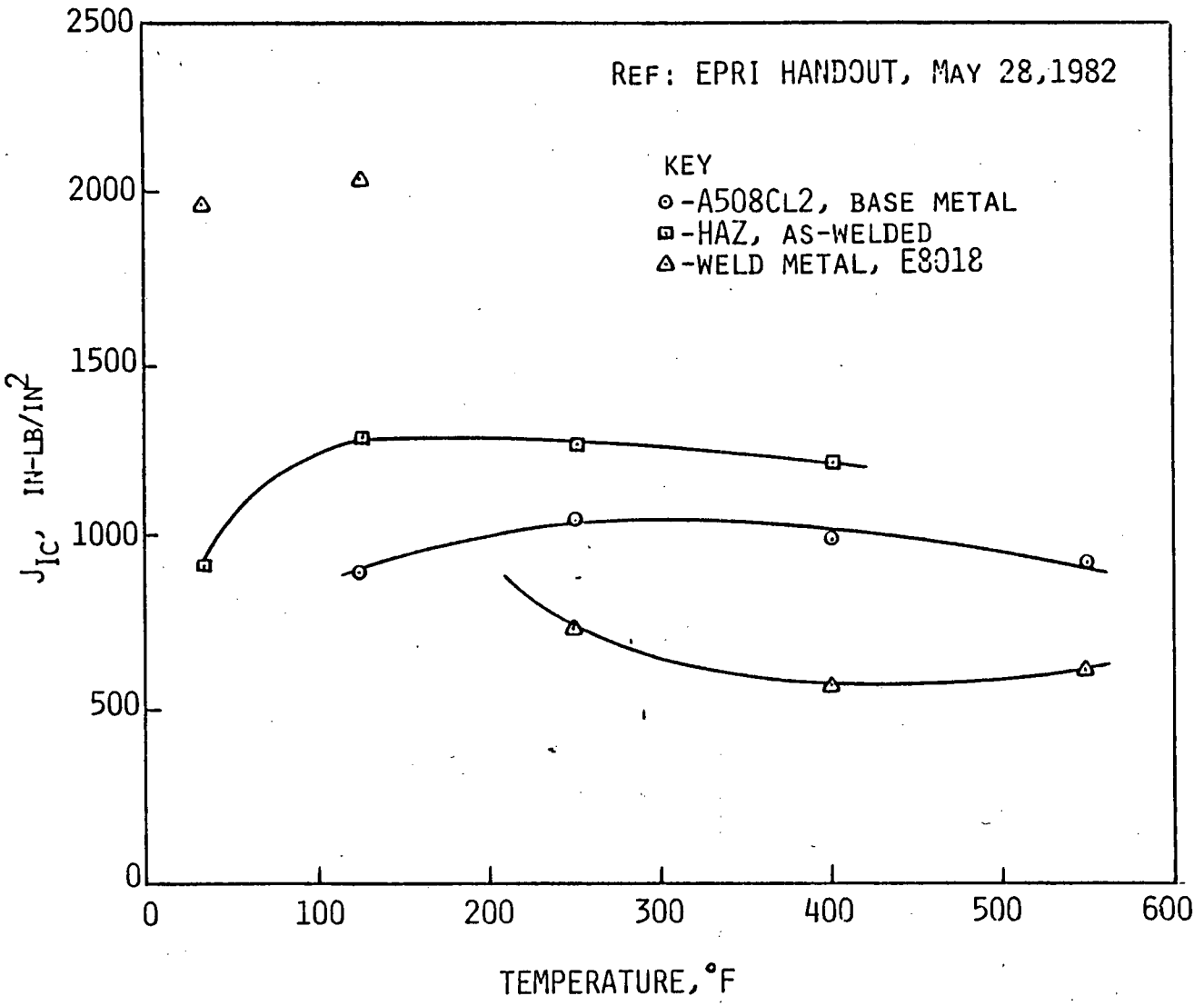
REF: EPRI HANDOUT, MAY 28,1982
KEY
⊙-A508CL2, BASE METAL
⊡-HAZ, AS-WELDED
△-WELD METAL, E8018
J_{IC}, IN-LB/IN^2
2500
2000
1500
1000
500
0
0
100
200
300
400
500
600
TEMPERATURE, °F

FIGURE A-23

FIGURE A-24

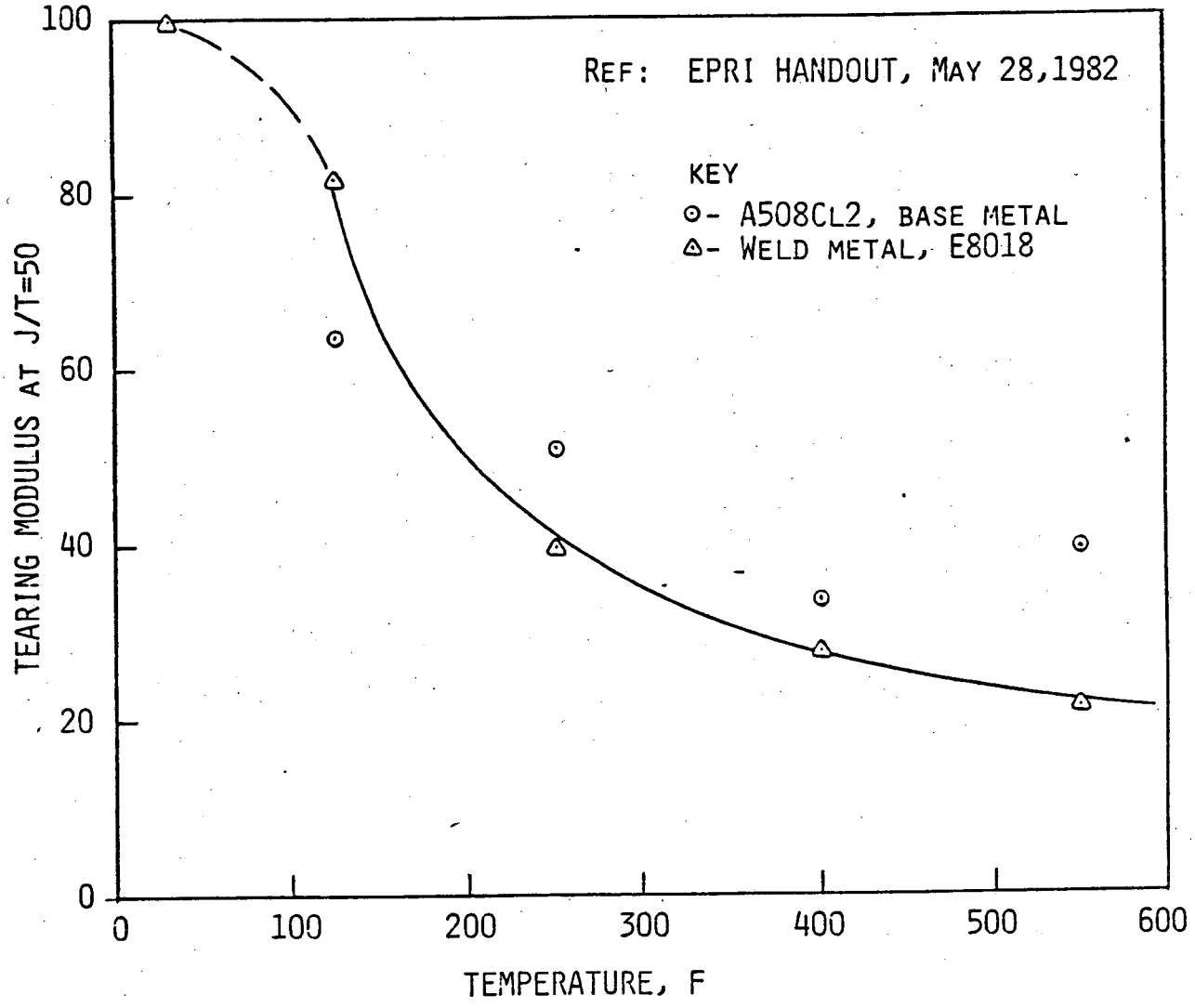
REF: EPRI HANDOUT, MAY 28,1982
KEY
⊙- A508CL2, BASE METAL
△- WELD METAL, E8018
TEARING MODULUS AT J/T=50
100
80
60
40
20
0
0
100
200
300
400
500
600
TEMPERATURE, F

FIGURE A-25

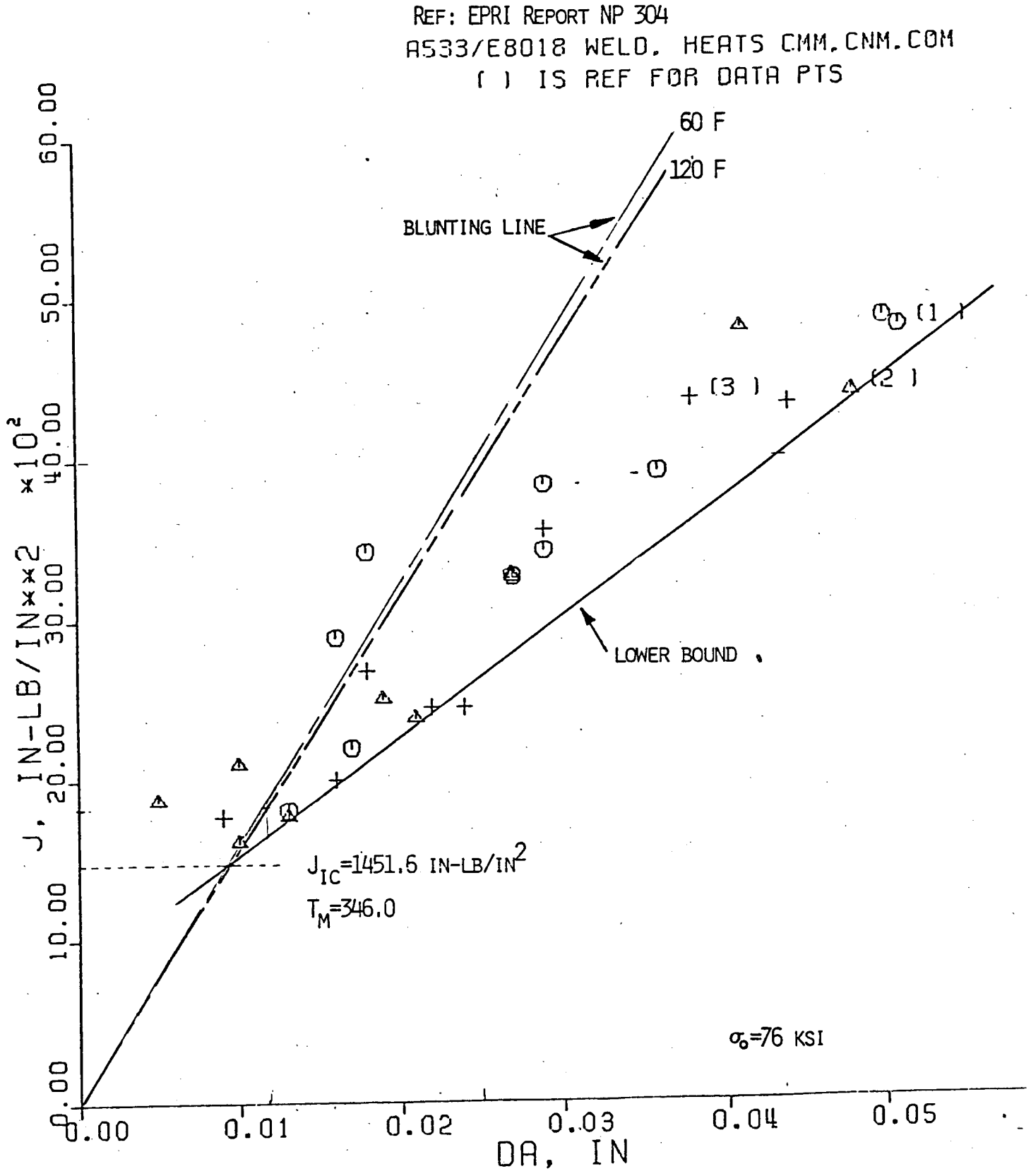
REF: EPRI REPORT NP 304
A533/E8018 WELD. HEATS CMM.CNM.COM
( ) IS REF FOR DATA PTS
60 F
120 F
BLUNTING LINE
LOWER BOUND
(1)
(2)
(3)
J_{IC}=1451.6 IN-LB/IN^2
T_M=346.0
σ_o=76 KSI
J, IN-LB/IN**2 *10^2
DA, IN
0.00
10.00
20.00
30.00
40.00
50.00
60.00
0.01
0.02
0.03
0.04
0.05

APPENDIX B

FPDSSM

The FPDSSM program is based on the computation of stress-intensity factors by means of the slice synthesis method.

B-1 THE SLICE SYNTHESIS METHOD

The slice synthesis method permits solutions for flawed 3-D geometries to be synthesized from 2-D solutions. Through application of this method, such powerful and well established 2-D analysis techniques as complex function theory and the universal weight function, i.e., influence coefficient, theory of Bueckner(1) can be extended to 3-D geometries. In this manner, the influence of finite boundaries can be completely included.

B-2 THEORY

Figure B.1 illustrates the application of the slice synthesis method to a typical reactor nozzle. The pressure vessel wall is idealized as an assemblage of flat radially cracked slices of infinitesimal thickness while the reinforcing ring on the inner boundary of the vessel wall and the nozzle proper are idealized as an assemblage of radially cracked rings of infinitesimal thickness. Mechanical coupling between the slices arises from the transverse shear stresses which exist

at the interface between adjacent slice elements. These transverse shear stresses arise from the restraining effect of neighboring slice elements on the crack opening displacement of each cracked slice element. The influence of these stresses is simulated by a 2-D system of line springs attached to faces of the cracked slice elements. The properties of these springs are determined by idealizing the reactor wall/nozzle as an assemblage of single edge crack slice elements as shown in Figure B.2.

In order for the radial crack and spring elements to be compatible, we must have:

$$(1/E) \int_{x-R}^{\xi=a(z)} \int_{R}^{u=R+\xi} [p^{o}(u)-p^{*}(u,z)]\ g(u,\xi)_{rc} g(x,\xi)_{rc}\ du d\xi = (1/E_s) \int_{z}^{\xi=b(x)} \int_{s_1}^{u=\xi} p^{*}(x,u) g(u,s)_s g(z,s)_s\ du ds \qquad \text{(B-1)}$$

where $p^{o}(x)$ is the crackline loading (i.e., the negative of the stresses existing in the unflawed structure along the plane of crack extension), $p^{*}(x,z)$ is the magnitude of the unknown stress transmitted across the springs, E is elastic modulus of the flawed material, E_s is the effective modulus of the spring elements, $g(x,\xi)_{rc}$ is the Bueckner universal weight function for the 2-D radial crack slice elements and $g(z,\xi)_s$ is the corresponding Bueckner universal weight function for the spring elements. The effective modulus E_s of the spring elements is a measure of the shear coupling between radial crack elements and is determined by the flaw aspect ratio a/b per the following equation:

$$E_s/E = (b/a)/(1-\mu^2) \int_{0}^{\phi=\pi/2} \sqrt{\sin^2\phi + (a/b)^2\cos^2\phi}\ d\phi \qquad \text{(B-2)}$$

where μ is Poisson's ratio.

Equation (2-1) is a singular integral equation with $p^{*}(x,z)$ the stresses

transmitted across the spring system, as the unknown function. The equation is solved numerically by treating $p^*(x,z)$ as a power series with unknown coefficients. These coefficients are determined by a multiple linear regression scheme by forming a redundant system of simultaneous equations. Values of the stress intensity factor at any point along the crack front can the be obtained by asymptotic expansion of the near tip displacement field. A complete description of the slice synthesis method is given in Reference(2).

B-3 APPLICATIONS

The slice synthesis method offers several significant advantages over other 3-D techniques such as the boundary integral method or the 3-D finite element methods. These advantages are:

(1) There is no need to model the crack-tip region or the interior domain or the boundaries with nodal elements. Hence, finite boundaries are readily accountd for. Also, the crack front can advance (as for fatigue crack growth computations) without the necessity of remodeling the geometry for each increment of growth.

(2) Computer solution time is drastically reduced. This reduction makes it feasible to incorporate the cycle-by-cycle flaw shape changes into the crack growth tracking algorithmn, thereby providing a more accurate and realistic representation of the flaw growth process in a reactor pressure vessel.

(3) Different crack loading conditions can be easily accommodated. This feature is a necessity for accurate prediction of crack growth behavior in a reactor vessel where the transients causing crack growth consist of various combinations

of internal pressure and temperature. During the crack growth process, checks must be made at each stage of growth to assure that the member possesses adequate residual strength to withstand any emergency or faulted conditions where the crackline loading associated with these conditions is different from the crackline loading producing the subcritical crack growth. Also, any changes in the crackline loading due to plastic yielding at the crotch of the nozzle or due to creep relaxation of the stress field can also be readily included.

B-4 VERIFICATION OF SLICE SYNTHESIS SOLUTIONS

Verification of FPDC's computer program (FPDSSM) for performing slice synthesis method stress analyses of flawed geometries was performed(__) by comparing predictions against published solutions for common 3-D flaw geometries. Slice synthesis method predictions for stress intensity factors were compared with available solutions in the literature for the following crack geometries: part-thru surface flaw, penny shaped embedded flaw, longitudinal part-thru and edge cracks in a pressurized cylinder, corner flaw in a quarter-infinite solid and the radial corner flaw emanating from an open hole. Very good correlation is found to exist between the slice synthesis method predictions and those obtained from other methods, thus verifying its suitability for the fracture mechanics analysis of nuclear safety related components.

B-5 REFERENCES

1. H. F. Bueckner, 'A Novel Principle for the Computation of Stress Intensity Factors,' Z. Angew. Math. Mech., 50, pp. 529-546, 1970.

2. W. T. Fujimoto, 'Determination of Crack Growth and Fracture Toughness Parameters for Surface Flaws Emanating from Fastener Holes,' Proceedings of the AIAA/ASME ISAE 17th SDM Meeting, Valley Forge, PA., May, 1976.

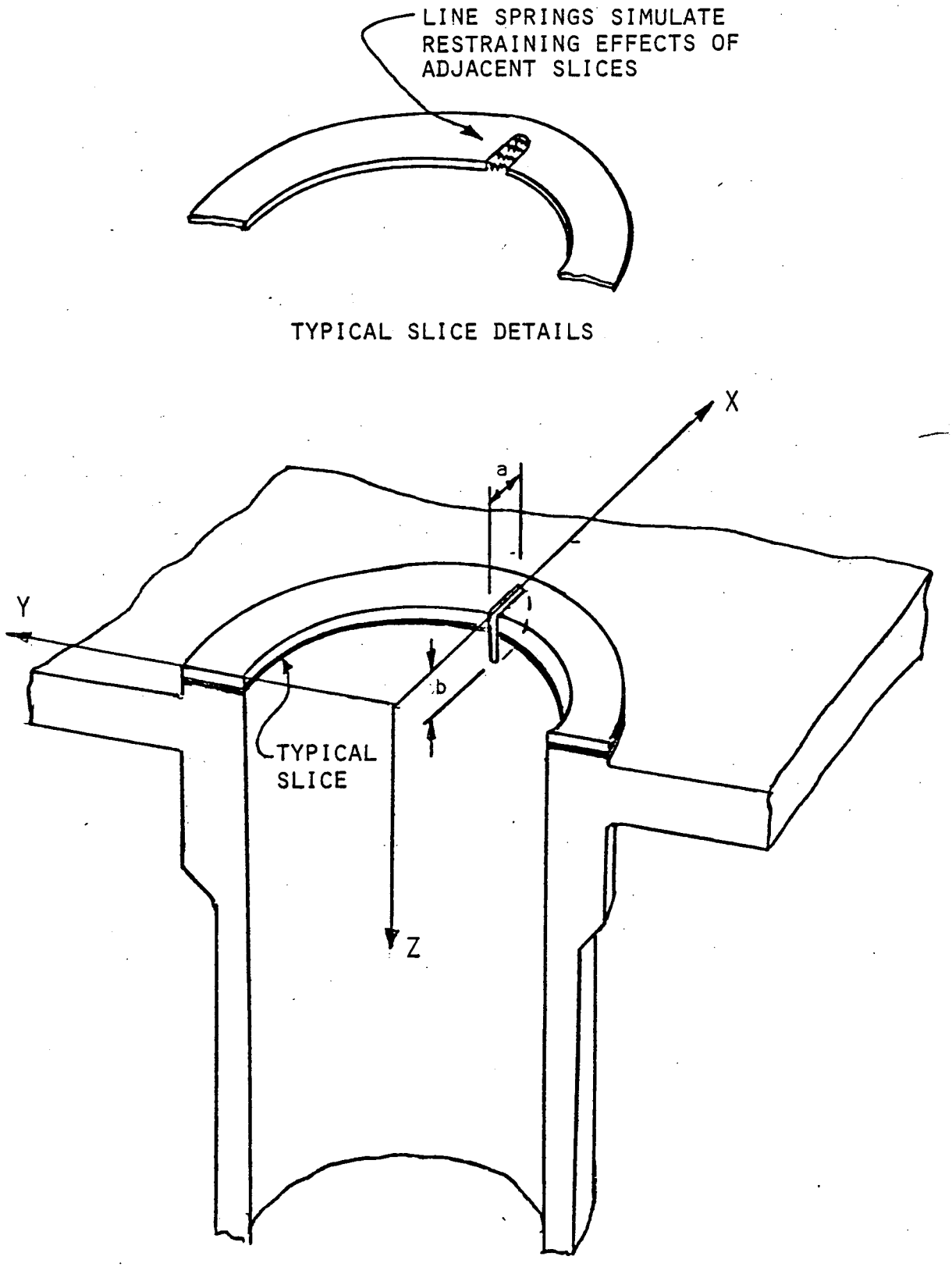

Fig. B-1 Cutaway View of Reactor Nozzle

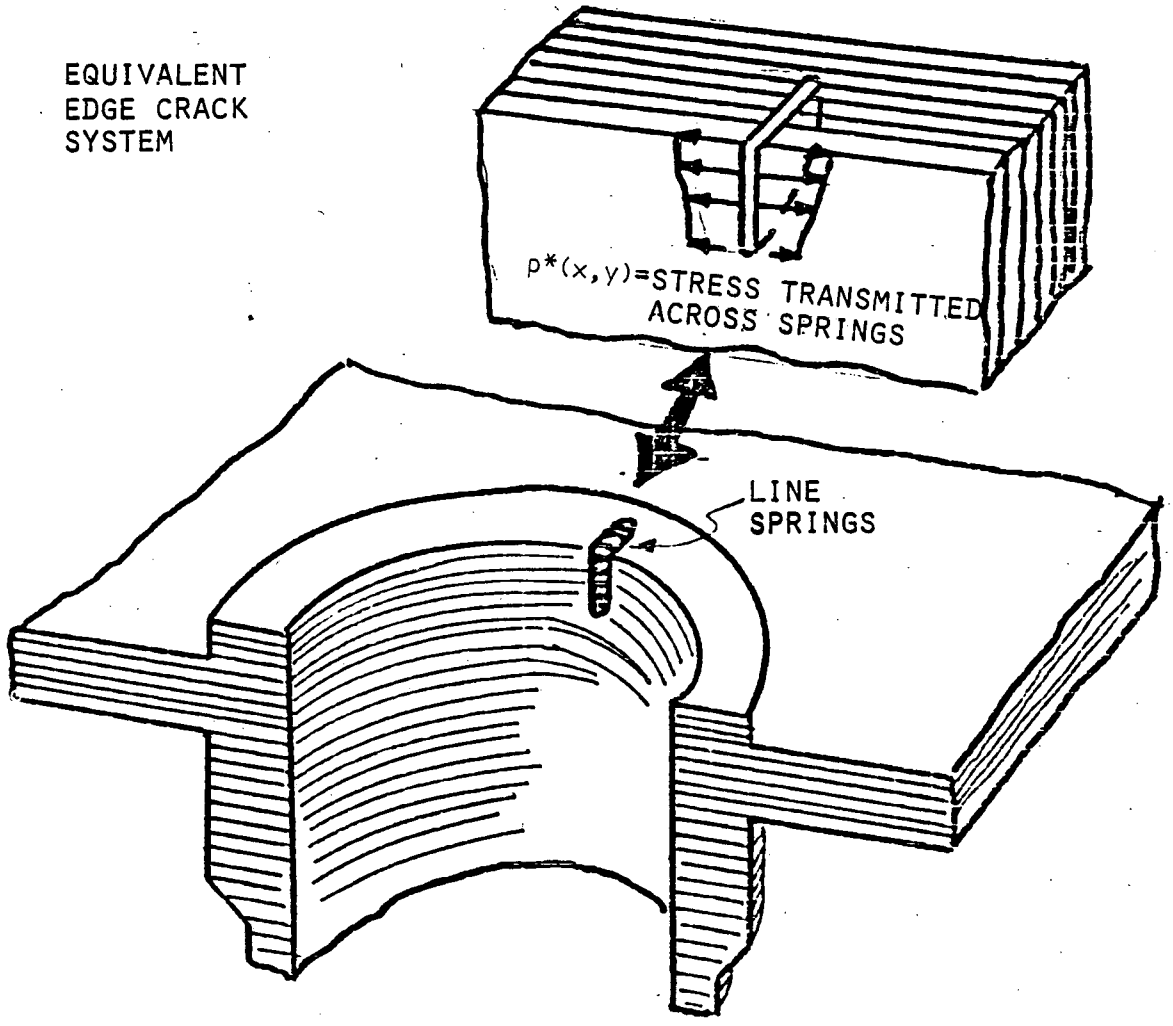

SLICE IDEALIZATION OF REACTOR NOZZLE

Fig. B-2 Spring Properties Determined From Equivalent Edge Crack System

APPENDIX C

HEAT TRANSFER CALCULATIONS

SOEST HILL
ENGINEERING
P.O. Box 1187
Rolla, Missouri 65401
March 31, 1983

Dr. Keyren H. Cotter
Fracture Proof Design Corporation
77 Maryland Plaza
St. Louis, Missouri 63108

Reference: Heat Transfer Near Heated Zone

Dear Dr. Cotter:

I have estimated the heat transfer coefficient for natural convection air flow over a heated vertical wall. I assumed a heated region 12 to 16 inches at 1200 degrees F. The calculation is relatively insensitive to the temperature difference and the heighth of the heated zone. The upper limit on the heat tranfer coefficient is 1.3 in English units. A value of 1.0 to 1.3 should be adequate for the calculations as you described them on the telephone. The finite element method as you outlined should properly describe the temperature distribution in the wall. The internals of the steam generator will serve as a heat sink and help keep the air temperature down and the delta-T up; this will in turn keep the value of h around 1.0.

If a larger heat transfer coefficient is desired, some type of forced flow must be utilized. The forced convection heat transfer coefficient would be at least an order of magnitude larger.

Sincerly yours,

D. Ray Edwards, P.E.

NATURAL CONVECTION

$$Gr = \frac{g\beta (T_w - T_\infty) L^3}{\nu^2}$$

Assume $T_w - T_\infty = 1100°F$

$\bar{T} = 650°F$

$Pr = 0.68$ $\quad \beta = 9.0 \times 10^{-4}/°F$

$\nu = 5.8 \times 10^{-4} \frac{ft^2}{sec}$ $\quad k = 27.4^{-3} \frac{Btu}{hr\,ft\,°F}$

$$Gr = \frac{(32.2\ ft/sec^2)(9.0\times10^{-4}/°F)(1100\ °F)(1.25)^3}{(5.9\times10^{-4}\ \frac{ft^2}{sec})^2}$$

$= 1.85^{10}$ LAMINAR FLOW $L = 1.25\ ft$ $\quad \Delta T = 1500$

$\overline{Nu} = \frac{4}{3} Nu_L$

$Nu_L = 0.508\, Pr^{1/2} (0.952 + Pr)^{-1/4}\, Gr_L^{1/4}$

$= 43.2$

$\overline{Nu} = 57.6$

$h = \frac{k}{L} \overline{Nu} = 1.26 \frac{Btu}{hr\,ft^2\,°F}$

$L = 1\ ft$ $\quad Gr = 9.47^{7}$

$Nu_L = 36.5$

$\overline{Nu} = 48.7$

$h = 1.33 \frac{Btu}{hr\,ft^2\,°F}$

USE $1.3\ Btu/hr\,ft^2\,°F$

$h \propto \Delta T^{1/4}$ AS WALL COOLS h WILL decrease

$h \propto \frac{1}{L^{1/4}}$ as heated belt widens h decreases

SOEST HILL
ENGINEERING
P.O. Box 1187
Rolla, Missouri 65401
March 20, 1983

Dr. Keyren H. Cotter
Fracture Proof Design Corporation
77 Maryland Plaza
St. Louis, Missouri 63108

Reference: PO 124

Dear Dr. Cotter:

The attached calculations are for the calculations of the temperature at the wall located 2 feet 9 3/4 inches below the inlet. I have detailed the assumptions in the calculations, noted appropriate steps, listed references, and noted assumptions. Basically, I assumed a free jet along a wall. This is conservative since a confined -jet will have a more restricted or narrow plume. In fact, the QA calculations were based on a restricted jet and the result is that the jet plume does not reach the wall at the weld. Hence, the predicted temperature of 517 to 524 degrees F is conservative.

The heat transfer coefficient calculated is given in a range based on the spacing of the "J" tubes. The coefficient is higher when the tubes are closer together. The range I calculated is from 49 to 90 in English units. This should cover the range required for any calculation of wall temperature.

Sincerely yours,

D. Ray Edwards, P.E.

ESTIMATE THE FLUID TEMP AT THE STEAM GENERATOR WALL FROM INLET FLUID AT 70°F INTO FLUID AT 547°F. FLUID ENTERS THROUGH J-TUBES WITH TOTAL FLOW OF 350 gpm. THERE ARE 35 - 38 J-TUBES PER GENERATOR. ELEVATION VIEW PROVIDED BY SKETCH DATED 3-9-83 NUMBER 80-121-1F

ASSUME 35 TUBES AND EQUAL FLOW/TUBE

$$\text{TUBE FLOW} = \frac{350\ \text{gpm}}{35\ \text{TUBES}} = 10\ \text{GPM}$$

2" SCHEDULE 80 PIPE

ID. 1.939" FLOW AREA 0.02050 ft²

$$\left(10\ \frac{\text{gal}}{\text{min}}\right)\left(\frac{1\ \text{min}}{60\ \text{sec}}\right)\left(\frac{1\ \text{ft}^3}{7.48\ \text{gal}}\right)\left(\frac{1}{0.02050\ \text{ft}^2}\right) = 1.087\ \text{ft/sec}$$

FLOW WILL BE CONSIDERED AS TWO DIMENSIONAL SET FOR CLOSELY SPACED TUBES AND AS CIRCULAR SET FOR WIDELY SPACED TUBES.

THE PROXIMITY OF THE J-TUBE TO THE INNER WALL IS SUCH THAT A WALL SET IS A CLOSE APPROXIMATION. BASED ON THE reference WORK CITED BELOW, A LINE OF SYMMETRY IS ASSUMED AT THE INNER SIDE OF THE J-TUBE.

ANOTHER BASIC ASSUMPTION IS THAT MOMENTUM IS CONSTANT AT ALL DISTANCES x BELOW THE SET

$$K = \pi R^2 u^2 = 0.02050\,(1.087)^2 = 0.0242\ \frac{\text{ft}^4}{\text{sec}^2}$$

2-D SET

SPACING = 5.75 IN

$$K = 2 \cdot \frac{0.0242\ \text{ft}^4/\text{sec}^2}{5.75\ \text{IN}/12\ \text{IN/ft}} = 0.101\ \frac{\text{ft}^3}{\text{sec}}$$

where the 2 is for symmetry & 5.75" is THE CLOSEST SPACING OF THE J-TUBES.

$$u = \frac{\sqrt{3}}{2}\sqrt{\frac{K\sigma}{x}}\left[1 - \tanh^2 \eta\right]$$

$\sigma = 7.67$ empirical constant

$\eta = \sigma \frac{y}{x}$ $y = 14.5''$ (d2 y SKETCH)

$x = 2'9\frac{3}{4}'' = 33.75''$ (h5 y SKETCH) DISTANCE FROM S-TUBE TO WELD OF INTEREST

$\eta = 7.67 \frac{14.5}{33.75}$

$= 3.295$

$$u = \frac{\sqrt{3}}{2}\sqrt{\frac{\alpha_t 101 \cdot 7.67}{33.75/12}}\left[1 - \tanh^2 3.295\right]$$

$u = (0.4545)(0.00548) = 0.00249$ ft/sec

$$\left(\frac{u}{u_{max}}\right)^{1/2} = \frac{T}{T_{max}}$$

$$\frac{T}{T_{max}} = \left(\frac{0.00249}{1.087}\right)^{1/2} = 0.0479$$

$T_{max} = 70 - 547 = -477$ °F

$T = -22.8$ or $T_{weld} = 524$ °F

CIRCULAR SET

$K = 2 \cdot 0.0242 = 0.0484$

$\frac{\epsilon_0}{TK} = 0.0161$ $\epsilon_0 = 0.003542$

$$\eta = \frac{1}{4}\sqrt{\frac{3}{\pi}}\ \frac{\sqrt{K}}{\epsilon_0}\ \frac{y}{x}$$

$$\eta = \frac{1}{4}\sqrt{\frac{3}{\pi}}\ \frac{1}{0.0161}\ \frac{14.5}{33.75} = 6.519$$

$$u = \frac{3}{8\pi}\ \frac{K}{\epsilon_0 x}\ \frac{1}{\left(1 + \frac{1}{4}\eta^2\right)^2}$$

$$= \frac{3}{8\pi}\ \frac{0.0484}{0.003542\ \frac{33.75}{12}}\ \frac{1}{\left(1 + \frac{1}{4}6.519^2\right)^2}$$

$$U = 0.00429$$

$$\left(\frac{U}{U_{max}}\right)^{1/2} = \frac{T}{T_{max}}$$

$$\frac{T}{T_{max}} = \left(\frac{0.00429}{1.087}\right)^{1/2} = 0.0628$$

$$T = -30.0 \qquad T = 517°F$$

HEAT TRANSFER COEFFICIENT

CONSTANT MOMENTUM $\quad 0.0242 \frac{ft^4}{sec^2} = \bar{u}^2 \frac{5.75 \cdot (14.5 + 1.88)}{144}$

$$\bar{u}^2 = 0.0370$$

fluid properties evaluated at 500°F

$$\bar{u} = 0.1923 \text{ ft/sec}$$

$$Re = \frac{D\bar{u}\rho}{\mu} = \left(\frac{16.38}{12}\right) \frac{(0.1923)(49.0)}{0.257} 3600$$

$$= 1.80 \times 10^5$$

$$Pr = \frac{c_p \mu}{k} = \frac{(1.176)(0.257)}{0.351} = 0.861$$

DITTUS BOELTER EQ'N FOR COOLING

$$Nu = 0.023\, Re^{0.8}\, Pr^{0.3}$$

$$= (0.023)(1.80 \times 10^5)^{0.8} (0.861)^{0.3}$$

$$Nu = 352$$

$$h = Nu \frac{k}{D} = (352) \frac{0.351}{16.38/12}$$

$$h = 90.5 \frac{Btu}{hr \cdot ft^2 \cdot F°}$$

FOR WIDELY SPACED TUBES $\bar{U}^2$ IS reduced by THE FACTOR 5.75/27

$$\bar{U}^2 = 0.0370 \frac{5.75}{27} = 0.00788$$

$$\bar{U} = 0.0888 \text{ ft/sec}$$

$$Re = 1.80 \times 10^5 \frac{0.0888}{0.1923} = 8.31 \times 10^4$$

$$Nu = 0.023 (8.31 \times 10^4)^{0.8} (0.861)^{0.3}$$

$$Nu = 189.6$$

$$h = 189.6 \frac{0.351}{16.38/12} = 48.8 \frac{Btu}{hr\,ft^2\,F^\circ}$$

References

JET FLOW: H. SCHLICHTING: BOUNDARY LAYER THEORY, 7th EDITION, McGRAW-HILL 1979

FLUID PROPERTIES & HEAT TRANSFER: S. RUST: NUCLEAR POWER PLANT ENGINEERING HARALSON 1979

MEMO TO: D. Ray Edwards
FROM: Gary E. Mueller
RE: Turbulent Jet Calculation

First of all I independently calculated an approximate temperature at the location of the weld. The value I obtained at the edge of the jet boundary layer was approximately 480°F which was about 8 inches out from the wall of the weld. This means the temperature at the weld should be relatively close to this value. After obtaining this value I reviewed your method of calculation and found out you obtained temperatures which were relatively close to this value. Thus, I feel that your method of calculation is valid for a first approximation.

Gary E. Mueller
Assistant Professor